A SYNTHESIS OF POINT SNOW DEPTH OBSERVATIONS AND A SATELLITE SNOW DEPTH PRODUCT

by

JINGMEI WEI

(Under the Direction of Thomas L. Mote)

ABSTRACT

Snow depth (SD) is one of the important parameters in the hydrologic cycle, contributing to water storage and runoff. This research compared volunteer, in situ SD observations from the National Weather Service cooperative (COOP) network with satellite-derived (Advanced Microwave Scanning Radiometer EOS, AMSR-E) SD values and then proposed a simple interpolation based synthesis incorporating AMSR-E SD, Interactive Multisensor Snow and Ice Mapping System (IMS) snow cover extent (SCE) and COOP SD observations. Daily AMSR-E SD means are found to have a good agreement with daily COOP SD means over time. However, a large difference in the spatial distribution is noted between the data sources. The Difference Correction approach improves the stand-alone AMSR-E SD values with lower mean absolute error and root mean square error, and a higher correlation coefficient (r), by using completely regularized spline interpolation.

INDEX WORDS: Snow depth, Satellite estimate, In situ observation, Interpolation

A SYNTHESIS OF POINT SNOW DEPTH OBSERVATIONS AND A SATELLITE SNOW DEPTH PRODUCT

by

JINGMEI WEI

B.A., Nanjing University, China, 2010

A Thesis Submitted to the Graduate Faculty of the University of Georgia in Partial Fulfillment of the Requirements for the Degree

MASTER OF SCIENCE

ATHENS, GEORGIA

2013

A SYNTHESIS OF POINT SNOW DEPTH OBSERVATIONS AND A SATELLITE SNOW DEPTH PRODUCT

by

JINGMEI WEI

Major Professor: Thomas L. Mote

Committee: Lan Mu
J. Marshall Shepherd

Electronic Version Approved:

Maureen Grasso
Dean of the Graduate School
The University of Georgia
August 2013

ACKNOWLEDGEMENTS

Three years fly by in the blink of an eye, with a cup of coffee holding in my hands, I would like to express my deepest gratitude for those without whose support and belief in this thesis it would not have been possible: Dr. Thomas Mote, Dr. Lan Mu, Dr. Marshall Shepherd, Theresa Andersen, Xiao Lv and last but certainly not least, my parents. Thank you.

I would like to mention NASA MEaSUREs Award NNX08AP34A, "Development of Northern Hemisphere Snow Climate Data Records" (Thomas Mote, Co-PI) which partially provided the financial support for my research. I also wish to thank Julian Turner for kindly sharing the CoCoRaHS snow data.

TABLE OF CONTENTS

Page

LIST OF TABLES

Page

LIST OF FIGURES

Page

LIST OF ABBREVIATIONS

AMSR-E	Advanced Microwave Scanning Radiometer-Earth Observing System
AMSR-E SWE	AMSR-E/Aqua L3 Global SWE EASE-Grids product
ANN	Artificial neural networks
ANSA	The Air Force Weather Agency (AFWA)-NASA
AVHRR	Advanced Very High Resolution Radiometer
CDRD	CV and DS rank difference
CO	cokriging
CoCoRaHS	Community Collaborative Rain, Hail and Snow Network
COOP	Cooperative Observer Program
CRS	completely regularized spline
CV	cross validation
DC	Difference Correction
DEM	Digital Elevation Model
DK	disjunctive kriging
DMC	Difference-Mixed Correction
DS	data splitting
EM	electromagnetic
EOS	Earth Observing System
GP	global polynomial interpolation

IFOV	instantaneous field of view
IK	indicator kriging
IMF	inverse multiquadric function
IMS	Interactive Multisensor Snow and Ice Mapping System
IMS SCE	IMS Daily Northern Hemisphere Snow and Ice Analysis at 4 km Resolution
LP	local polynomial interpolation
LR	linear regressions
LST	Local Standard Time
MAE	mean absolute error
MF	multiquadric function
MODIS	Moderate Resolution Imaging Spectroradiometer
NMC	Normalization-Mixed Correction
NSIDC	National Snow and Ice Daata Center
OK	ordinary kriging
PK	probability kriging
QSCAT	QuikSCAT
RBF	racial basis functions
RC	Ratio Correction
RK	residual kriging
RMC	Ratio-Mixed Correction
RMSE	root mean square error
RT	regression tree

SAR	synthetic aperture radar
SCF	snow cover fraction
SD	snow depth
SK	simple kriging
SMMR	Scanning Multi-channel Microwave Radiometer
SSM/I	Special Sensor Microwave / Imager
SWE	snow water equivalent
SWT	spline with tension
T_B	brightness temperature
TIROS-1	Television Infrared Observation Satellite
TPS	thin plate spline
UK	universal kriging
WMO	World Meteorological Organization
WMPSR	Wilcoxon Matched-Pairs Signed-Ranks

CHAPTER 1

INTRODUCTION

Among various surface cover features, snow is very unique and maybe one of the most variable on the planet. Notably, snow can cover a large area over the Northern Hemisphere, varying from 3.8 x 10^6 km^2 to 6.5 x10^6 km^2 (Engen et al. 2004, Green et al. 2012). Snow plays an important role in natural systems and our human society. For example, snow is one of the crucial water resource providers (i.e. snow provides 70% of the fresh water supply in the western United States) (Chang et al. 2005). Secondly, snow is an important contributor to the global hydrologic cycle, particularly in river basins over areas with high elevation and latitude attributes (Konstantinos et al. 2009). Thirdly, the lack or abundance of snow can have significant impacts on agriculture, water resources, ecosystems, infrastructure, travel safety, and winter tourism and recreation (Burakowski et al. 2008, Kunkel et al. 2009, Peng et al. 2010). Therefore, a more accurate estimation of snow can be an advantage in many aspects.

Currently, snow depth (SD), snow water equivalent (SWE), and snow cover extent (SCE) are three major metrics that have been extensively used to study the large-scale distribution of snow. By definition, SCE refers to the total land area covered by snow, SD is the total depth including both old and new snow above the ground, and SWE is the water content obtained from melting snow (GCOS 2009). Typically, SCE, SD and SWE are reported in square kilometers (km^2), centimeters (cm), and millimeters (mm), respectively (GCOS 2009). As shown in previous studies, these metrics are important for initializing meteorological and hydrological

models, particularly during spring snowmelt (Hyvarinen et al. 2009). Snow cover can have influence on both energy budgets by regulating solar radiation (Tedesco 2012) and temperature over land (Mote 2008). As a result, it can affect the large-scale climate through altering thermal circulation patterns (e.g., Ge and Gong 2009).

1.1 Motivation

Traditionally, surface meteorological stations, or in-situ measurements using rulers, fixed snow stakes, snow boards or automated monitors at surface meteorological stations are the main source for SCE and SD data. However, given the high spatial variability of snow distribution in many regions of the world, surface meteorological stations are too sparse to provide sufficient data to accurately reproduce and assimilate large-scale snow cover distributions.

To address the problem of sparse ground station networks, satellite remote sensing offers an alternative source of snow information (e.g., Romanov et al. 2000). Visible, infrared, and microwave ranges of the electromagnetic spectrum are widely used to measure SCE, SWE, and SD values. Although visible and near infrared can give reasonable of SCE under cloud-free conditions with relatively high resolution (e.g. 500 m, 1 km, and 4 km), both signals may be significantly obscured by clouds. In addition, visible sensor retrievals can also be affected by lack of illumination at high latitude or night. In comparison, passive microwave sensors can penetrate clouds and are unaffected by illumination and with wide scanning swath, repeat coverage can be provided. A consistent time series of passive microwave data exists since late 1978 (Takala 2011).

However, passive microwave sensors have some disadvantages. These include a relatively low resolution (25 km) and high uncertainty due to either systematic errors or random errors (i.e. Takala 2011). Moreover, many other factors can also affect microwave retrievals and

increase uncertainties in results such as snow density, snow grain distribution, snow wetness, and vegetation. Besides in situ observations and passive microwave remote sensing, airborne and spaceborne synthetic aperture radar (SAR) and airborne LIDAR are noted for being able to provide valuable SD, SWE and snow density values with a higher resolution; however, these approaches are relatively more expensive and are still in active development (Luzi et al. 2009, Larson et al. 2009).

Considering all of the snow measurement approaches mentioned, different methods have their own advantages and disadvantages. Snow scientists are trying to advance snow detection over large areas by improving stand-alone satellite estimates, developing advanced interpolation methods, building snow models, and incorporating multiple data sources. In order to improve snow and snowmelt detection, an increasing number of researchers focus on incorporating different existing snow products, especially satellite products, instead of developing more complex interpolation techniques, or building advanced snow models with more physical characteristics. For example, Liang et al. (2008) combined products of Moderate Resolution Imaging Spectroradiometer (MODIS) snow cover with Advanced Microwave Scanning Radiometer-Earth Observing System (AMSR-E) SWE in order to develop a new daily snow cover product. As a result, the newly proposed product has increased the accuracy of snow cover detection from 33.7% to 75.4% compared to in situ measurements over northern Xinjiang, China. Foster et al. (2011) developed a global snow product, The Air Force Weather Agency (AFWA)-NASA (ANSA), by integrating AMSR-E, MODIS and QuikSCAT (QSCAT) snow products to yield improved snow products. The ANSA SCE product was evaluated over the lower Great Lakes region and Finland, and was found to have better results compared to either the MODIS or the AMSR-E products alone. While some studies have incorporated satellite

products and ground observations in SCE and SWE retrievals and other climatic fields, such as precipitation (e.g. Rozante et al. 2010), this has not been done extensively in SD retrievals.

Cao et al. (2012) proposed five algorithms (Difference Correction, Ratio Correction, Difference-Mixed Correction, Ratio-Mixed Correction and Standardized Correction) in order to enhance MODIS cloud fraction detection by assimilating satellite estimates and ground observations over China. Their results showed that all of the proposed algorithms enhanced the accuracy of satellite cloud fraction retrievals. Like cloud cover, snow cover is also an ephemeral discontinuity property of the climate. Therefore, the Cao et al. (2012) methods may also be applicable to snow cover.

1.2 Research objectives

The objectives in this research are three fold: (1) to compare the AMSR-E SD retrievals to COOP SD observations to determine when and where they are significantly different; (2) to evaluate the error of 10 classic interpolation techniques on the COOP SD in order to select the optimum interpolation method; (3) to use five interpolation methods from Cao (2012) and produce a best synthesis combining satellite SD, SCE and COOP SD observations and then compare to stand-alone SD products.

A review of literature on microwave satellite remote sensing and its application for snow depth, as well as interpolation techniques, are discussed in Chapter 2. Chapter 3 discusses five datasets that are used in this research: AMSR-E SWE and Interactive Multisensor Snow and Ice Mapping System (IMS) SCE products from National Snow and Ice Data Center (NSIDC), National Weather Service (NWS) COOP SD and CoCoRaHS ground observations. AMSR-E SD values retrieved from AMSR-E SWE and COOP SD measurements are used to conduct a comparison with the aim of assessing the accuracy of satellite SD estimates. An interpolation

optimization process is generated subsequently for 10 interpolation techniques based on COOP SD measurements, using ancillary DEM data and IMS SCE data. An optimal synthesis is proposed by incorporating AMSR-E SD, IMS SCE and COOP in situ data. CoCoRaHS SD is used to evaluate the synthesis performances. This methodology is described in detail in Chapter 3. Chapter 4 includes findings and discussion organized by the research objectives. Conclusions and possible future areas of research are included in Chapter 5.

CHAPTER 2

LITERATURE REVIEW

2.1 In situ snow observation networks and their application to snow depth

In situ SD observations have been used to study snow trends over regions at various scales (e.g., Dyer and Mote 2006), interpolation of different snow characteristics (e.g., López and Bravo 2006, Harshburger et al. 2010), and the evaluation of satellite snow algorithms (e.g., Tekeli 2008). There are numerous networks observing snow characteristics (e.g., SWE, SD and snowfall). Among the most common in situ measurements in the United States are observations taken at National Weather Service offices, at snow-telemetry sites (SNOTEL), at Cooperative Observer Program stations (COOP), at automated surface observing systems sites (ASOS) and by Community Collaborative Rain, Hail and Snow (CoCoRaHS) observers. Fiebrich (2009) provides a thorough review of surface weather observations in the United States.

Many studies in the U.S. using in situ data have relied on the COOP data either in original form or as part of screened and quality controlled data sets, such as the U.S. Historical Climatology Network (USHCN, Easterling et al. 1996). For example, Dyer and Mote (2006) used COOP surface observations to study the SD trends and spatial variability over North America. Fuhrmann et al. (2010) used observations of snowfall and SD from stations within the COOP network to study the snow cover spatial pattern in North Carolina, and Burakowski et al (2008) examined changes in northeastern U.S. snow depth. In the western U.S., many studies have focused on the SNOTE network. For example, Moser et al. (2011) used SNOTEL SWE measurements to conduct a comparison with AMSR-E SWE in the watersheds over western U.S.

In a few cases, both COOP and SNOTEL networks have been used in concert. Both SNOTEL SWE observations and COOP SD observations were used to validate estimates from satellite, model and assimilation in northern Colorado (De Lannoy et al. 2012).

Many studies regarding snow cover have focused on decreasing snow extent and depth, particularly during the spring, during the past 50 years (IPCC 2007, Grundstein and Mote 2010). For example, decreases of over 50% and 15-30% of SD and SWE on April 1st were noted at sites in the Cascade Mountains and Rocky Mountains respectively (Mote et al. 2005, Grundstein and Mote 2010). However, some other areas were found to have increasing SD and SWE such as the southern Sierra Nevada Mountains and southwestern U.S. (Mote et al. 2005, Grundstein and Mote 2010). According to Kunkel et al. (2009), since 1930, a sharp decrease trend in snowfall has been detected in the far West, and an increase is apparent in the Great Lakes-northern Ohio Valley, the upslope regions in the lee of the Rocky Mountains, and parts of the north-central U.S. A slight downward trend is also found in New England. Dyer and Mote (2006) cited a decreasing trend in snow depth coinciding with the beginning of the melt season in the northern U.S.

2.2 Passive microwave remote sensing and its application to snow depth

The history of snow detection by satellites started in 1960 when the Television Infrared Observation Satellite (TIROS-1) provided the first source of remotely sensed information on SCE (Zhu 2009). Since then, higher spatial resolution instruments such as the Advanced Very High Resolution Radiometer (AVHRR) and Landsat have improved snow detection (Lucas and Harrison 1990). The skill of estimating snow cover has become even more mature in the Earth Observing System (EOS) era with instruments such as MODIS (Hall et al. 2001).

Passive microwave radiometry not only provides information on SCE but also SWE and SD**.** Different from visible and infrared radiometers, the longer wavelength microwave

radiometers can penetrate clouds and continuously monitor the earth surface (Lucas and Harrison 1990). The scattering of microwave radiation by snow crystals was first reported by England (1975), Chang et al. (1976), among others. The scattering effect reduces the upwelling radiation, particularly at longer wavelengths, as a function of the number and size distribution of snow grain This offers the physical basis of microwave detection of snow (Singh et al. 2000). When the depth and water equivalent of snow pack increases, snow microwave emission decreases at frequencies above 15 GHz (Hallikainen 1984). This is due to the preferential scattering of microwave radiation by snow grows at higher frequencies.

A number of microwave algorithms and techniques have been developed to estimate SD and SWE in the past three decades. SD can be retrieved from space-borne data through linear regression against the microwave brightness temperature (T_B) difference between 19 and 37 GHz (or similar frequencies). Other methods use physical and/or electromagnetic (EM) snow models to estimate SD. An in-depth review of microwave snow algorithms was provided by Tedesco et al. (2010). SWE estimates are higher when the difference between the T_B measurements at the two frequencies is larger (Takala et al. 2011).

Chang et al. (1987) first suggested a linear relationship between the snow depth and the T_B difference at 37 and 18 GHz (i.e., the frequency gradient), horizontal polarization. Goodison et al. (1986) and Hallikainen (1989) developed SWE algorithms using vertical polarization channels. The algorithm was used with global observations of Scanning Multi-channel Microwave Radiometer (SMMR) and Special Sensor Microwave Imager (SSM/I) (Foster et al. 1997). Singh and Gan (2000) developed multivariate regression algorithms for retrieving SWE. Pulliainen (2006) proposed a Bayesian approach weighing the satellite data and the corresponding interpolated snow depth field. An artificial neural network (ANN) model

including physiographic and atmospheric data was developed by Gan et al. (2009). Foppa et al. (2007) improved the snow depth mapping in the Swiss Alps by merging interpolated ground observations with AVHRR SCE data. Harshburger et al. (2010) estimated SWE using a simple methodology incorporating SNOTEL surface observations and MODIS SCA estimates. Tedesco et al. (2010) introduced retrieval approaches that dynamically combine ancillary SD information (e.g., from snow physical models driven with surface meteorological data) with established algorithms based on EM modeling. Liu et al. (2013) suggest that snow prediction can be improved by assimilating several satellite-based snow products into the Noah land surface model including MODIS snow cover fraction (SCF) and SD from AMSR-E over Alaska.

Though estimates of snow depth from microwave radiometry have already been widely used, the accuracy can be affected by vegetation, topography, snow wetness (i.e., liquid water content), snow grain size, and snow density. Landscape features affect accuracy in various ways. Matzler (1994) elaborated that topography affects the accuracy in two ways. One effect is due to the distance between the radiometer and the surface. With greater distance, the spatial resolution will be coarser and a thinner layer of atmosphere will be situated between the sensor and target. Another effect is due to the complex terrain itself because the emitted radiation will propagate in different directions from unsmooth surfaces. Chang et al. (1991) cite that vegetation is a significant factor affecting the accuracy of snow depth. Vegetation can attenuate the microwave radiation from the underlying snow cover. Meanwhile, the radiation from the canopy increases the microwave radiation received by the satellite, even at high frequencies, reducing the T_B difference between low and high frequencies (i.e., the frequency gradient). Wet snow reduces volume scattering, increases the emissivity of the snow, and reduces the frequency gradient

(Hallikainen et al. 1987). Liu et al. (2013) found that the sensors have difficulty detecting thin snow layers and may overestimate snow in dry and cold regions.

2.3 Interpolation methods

Interpolation is a method which uses a limited number of sample data points to estimates unknown values for any location. It has historically been applied to various scientific fields such as ecology, health, forestry, meteorology and climatology. Interpolation technique plays an important role in this research as it is part of the synthesis.

Based on researchers' knowledge and research need, interpolation methods can be classified into different categories. For example, Sluiter (2009) compared different interpolation methods for climate data and grouped the methods into three categories: deterministic methods, probabilistic methods, and other methods. Lopez (2006) classified the interpolation techniques into local methods, geostatistical methods, and global methods. Deterministic and geostatistical techniques are two interpolation categories of interest for the current study discussed below.

Before deciding which interpolation to use, there are several assumptions to be considered especially for geostatistical techniques. The assumptions are stationarity, intrinsic hypothesis, stochastic and normal distribution. According to Tveito et al. (2006), stationarity implies there should be a certain probability distribution function (mean, covariance and standard deviation) in every place with no relation to the location. Intrinsic hypothesis states that the difference between two sample points only depends on a distribution of the distance not the location. Unlike deterministic interpolation, geostatistical techniques are stochastic which implies that the results of all sample values are random processes in the study area. None of the samples are independent. A normal distribution is another assumption for some geostatistic interpolation techniques, which implies that a large number of samples follow a normal

distribution. If the data is not normally distributed, then a transformation is suggested (Chi et al. 2011).

Deterministic methods generate a continuous surface by only using the geometric characteristics of measured point observations (Sluiter 2009). They can be divided into global and local techniques. Global techniques (e.g., global polynomial interpolation) predict unknown values using the entire dataset. Local techniques (e.g., spline) predict unknown values using the measured points within neighborhoods, which are smaller spatial areas within the larger study area (Wu et al. 2009). They can also be classified into exact and approximate interpolations. Exact interpolations produce the same value as the measured value on sampled points. Different from exact interpolation, approximate interpolations produce different values, assuming uncertainty in these values will reduce errors by smoothing. By using exact interpolations, the output surface can avoid obvious peaks and troughs (Wu et al. 2009). Inverse distance weighted (IDW) is one of the most popular deterministic methods. It uses the measured values surrounding the prediction location to predict a value for any unmeasured location. The measured values closest to the prediction location have more influence on the predicted value than those farther away by assigning different weights. The weight of each observation is determined by distance (Chi, et al. 2011). IDW is an exact interpolator, which means there is no larger or smaller value than the maximum and minimum value of the sample data. According to Sluiter (2009), IDW is quick, simple to implement and easily tailored for specific applications. However, the output surface is sensitive to clustering and the presence of outliers, which produce "bull's eye patterns." In addition, it does not incorporate ancillary data or trends (Wu et al. 2009). Linear regressions (LR) give predictions based on the relationship between the predicted and response variables. They are most often global interpolators (Wu et al. 2009). The technique has been

widely used in combination with other interpolation methods such as IDW. Radial basis functions (RBF) are a series of exact interpolation techniques. The surface must pass through each measured sample value (Wu et al. 2009). The basic functions include spline functions and multiquadric function. RBFs are similar to fitting a rubber membrane through the measured sample values at the same time minimizing the total curvature of the surface (Wu et al. 2009). Different from IDW, RBF can produce values larger than the maximum and below the minimum measured values (Wu et al. 2009). By x-order polynomials, polynomial functions (PF) are techniques that fit trend functions through the sampled data. In general they are global interpolators and fulfill the criteria of exact interpolators by fitting any polynomials in regions with overlapping neighborhoods (Sluiter 2009). PFs are ideal for interpolating monthly and yearly climate elements and are not suggested for higher temporal resolutions like days and hours (Sluiter 2009).

Geostatistical interpolation techniques create surfaces based on the statistical properties of the sampled points (Wu et al. 2009). Geostatistical techniques quantify the spatial autocorrelation by means of either covariance or semi-variances between measured points and account for the spatial configuration of the sample points around the prediction location (Lopez 2006). The variogram is the central tool of geostatistics and describes the randomness and structural characteristics of regional variation. Assuming that two regional variations *Z(xi)* and *Z(xi+h)* are the measured value of *Z(x)* at the spatial location of *xi* and *xi+h (I = 1, 2, ...N(h))*, the variogram can be estimated by the following equation:

$$r(h) = \frac{1}{2N(h)} \sum_{i=1}^{N(h)} [Z(xi) - Z(xi + h)]^2 \qquad \textbf{(2.1)}$$

where,

N(h) is the sample size when the distance between two points is *h*.

The variogram is defined under the assumption that *Z(x)* is regional variation and meets the stationary condition and intrinsic hypothesis. It can be proved mathematically that spatial correlation decreases when the variogram increases, and vice versa. The variogram of two-dimensional regional variations is not only based on distance *h*, but also direction. Assuming that *r(h, θ1)* represent a variogram of one direction, *r(h, θ2)* represents a variogram of another direction, the ratio of two values is:

$$k(h) = r(h,\theta 1)/r(h,\theta 2) \quad \textbf{(2.2)}$$

If the result equals to 1 or close to 1, it indicates isotropy. Otherwise, the result implies anisotropy. The lower the ratio value, the higher the anisotropy and larger degree of spatial variation will be (Wu et al. 2009).

There are many geostatistical techniques, which can be applied for different research needs. Ordinary kriging (OK) generates prediction based on a linear combination of the measured values, and OK assumes intrinsic stationarity and an unknown mean (Sluiter 2009). The weighting factors are determined by a variogram, which summarizes the spatial structural of semi-variances (Lopez et al. 2006). OK is frequently applied in meteorology, often as part of residual kriging (RK) or indicator kriging (IK). Simple kriging (SK) is OK with a known mean. Therefore, it is slightly more powerful than OK, however, the mean is often difficult to derive. Universal kriging (UK) is also known as "kriging with a trend/external drift." As part of the kriging process, UK uses regression to model the mean value expressed as a linear or quadratic trend. Kriging with an external drift is a very common method in meteorology. It assumes

intrinsic stationarity and that the number of "drift" variables should be much higher that the variable of interest (Sluiter 2009). Cokriging (CO) can incorporate multiple variables. The calculation of the weights is based on cross-variograms (Lopez et al. 2006). According to Chi et al. (2009), the autocorrelation of the major variable (i.e., SD) and the cross-variograms between the major variable and other variables can help predict better results. However, more uncertain factors will be introduced when incorporating multiple variables. Disjunctive kriging (DK) is a non-linear procedure in which the dataset is transformed using a series of additive functions. DK assumes that all data pairs originate from a bivariate normal distribution (Wu et al. 2009). IK uses thresholds to create binary data (0/1) and then uses OK for interpolation. The results indicate the probability that a certain threshold is exceeded. IK can be seen as special version of DK (Sluiter 2009). According to Tveito et al. (2006), the method is not suitable for data with a trend. Probability kriging (PK) is a non-linear method using indicator variables. The method can be seen as a form of CO where the first variable is the indicator and the second variable is the original untransformed data (Tveito et al., 2006). PK is more powerful than IK but it requires more calculations because cross variances have to be fitted. Similar to IK, the method is not suitable for data with trends. More uncertain factors will be introduced when predicting unknown autocorrelation functions (Chi et al. 2009)

The performance of different interpolation techniques can be evaluated by cross validation (CV) and data splitting (DS). By generating CV, the interpolation procedure will be executed many times in a bootstrap approach. One observation will be omitted and the interpolation will be calculated based on neighboring observations each time. The procedure will not stop until the difference between the calculated and observed value of all the points has been estimated (Sluiter 2009). DS is the process of splitting the dataset into two parts: one part for

estimation and another part for validation. This method is applicable if there is a large quantity of observations and they are regularly sampled (Sluiter 2009).

Interpolation techniques in meteorology and climatology fields have been in use for several decades. Erxleben et al. (2002) compared IDW, OK, modified RK and CO, and a combined method (binary regression trees and geostatistical methods) for estimating snow distribution in the Colorado Rocky Mountains and found that tree-based models provide the most accurate estimates. In a few instances, interpolation methods have been applied to SD. Molotch et al. (2005) presented a comparison of regression tree models and different residual interpolation techniques to study the impact of digital elevation data and independent variable selection on estimating the spatial distribution of SWE, and the result showed CO with maximum upwind slope and elevation performed the best. Chang et al. (2005) used optimum interpolation to study the variations between ground-measured and passive microwave-derived snow depth (SD) across the Northern Great Plains. Dyer and Mote (2006) used IDW to study the snow depth trend over North America. Zhu et al. (2009) used OK to interpolate station data in order to validate microwave snow depth data and compared to IDW and found that OK had a better performance.

Interpolation methods have been studied over the past few decades and significant improvements have been achieved. However, the optimum interpolation method varies by study and region. Many factors can influence interpolation performance, such as spatial autocorrelation and station density. “Moran’s eye” is widely identified to be a statistical index to determine the significance of the spatial autocorrelation of the data source. Nevertheless, there is no widely used statistical index providing helpful suggestions on which interpolation methods work better on certain ground observation density. Additionally, few studies have compared different

interpolation techniques on SD in a large spatial scale. Furthermore, for most of interpolation optimum studies, either CV or DS is used for interpolation evaluation, however, little paper used both CV and DS.

2.4 Summary

The history of snow detection by satellite sensors can be traced back to the 1960s. The first SD algorithm based on brightness temperature values was proposed by Chang et al. (1976). Since then, many stand-alone satellite algorithms, advanced interpolation methods and snow models combining satellite retrievals with other data sets have been developed. However, many of them have high computational requirements for modeling, and some of them are limited to certain regions where ground stations are dense. Recently, a number of studies have assimilated existing data by adopting a simple modeling procedure (i.e., ANSA). Many of the studies combine satellite products to increase the satellite SD detection. In this research, I propose a simple interpolation based synthesis aimed at improving satellite SD retrievals by combining AMSR-E SWE, IMS SCE products with COOP ground observations. The synthesis follows the algorithms proposed by Cao et al. (2012).

CHAPTER 3

DATA AND METHODOLOGY

3.1 Study area and data

The study area for this research is the contiguous U.S. As one of the crucial components of water supply, runoff, and recharge, snow significantly affects water management in the western and northern U.S. Rapid snow melt was identified as a major cause of floods in the northern U.S. (Kunkel et al. 2009). During the winter season (December-March), snow affects most northern areas, especially the Great Plains New England, Great Lakes, Rocky Mountains, and the mountainous areas of Washington, Oregon and California.

3.1.1 AMSR-E

To carry out the objectives of this research, five datasets are used. AMSR-E/Aqua L3 Global SWE EASE-Grids product (AMSR-E SWE) and IMS Daily Northern Hemisphere Snow and Ice Analysis at 4 km Resolution (IMS SCE) are used as satellite data. The Cooperative Observer Program (COOP) data and Community Collaborative Rain, Hail and Snow Network (CoCoRaHS) are used as in situ data. Digital elevation model (DEM) data is used as ancillary data.

AMSR-E SWE product is a microwave product available on a daily time scale, covering the Northern Hemisphere on a 721 by 721 pixel grid in EASE-Grid projection beginning 19 June 2002 with a 25 km by 25 km resolution. Based on AMSR-E SWE algorithm theoretical basis document (Tedesco 2012) and AMSR-E SWE product documentation from NISDC, the algorithm is described as:

(1) A climatological snow cover map (Dewey and Heim 1981) and a land/ocean/ice mask (retrieved from MODIS MOD12Q1 1GBP land cover data) is first used to determine the possibility of snow. If snow is impossible, a flag is assigned to the pixel and go to the next pixel, otherwise, AMSR-E/Aqua L2A Global Swath Spatially-Resampled Brightness Temperature is applied;

(2) A melting snow detection procedure is conducted for areas where snow is possible. This procedure aims at distinguishing areas where SWE retrievals are impossible. Melting snow is defined when $T_{B36\,H} < 245$ K and $T_{B36\,V} < 245$ K, if the pixel is found to be dry snow, a step to identify shallow or deep snow is conducted;

(3) Medium to deep snow is noted when $T_{B10V} - T_{B36V} > 0$ K or $T_{B10H} - T_{B36H} > 0$ K, otherwise (i.e., $T_{B10V} - T_{B36V} <= 0$ K or $T_{B10H} - T_{B36H} <= 0$ K), shallow snow is identified when $T_{B89V} <= 255$ K, $T_{B89H} <= 265$ K, $T_{B23V} - T_{B89V} > 0$ K or $T_{B23H} - T_{B89H} > 0$ K and $T_{snow\_K} < 267$ K. A 5.00 cm is assigned when shallow snow is noted and a SD algorithm (Eqn. 3.1) combining retrievals for both forested and unforested fractions is applied if medium to deep snow is found;

$$SD = \left(ff \times (SDf)\right) + \left((1 - ff) \times (SDo)\right) \quad (\mathbf{3.1})$$

where:

SD_f = snow depth from the forested component of the instantaneous field of view (IFOV) and is calculated following Eqn. 3.2,

SDo= snow depth from the non-forested component of the IFOV and is calculated following Eqn. 3.3,

ff = forest fraction (1.00 = 100% forest fraction and 0.00 = 0% forest fraction), and

$$SDf[cm] = polfact36 \times (TB18V - TB36V)/(1 - fd \times 0.6) \quad \textbf{(3.2)}$$

where:

$polfact_{36}$ = $1/\log_{10}(pol_{36})$,

pol_{36} = T_{B36V} - T_{B36H} (if $pol_{36} < 1.1$, pol_{36} is set to 1.1 to make sure $\log(pol_{36}) > 0$),

fd = forest density (g cm^{-3}) from 500 m MODIS Vegetation Continuous Fields (VCF) data, and

$$SDo[cm] = [polfact36 \times (TB10V - TB36V)] + [polfact18 \times (TB10V - TB18V)] \quad \textbf{(3.3)}$$

where:

$polfact_{18}$ = $1/\log_{10}(pol_{18})$, and

pol_{18}=T_{B18V} - T_{B18H}.

(5) The SD values are calculated and projected to a 25 km EASE-Grid (Brodzik and Knowles 2002) cell;

(6) SWE is estimated for each cell using the SD and a static snow density data (Stum et al. 1995) following Eqn. 3.4.

$$\text{SWE} = \text{SD(cm)} \times \text{density(g cm} - 3) \times 10.0\text{(mm)} \quad \textbf{(3.4)}$$

For the purposes of this study, the SWE values were converted back into SD estimates by dividing a spatially varying but temporally static snow density data file (Figure 3.1). An example of AMSR-E SWE on 29 Jan. 2009 is shown in Figure 3.2 where water is blue, ground is orange, the darker green depicts lesser SWE, and the darker red depicts greater SWE. Additional

documentation can be found on the National Snow and Ice Data Center (NSIDC) website at http://nsidc.org/data/docs/daac/ae_swe_ease-grids.gd.html.

3.1.2 IMS

The IMS product is also available on a daily time scale, covering the Northern Hemisphere on a 6144 by 6144 pixel grid in a polar stereographic projection beginning 23 February 2004. According to Brubaker et al. (2005), this product involves an analysis with primary input from motion loops in the visible wavelength images from geostationary satellites and polar orbiting satellites and also heavily relies on passive microwave images. Figure 3.3 shows an IMS SCE example on 29 February 2004. Additional documentation can be found on the NSIDC website at http://nsidc.org/data/docs/noaa/g02156_ims_snow_ice_analysis/. Both AMSR-E SWE and IMS products over December 2007–March 2008, and December 2008–March 2009 were retrieved from NSIDC.

3.1.3 COOP

The COOP network was founded in 1890, now it has over 11,000 volunteers who make observations at various places such as farms, national parks, cities and suburban areas. The meteorological data contain SD, snowfall, 24-hour precipitation totals and daily maximum and minimum temperatures (Cooperative Observer Program 2013). The COOP data proposed for use in this thesis have been modified following the TD3200 format and have been quality controlled (Dyer and Mote 2006) using a procedure recommended by Robinson (1989).

3.1.4 CoCoRaHS

CoCoRaHS is a non-profit, community-based network to obtain rain, hail and snow measurement and mapping. The network consists of volunteers from all backgrounds and ages. The aim of CoCoRaHS is to offer the best quality data for education, research applications and

natural resources at low cost. It features an interactive web-site and provides training and education in all 50 states (CoCoRaHS 2013). An example of COOP (blue) and CoCoRaHS (red) station distribution on 29 January 2009 is shown in Figure 3.4.

3.1.5 Ancillary data

The elevation data used in this research is a 30 by 30 meter DEM dataset used for CO interpolation. It can be acquired from the National Map Seamless Server (http://seamless.usgs.gov). The National Map Seamless Server enables a user to view and download many geospatial data layers, such as the National Elevation Dataset, National Land Cover Dataset, High Resolution Orthoimagery, and many others. Figure 3.5 provides an overview of the DEM data. The brighter tone depicts higher elevation and the darker depicts lower elevation.

3.2 Methodology

Some data preprocessing steps were conducted after acquiring the AMSR-E SD from AMSR-E SWE, snow density and IMS data from NSIDC, DEM from USGS and the raw CoCoRaHS data. The major procedures conducted for CoCoRaHS data were as follows: (1) records with SD measurements were filtered; (2) records with "T" as a SD measurement were changed to "0.01" (normally "T" is set to "0.00", however, because "T" is lower than the smallest unit (i.e. the nearest tenth of an inch) and larger than zero, "T" is set to a small positive number, "0.01"); (3) records without latitude and longitude information were removed. AMSR-E SD data were calculated by multiplying AMSR-E SWE with snow density following Eqn. 3.2, as suggested in the AMSR-E SWE documentation. DEM data were merged into one shapefile over study area.

3.2.1 Comparison of in situ and passive microwave snow depth

Next, a spatial and temporal comparison between SD from satellite and ground based observations in the 2007/2008 and 2008/2009 winter seasons were generated to determine whether satellite estimates are significantly different from ground observations and how they differed. A time series study and spatial comparison were conducted to achieve the goal. For the time series analysis, the procedure was as follows: (1) daily COOP records were filtered based on satellite coverage, and only stations within satellite coverage were kept for further analysis; (2) daily COOP SD spatial mean were calculated based on filtered data; (3) AMSR-E SD estimates were extracted for locations corresponding to the filtered COOP stations locations, and daily averaged SD per location was treated as daily AMSR-E mean; (4) COOP daily means were compared to AMSR-E daily means over time. The time series study was based on daily COOP SD observations and daily mean AMSR-E estimates.

A statistical hypothesis test, the Wilcoxon Matched-Pairs Signed-Ranks (WMPSR) test (Eqn. 3.5) was used to determine whether or not there are significant differences between the ground and AMSR-E SD. The WMPSR test is defined as follow:

$$Zw = \frac{T - \frac{n(n+1)}{4}}{\sqrt{\frac{n(n+1)(2n+1)}{4}}} \qquad (3.5)$$

where:

n = number of matched pairs (n>10), and

T = rank sum.

Ranks are based on matched-pair absolute differences (lowest rank corresponding to smallest absolute difference, and highest rank corresponding to largest absolute difference).

When the same absolute difference values occur, the mean rank values are set to each pair. However, if the absolute difference between two data sources is zero, the data would be ignored and the number of matched pairs would be reduced accordingly. The null hypothesis states that the matched-pairs absolute difference (in ranks) for the population equals to zero (McGrew and Monroe 2000). This indicates that there is no significant difference between the two data sets. As opposed to the paired t-test, a normally distributed population is not required by the WMPSR test.

SD can change quickly after a storm passage. Also, missing data locations vary day-to-day, therefore, the SD was studied on a daily time-scale for spatial analysis. The dates for further analysis were chosen based on: (1) five nonconsecutive days with maximum COOP daily SD and three nonconsecutive days with minimum COOP daily SD with at least an average number of reporting stations, (2) the selected COOP SD values were interpolated by using IDW, and (3) the interpolated in-situ SD were compared with AMSR-E SD estimates spatially.

3.2.2 Analysis of interpolation performance

An optimum interpolation method for the COOP data was identified from a suite of interpolation techniques. These include eight deterministic methods (IDW, global polynomial interpolation (GP), local polynomial interpolation (LP), thin-plate spline (TPS), spline with tension (SWT), completely regularized spline (CRS), multiquadric function (MF) and inverse multiquadric function (IMF)) and two geostatistical techniques (ordinary kriging (OK) and ordinary cokriging (CO) with DEM). Cross validation (CV) and data splitting (DS) were used to evaluate the interpolation results. Root mean square error (RMSE, Eqn. 3.6) was adopted as the statistical metric:

$$RMSE = \sqrt{\frac{1}{n}\sum_{k=1}^{n}(y(i)pred - y(i)true)2} \quad (3.6)$$

where:

n=number of total station in use,

y(i)pred=predicted value, and

y(i)true=observation measurements.

The validation procedures were: (1) extracted COOP stations within IMS SCE (i.e., evaluation were based on interpolated values within snow boundary) and interpolated using the individual methods discussed above; (2) evaluate using cross validation; (3) separated each daily COOP data (i.e., data splitting) with 20% of the data for performance evaluation and 80% of the data for generating interpolation methods; (4) extracted evaluation stations within SCE and calculate RMSE; (5) assigned weights to two evaluation results in order to assess which interpolation methods are better suited to sparse or dense station networks.

Several parameters in ArcGIS were chosen based on data characteristics prior to generating interpolations. Fifteen and 10 were selected as values for maximum neighborhood and minimum neighborhood parameters, respectively. Sector 1 (i.e., one sector) was chosen as the sector type, and 0.2 was used as the output cell size. Other parameters, such as power, were optimized based on cross validation results. Lag size and lag number are default values calculated by ArcGIS. Data preprocessing was performed using MATLAB, while interpolations and interpolation evaluations were performed using ArcGIS.

3.2.3 Synthesis modeling and evaluation

Five interpolation based techniques incorporating ground observations with satellite estimates aimed at improving satellite SD retrievals were generated based on Cao et al. (2012). AMSR-E SD estimates and COOP observations were first combined using the equations listed

below with ArcGIS model builder. The exported scripts were modified for batch data processing. IMS SCE was utilized after retrieving the post correction SD values, the SD retrievals within the SCE were left, and the SD estimates outside the boundary were all set to 0 cm. While conducting ratio correction (RC), ratio-mixed correction (RMC) and normalization-mixed correction (NMC), both in-situ data and microwave retrievals with 0 values were reset to 0.01 in order to get meaningful results.

Difference correction:

$$SD = SD_S - \Delta_{SD}^{i} \quad (3.7)$$

$$\Delta_{SD}^{i} = interpolate\left(SD_S^P - SD_g\right) \quad (3.8)$$

where:

SD = corrected snow depth satellite data;

SD_S = AMSR-E snow depth satellite data;

SD_S^P = satellite data corresponding to the station locations;

SD_g = observation data;

interpolate() = interpolation function (using the best method resulting from step 2);

Δ_{SD}^{i} = the interpolated difference of satellite data corresponding to the observation locations and data;

Ratio correction:

$$SD = \frac{SD_S}{R_{SD}^{i}} \quad (3.9)$$

$$R_{SD}^{i} = interpolate\left(\frac{SD_S^P}{SD_g}\right) \quad (3.10)$$

where:

R_{SD}^{i} = the interpolated ratio of satellite data corresponding to the observation locations and observation data;

Difference-mixed correction:

$$SD_D = SD_S - interpolate\left(SD_S^P - SD_g\right) * SD_S \quad \textbf{(3.11)}$$

$$SD_g = a_D + b_D * SD_D^P \quad \textbf{(3.12)}$$

$$SD = a_D + b_D * SD_D \quad \textbf{(3.13)}$$

where:

SD_D = the satellite snowdepth data after difference-mixed correction;

SD_D^P = the difference-mixed corrected satellite data corresponding to the observation locations;

Ratio-mixed correction:

$$SD_R = SD_S - interpolate\left(\frac{SD_S^P - SD_g}{SD_g}\right) * SD_S \quad \textbf{(3.14)}$$

$$SD_g = a_R + b_R * SD_R^P \quad \textbf{(3.15)}$$

$$SD = a_R + b_R * SD_R \quad \textbf{(3.16)}$$

where:

SD_R = the satellite snowdepth data after ratio-mixed correction;

SD_R^P = the ratio-mixed corrected satellite data corresponding to the observation locations;

Normalization-mixed correction:

$$SD_N = SD_S - 2 * interpolate\left(\frac{SD_S^P - SD_g}{SD_S^P + SD_g}\right) * SD_S \quad (\mathbf{3.17})$$

$$SD_g = a_N + b_N * SD_N^P \quad (\mathbf{3.18})$$

$$SD = a_N + b_N * SD_N \quad (\mathbf{3.19})$$

where:

SD_N = the satellite snow depth data after normalization-mixed correction;

SD_N^P = the normalization-mixed corrected satellite data corresponding to the observation locations;

a_D,b_D; a_R,b_R; a_N,b_N represent revised empirical coefficients of difference-mixed correction, ratio-mixed correction and normalization-mixed correction individually (Cao et al. 2012).

A synthesis optimization was conducted statistically and spatially. Specifically, (1) mean absolute error (MAE), correlation coefficient (r), and RMSE were calculated based on CoCoRaHS SD observations and the corresponding synthesis outputs; (2) a spatial analysis of all synthesis results on 29 January 2009 was created. For both evaluation procedures, the optimum synthesis results were compared to stand-alone satellite estimates and stand-alone interpolated COOP SD. A flow chart of the entire procedure is shown in Figure 3.6.

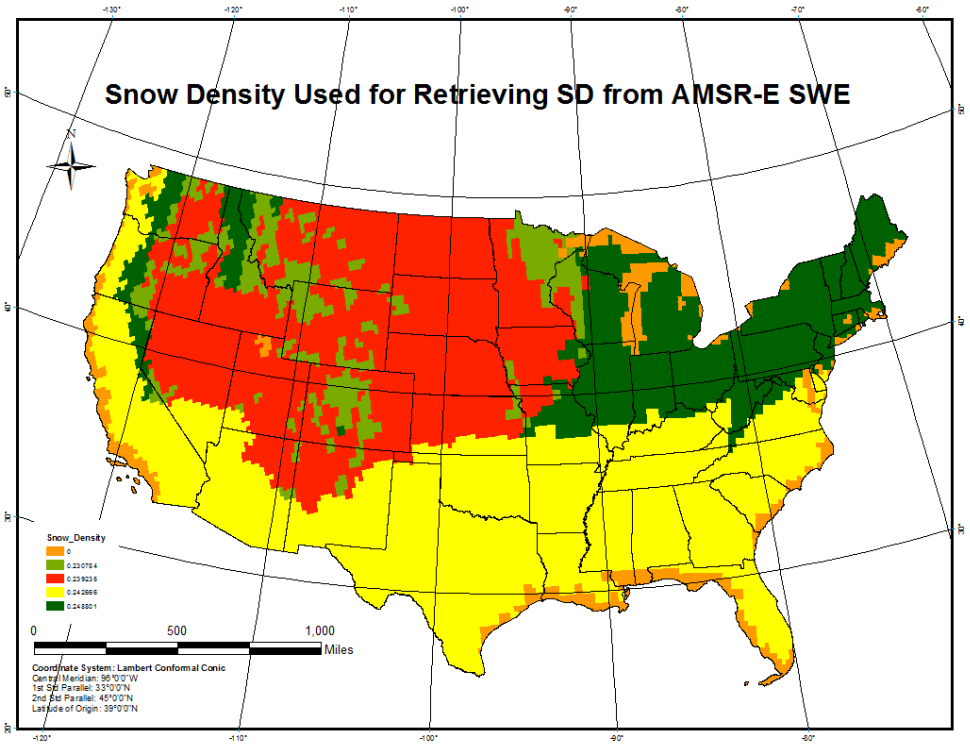

Figure 3.1: Snow density used for retrieving SD from AMSR-E SWE.

Figure 3.2: AMSR-E SWE on 29 Jan. 2009.

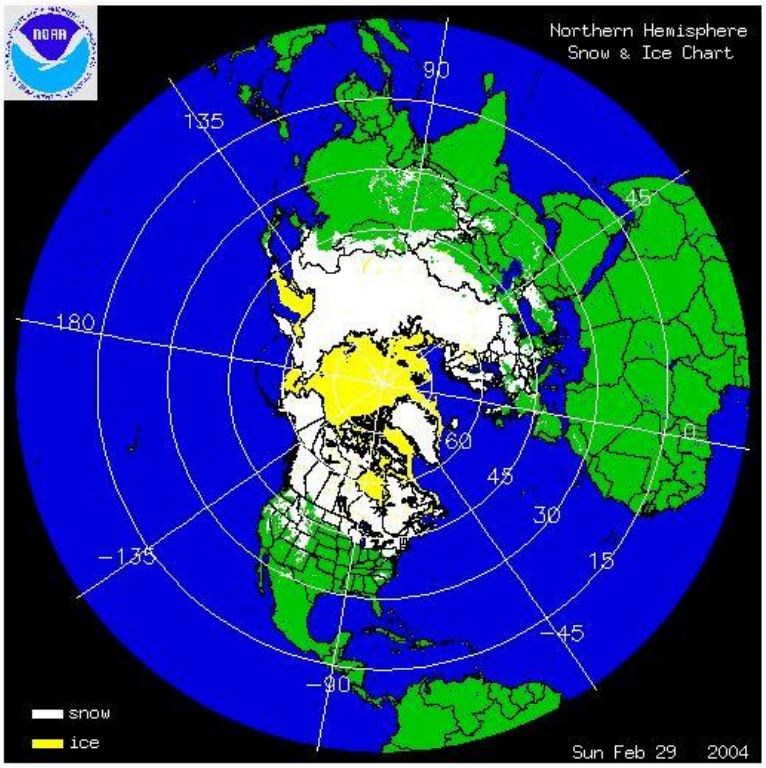

Figure 3.3: IMS SCE example from official website for 29 Feb. 2009.

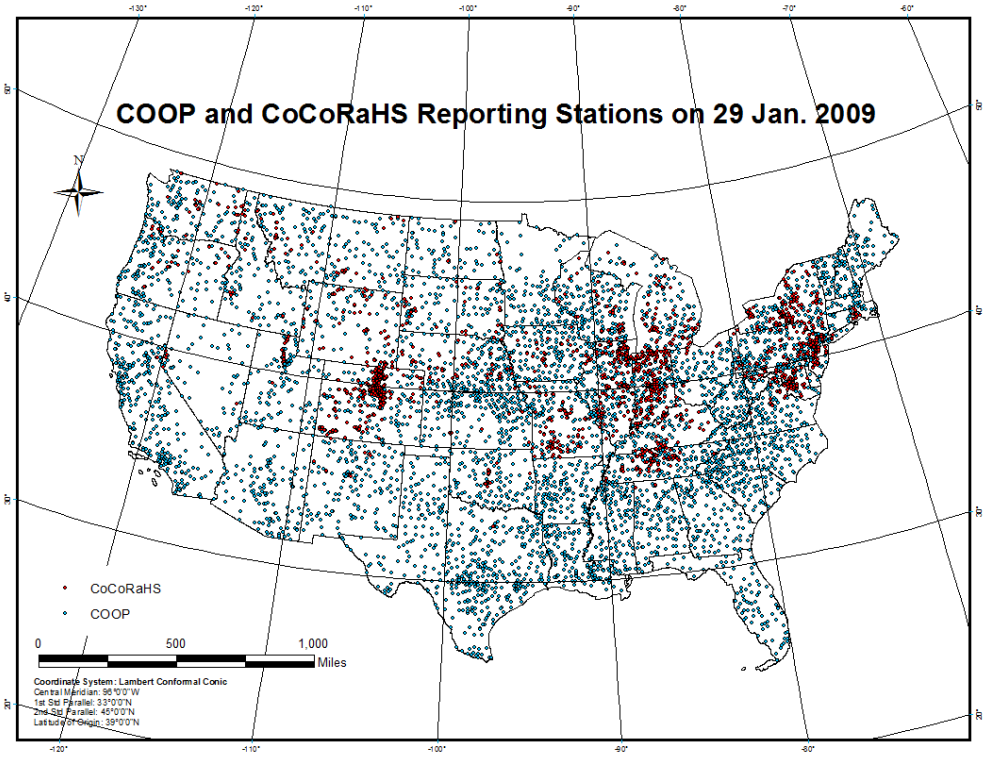

Figure 3.4: COOP and CoCoRaHS station distribution on 29 Jan. 2009.

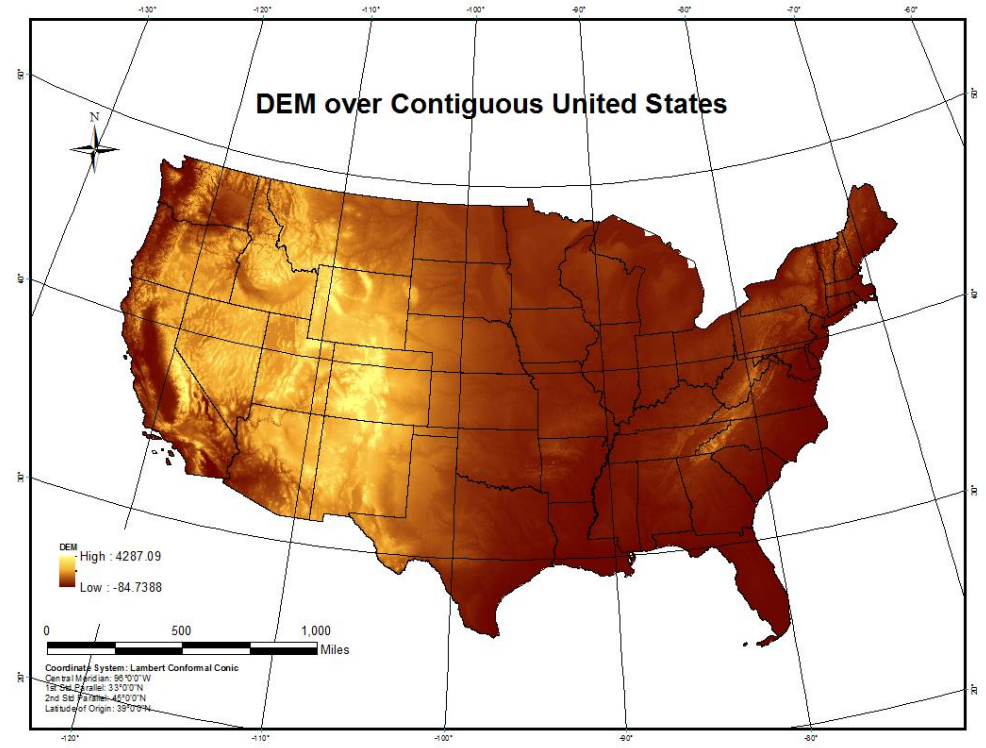

Figure 3.5: DEM over the contiguous U.S.

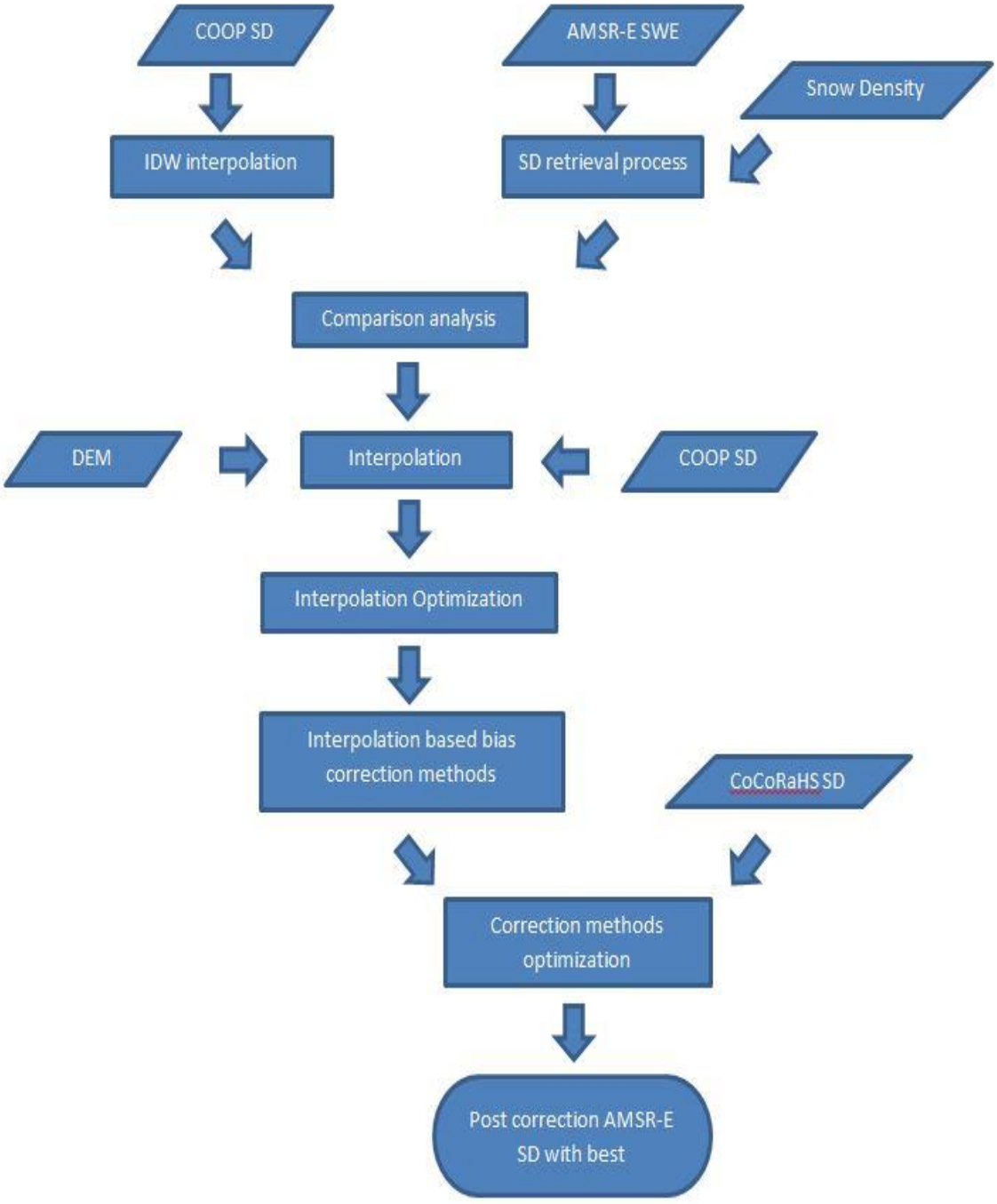

Figure 3.6: Flow chart of methodology.

CHAPTER 4

RESULTS AND DISCUSSION

4.1 Comparison of in situ and passive microwave snow depth

The first objective of this research was to compare satellite SD estimates with in situ SD measurements in the 2007/2008 and 2008/2009 winter (December–March) seasons. The methods used to address this objective were: (1) a time series study based on daily in situ SD means and the corresponding AMSR-E SD means; (2) a statistical hypothesis test, the Wilcoxon Matched-Pairs Signed-Ranks (WMPSR) test, was used to determine whether there are significant differences between the two datasets; (3) a spatial comparison was generated for eight nonconsecutive days to determine spatial differences between the two data sets.

4.1.1 Results of comparison of in situ and passive microwave snow depth

Figure 4.1 showed the time series of both COOP (blue) and AMSR-E SD (red) estimates. Several peak SD values were clearly identified as major snowfall events in the latter season. The dashed blue and red lines represent COOP SD and AMSR-E SD seasonal means. The COOP 2007/2008 and 2008/2009 seasonal SD station mean values (2007/2008 seasonal mean was 6.23cm, 2008/2009 seasonal mean was 5.41 cm) were 1.78 cm and 1.80 cm greater, respectively, than the corresponding AMSR-E seasonal SD means (2007/2008 seasonal mean was 4.45 cm, 2008/2009 seasonal mean was 3.61 cm). The Pearson correlations between daily COOP SD and AMSR-E SD in 2007/2008 and 2008/2009 winter seasons were 0.71 and 0.70, respectively. The correlation was significant at the $p = 0.01$. The detailed daily COOP and AMSR-E SD values over time were shown in Tables 4.2 and 4.3.

A directional alternate hypothesis (WMPSR) was used to determine whether the difference between COOP SD and AMSR-E SD was significant. As the frequency of negative differences in SD was less than the frequency of positive differences, the negative rank sum (Tn) was selected for the computation. The Zw values of the WMPSR test were calculated as -9.26 and -8.00 for 2007/2008 and 2008/2009 winter seasons, respectively, and both result in one-tail p-values equaled to 0.0. These results suggested that the differences between COOP SD measurements and AMSR-E SD estimates were significant for both seasons. The detailed WMPSR results were displayed in Table 4.1.

Figure 4.2 showed the daily COOP spatial SD means, AMSR-E spatial SD means, and number of COOP reporting stations. The daily number of COOP reporting stations did not change much over time, with the exception of two days with relatively low values (i.e., 1 February 2009 and 1 March 2009). On both 1 February 2009 and 1 March 2009, the SD means were unusually high (14.30 cm and 10.90 cm). Therefore, the number of reporting stations into consideration was important when selecting individual days for spatial comparison because the SD mean was likely to be affected by the number and distribution of stations. The days with an abnormal number of reporting stations were excluded even if they had the largest or smallest daily SD spatial means. The detailed daily numbers of COOP reporting stations is shown in Table 4.4.

Five days with the largest mean SD and three days with the smallest mean SD (with a normal daily number of reporting stations) were selected for further analysis. Tables 4.5 and 4.6 showed the results of the 15 days with the largest SD daily mean and the 15 days with the smallest SD daily mean with associated number of reporting stations. As stated previously, an anomalous number of reporting stations may lead to skewed daily SD spatial means; therefore, 1

February 2009 and 1 March 2009 were not selected. Consecutive days may lead to very similar results (Tables 4.4 and 4.5) because of temporal autocorrelation of snow depth at an individual station, so consecutive days were also excluded. Thus, the five days with largest SD value selected for the individual spatial comparison were 13 February 2008, 22 February 2008, 6 February 2008, 22 December 2008 and 29 January 2009. The three days with the smallest SD value were 1 December 2007, 6 February 2008 and 21 March 2009.

Figures 4.3–4.10 depict the COOP and AMSR-E SD. Note that interpolated COOP SD values were omitted over areas where the AMSR-E data were missing. Compared to interpolated COOP, AMSR-E was likely to underestimate SD over Northern Idaho, northwestern Montana, northeastern Washington (Figures 4.3 – 4.7, 4.10) and mountainous areas over Washington, Oregon, California (Figures 4.3 – 4.7, 4.9), the Great Lakes areas (Figures 4.3, 4.7), the New England regions (Figures 4.3 – 4.5, 4.7) and mountainous areas over Montana, Wyoming and Colorado (Figure 4.3 – 4.7). Overestimations of SD were noted over northeastern Utah (Figures 4.3 – 4.6), northern and eastern Montana (Figures 4.3, 4.6), North Dakota (Figures 4.5, 4.6, 4.10), eastern South Dakota (Figures 4.4 – 4.6), eastern Nebraska (Figures 4.4 – 4.6), northern Kansas (Figure 4.7), Missouri (Figures 4.4, 4.7), northern Illinois, Indiana and northern Ohio (Figure 4.7).

4.1.2 Discussion of comparison of in situ and passive microwave snow depth

From the visual and statistical analyses of COOP SD observations in combination with AMSR-E SD estimates over the 2007/2008 and 2008/2009 winter seasons, there were several important findings. Daily AMSR-E SD means had a relatively high correlation (2007/2008 = 0.71, 2008/2009 = 0.70) with daily COOP means over time, though AMSR-E SD was noted to be significantly different from COOP observations based on WMPSR. The possible explanation

was that the overall lower satellite SD estimates compared to ground SD observations strongly affect the WMPSR results.

The largest daily mean difference between AMSR-E and ground observations was noted in January and February for 2007/2008 and 2008/2009 seasons, respectively (i.e., the difference is greater while there are larger SD values, possibly due to snow depth penetration by passive microwave). The smallest daily mean difference between AMSR-E and ground observations was noted in March for both 2007/2008 and 2008/2009 seasons. This finding was possibly related to frozen snow. In March, the process of snow refreezing (i.e., increased grain size) occurs more often compared to December, January and February. Increased snow grain size can enhance the brightness temperature gradient, which leads to larger SD detection.

AMSR-E underestimated SD over Northern Idaho, northwestern Montana, northeastern Washington and mountainous areas over Washington, Oregon, California. However, overestimation of SD is noted over Northeastern Utah. The ability of AMSR-E snow detection over the Great Lakes region, the New England areas, northern and eastern Montana, North Dakota, eastern South Dakota, eastern Nebraska, northern Kansas, Missouri, northern Illinois, Indiana and northern Ohio and mountainous areas over Montana, Wyoming and Colorado varied over time.

AVHRR 1km land cover image (Figure 4.11), forest density (Figure 4.12), and SNODAS SD, snow melt and average snowpack temperature products (Figures 4.13–4.15) were used to identify possible factors influencing satellite SD detection. Three days (29 January 2009, 13 February 2008 and 22 December 2008) were selected for the analysis. SD and snow melt products were from the NOAA National Weather Service's National Operational Hydrologic Remote Sensing Center (NOHRSC) Snow Data Assimilation System (SNODAS). SNODAS is a

modeling system aimed at providing the best possible estimates of snow related parameters by integrating snow data from different sources including ground stations, satellite, airborne platforms, and output from the NWP models (Barrett 2003).

For 29 January 2009, from Figures 4.3 and 4.13a, interpolated COOP SD was noted to have a higher agreement with SNODAS product, however, little SD was detected by both COOP and AMSR-E over Tennessee, Kentucky, West Virginia and Virginia. This may due to the different measurement/observation times and techniques of the three datasets. Both interpolated COOP SD and SNODAS SD product showed no SD over northeastern Montana, southwestern North Dakota and central South Dakota (Figures 4.3a and 4.13a). However, AMSR-E showed large SD over those areas. Underestimations over mountainous areas over Washington, Oregon and California might have been due to snow melt, evident as snow temperatures close to freezing in SNODAS (Figure 4.13b). With the onset of snow melt, the T_B gradient will be reduced.

Dense forests over New England, northern Idaho, northwestern Montana, northeastern Washington, and mountainous areas over Washington, Oregon and California (Figures 4.3 and 4.12) mask snow detection in AMSR-E. Forests emit microwave radiation and decrease the T_B gradient. Therefore, significant underestimations of SD by AMSR-E over those areas may relate to forest density.

By comparing SD distribution with the AVHRR 1 km land cover image (Figure 4.11) from the Global Land Cover Facility website, AMSR-E SD detection did not perform well over the western forested areas of mountainous Oregon, Washington, California, Colorado and Wyoming where the forest types are evergreen needle leaf forest and evergreen broadleaf forest. Occasionally, AMSR-E detected SD well over the Great Lakes and the New England areas where the forest types were mixed forest and deciduous broadleaf forest; however, the

performance was not consistently accurate. Underestimation of AMSR-E SD over mountainous areas may also relate to elevation. The spatial resolution of AMSR-E is very coarse (i.e., 25 × 25 km), therefore, AMSR-E cannot display regional SD change over mountainous areas.

For 13 February 2008 (Figure 4.4), a significant overestimate of AMSR-E over northeastern Utah was identified. For 22 December 2008 (Figure 4.7), a large difference was noted between COOP SD and AMSR-E SD (i.e., AMSR-E significantly overestimated SD over northeastern Kansas, southern Iowa, northern Indiana, northern Illinois, northern Indiana and northern Ohio). This finding may be due to refrozen snow. The average snowpack temperature on 21 December 2008 showed relatively high temperature over the AMSR-E SD overestimation regions (Figure 4.15a). However, the average snowpack temperature on 22 December 2008 suggested a sharp decrease of snowpack temperature (Figure 4.15b). This finding may indicate a snow refreezing process. The snow grain size increases during snow refreeze which will increase radiation scattering and eventually enhance the T_B gradient.

To date, there were only a limited number of studies focusing on AMSR-E assessments. Tekeli (2008) found that AMSR-E overestimated the SWE during either precipitation events or warm period events, however, overestimates occurred during refreezing events. Tedesco and Narvekar (2010) compared the SD values derived from AMSR-E SWE with SNODAS SD estimates (re-sampled to a 25×25 km^2 spatial resolution) and SD measurements by various stations in the Northern Hemisphere collected by the World Meteorological Organization (WMO). They found the correlation and RMSE between AMSR-E SD and WMO are 0.41 and 6 cm, respectively, during 2005–2007. The correlation (2007/2008 = 0.27, 2008/2009 = 0.23) between AMSR-E SD and COOP SD observations in the present study was lower than found by Tedesco and Narvekar (2010). The number and distribution of ground stations used may affect

this difference. Stations selected by Tedesco and Narvekar (2010) were located where snow is likely to be found. Compared to Tedesco and Narvekar (2010), instead of using 42 selected stations over Canada, Alaska, Sweden, Norway and Finland, the ground stations used in the present study were the COOP stations available daily over contiguous U.S. with greater variation in land cover and more ephemeral snow cover. In addition, as found in this research, beside areas with relatively high latitude, AMSR-E SD was also noted to have significant spatial difference over dense evergreen forest (e.g. mountainous areas over California) and melting snow areas (e.g., northern Missouri) compared to interpolated COOP SD. Therefore, by including larger areas where AMSR-E SD was also noted to be largely different from in situ SD measurements (may due to vegetation, complex land cover and melt snow) may contribute to the lower correlation found in this research. If only stations with SD above 0 cm are used for the comparison analysis, a further decrease in correlation is likely to happen.

Tedesco and Narvekar (2010) also conducted an AMSR-E SD assessment over forest cover boundaries. By comparing to SNODAS, they found that SD over forested areas were underestimated by the AMSR-E algorithm. In this research, we compared the selected individual days with AVHRR 1km Landcover (Figure 4.11) and found an overall underestimation of SD detection over forest, especially the northern Rocky Mountains and western mountainous regions with evergreen forest. Snow detection over deciduous and mixed forest over New England and the Great Lakes region is inconsistent. When examining AMSR-E SD detection performance by forest types, satellite SD estimates are consistently less accurate over evergreen forests. Tedesco and Narvekar (2010) indicated a comparatively greater correlation between AMSR-E and WMO for dense forest cover than for sparse forest cover. This phenomenon, as mentioned by the authors, may be related to the greater snow depth on average over the dense forests in their study

region. Poor correlation occurred over sparse forest cover likely due to a large number of shallow snow cases.

Frei et al. (2012) compared the AMSR-E SD to the Canadian Meteorological Center (CMC) snow product over Northern Hemisphere. Figure 4.16 from Frei et al. (2012) showed the comparison between AMSR-E and CMC snow depth in January. There were discrepancies between CMC and AMSR-E snow accumulations in many regions. Underestimation of snow was detected over the mountainous areas of Washington, Oregon and California, northern Rocky Mountains, mountainous areas of northwestern Wyoming and western Colorado and the northeastern contiguous U.S. Overestimation of snow was largely detected over the central U.S. The AMSR-E SD distribution over the U.S. found in this research closely resembles results from Frei et al. (2012).

Frei et al. (2012) also suggested that AMSR-E tends to overestimate the SD values provided by CMC based on histograms of the SD difference between the two datasets. Siberia were found to be the primary area with AMSR-E SD overestimation, however, other regions (e.g., Tibetan plateau and North American northeastern coast) were noted with AMSR-E SD underestimation. By conducting a coefficient of variation analysis, the largest difference between the two datasets is in October and smallest difference was in January. The difference began to increase again in April. In this research, February and January had the smallest difference for both winter seasons, while December had the largest data discrepancy for 2007/2008 and 2008/2009 seasons, respectively. The difference may be explained by the studies' spatial scales. Frei et al. (2012) performed a hemispheric scale study, however, the present study area is the contiguous U.S.

Overall, AMSR-E underestimates SD compared to ground observations. Compared to interpolated COOP, AMSR-E underestimated SD over Northern Idaho, northwestern Montana, northeastern Washington and mountainous areas over Washington, Oregon, California, the Great Lakes areas, the New England regions and mountainous areas over Montana, Wyoming and Colorado at times. Overestimations of SD were noted over Northeastern Utah, northern and eastern Montana, North Dakota, eastern South Dakota, eastern Nebraska, northern Kansas, Missouri, northern Illinois, Indiana and northern Ohio. Other significant factors must have influenced the accuracy of AMSR-E retrievals along with vegetation, snow melt, snow grain size and elevation. Based on previous studies, other influencing factors can be the physical structure of snow packs; for example, spatio-temporal varying snow density.

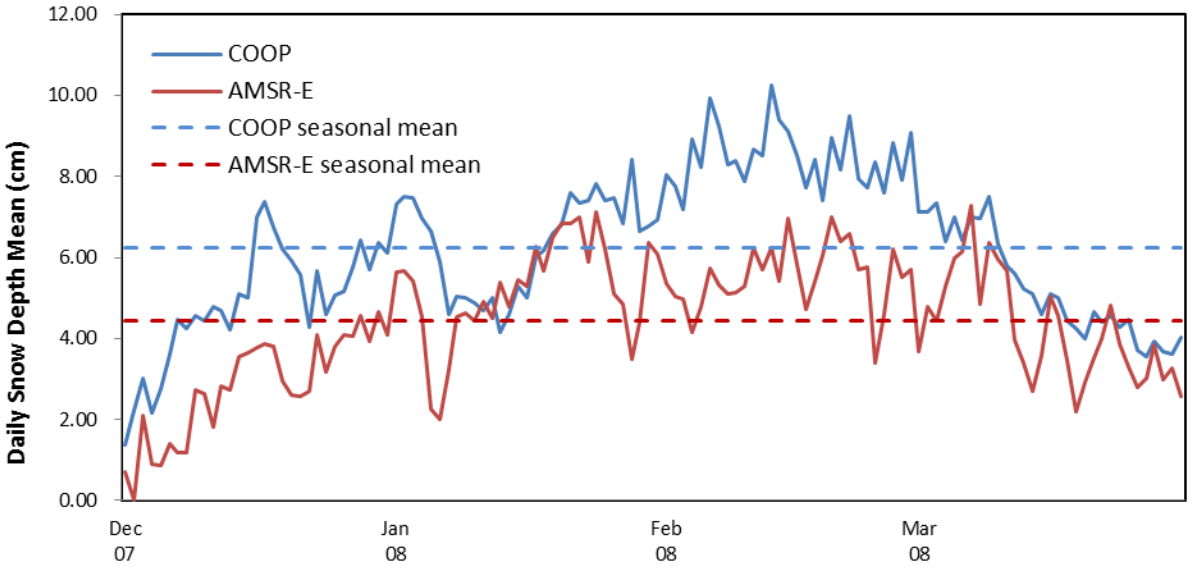

(a)

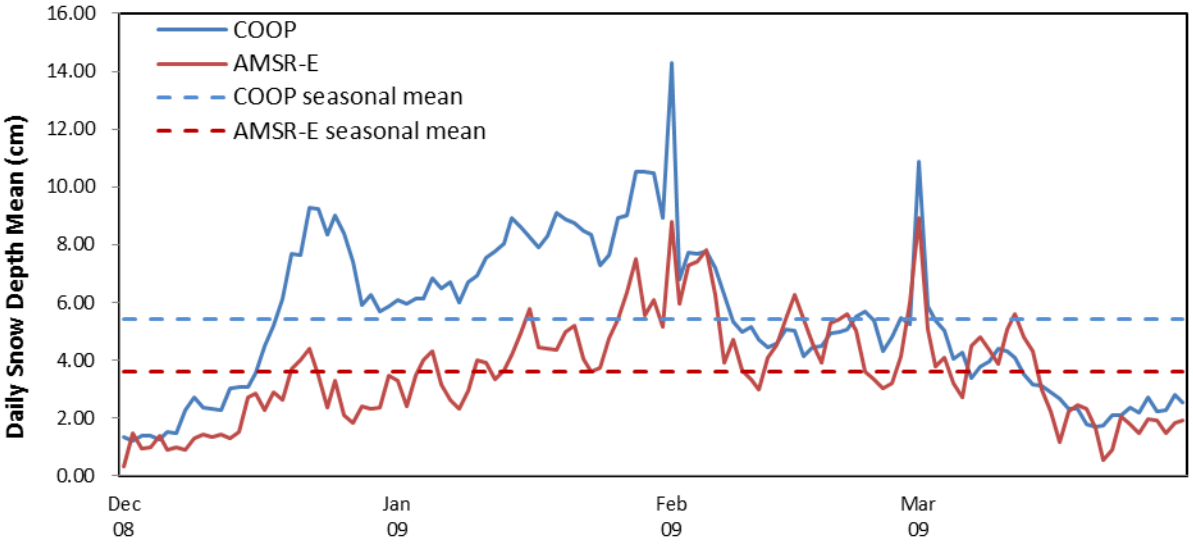

(b)

Figure 4.1: Daily COOP (blue) and AMSR-E (red) Snow Depth averaged mean over all stations for 2007/2008 (a) and 2008/2009 winter (b). Seasonal means shown with dashed lines.

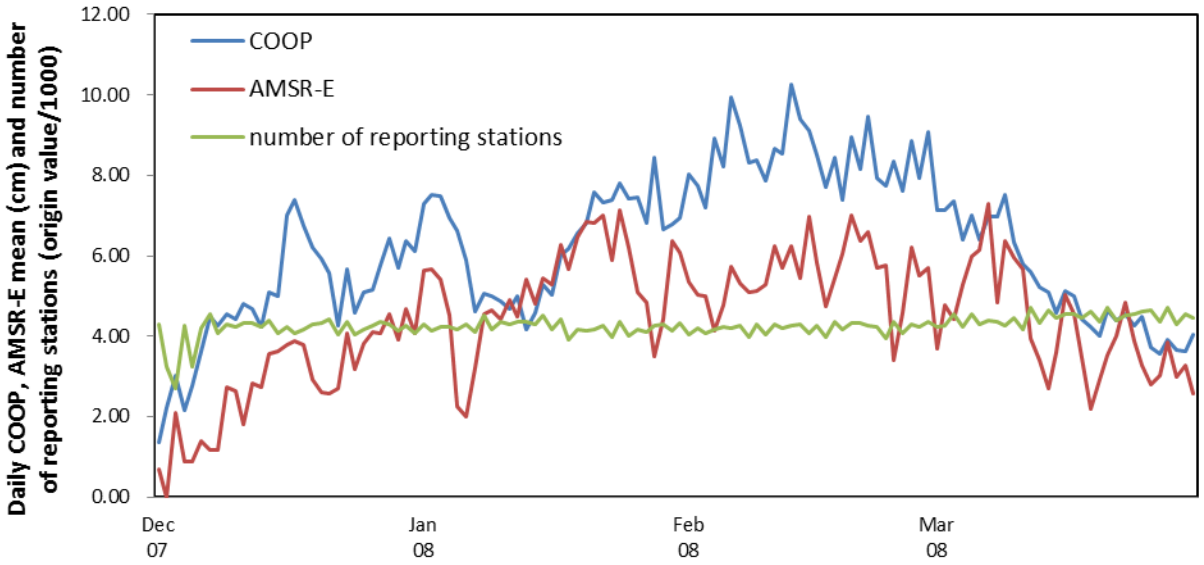

(a)

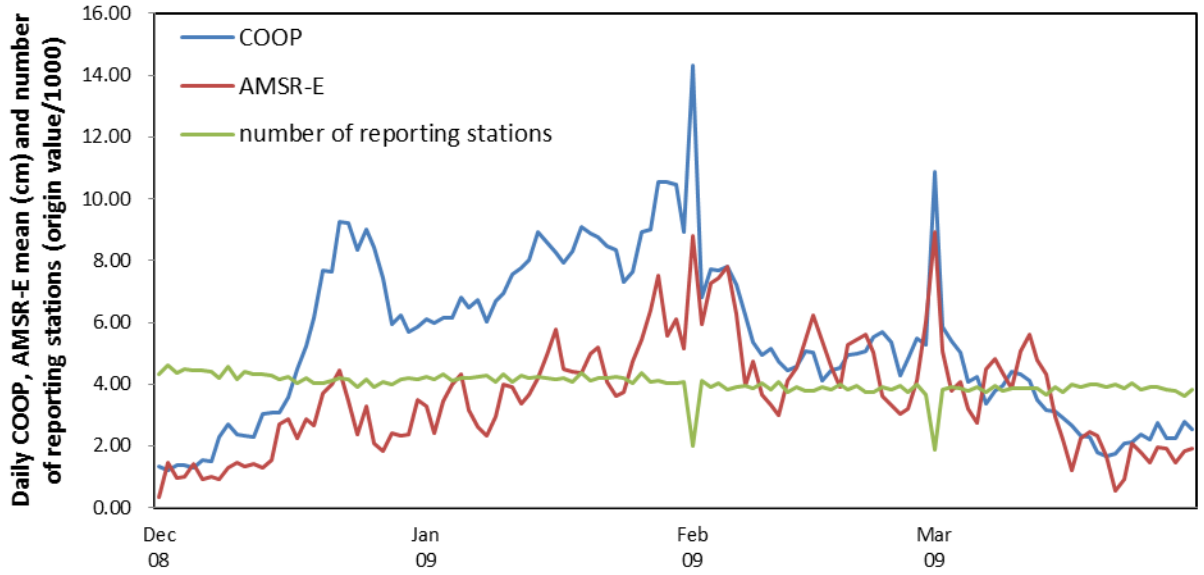

(b)

Figure 4.2: Daily COOP (blue), AMSR-E (red) Snow Depth averaged mean and daily number of reporting stations (green) for 2007/2008 (a) and 2008/2009 (b) winter.

Table 4.1: WMPSR hypothesis test results.

Date	Tn	Tp	N	Zw	p-value
2007/2008	110	7271	121	-9.26	0
2008/2009	596	6785	121	-8	0
2007/2008 (stations with snow)	0	7381	121	-9.55	0
2008/2009 (stations with snow)	0	7381	121	-9.55	0

Table 4.2: Daily COOP SD mean (cm) within satellite coverage over 2007/2008 and 2008/2009 winter seasons.

Day	Dec 2007	Jan 2008	Feb 2008	Mar 2008	Dec 2008	Jan 2009	Feb 2009	Mar 2009
1	1.38	7.30	8.04	7.13	1.33	6.10	14.30	10.88
2	2.23	7.51	7.74	7.13	1.23	5.97	6.81	5.86
3	3.01	7.47	7.20	7.34	1.39	6.13	7.73	5.40
4	2.17	6.96	8.92	6.39	1.38	6.13	7.67	5.04
5	2.76	6.64	8.22	7.01	1.28	6.82	7.79	4.06
6	3.62	5.89	9.92	6.41	1.54	6.47	7.21	4.26
7	4.48	4.61	9.25	6.99	1.50	6.73	6.25	3.37
8	4.25	5.05	8.31	6.96	2.28	6.01	5.34	3.77
9	4.56	5.01	8.38	7.50	2.72	6.70	4.96	3.94
10	4.43	4.86	7.87	6.35	2.37	6.95	5.14	4.42
11	4.79	4.69	8.66	5.80	2.32	7.56	4.72	4.31
12	4.68	5.00	8.52	5.59	2.29	7.78	4.46	4.11
13	4.22	4.15	10.25	5.23	3.02	8.03	4.57	3.51
14	5.08	4.60	9.40	5.09	3.06	8.91	5.08	3.15
15	4.99	5.28	9.11	4.60	3.08	8.60	5.04	3.13
16	7.01	5.02	8.51	5.11	3.57	8.25	4.13	2.90
17	7.39	6.02	7.72	5.00	4.51	7.93	4.46	2.68
18	6.75	6.18	8.43	4.42	5.21	8.29	4.51	2.31
19	6.20	6.57	7.40	4.23	6.13	9.09	4.93	2.30
20	5.93	6.81	8.96	4.00	7.67	8.90	5.00	1.79
21	5.58	7.58	8.16	4.66	7.66	8.76	5.09	1.68
22	4.27	7.33	9.48	4.39	9.26	8.48	5.52	1.76
23	5.67	7.40	7.93	4.56	9.23	8.33	5.70	2.09
24	4.59	7.81	7.73	4.27	8.36	7.31	5.36	2.12
25	5.08	7.41	8.35	4.47	9.00	7.64	4.30	2.36
26	5.17	7.46	7.61	3.71	8.41	8.94	4.80	2.19
27	5.76	6.83	8.84	3.55	7.43	9.03	5.48	2.74
28	6.42	8.43	7.92	3.92	5.94	10.54	5.26	2.25
29	5.70	6.66	9.08	3.67	6.25	10.54		2.27
30	6.37	6.77		3.63	5.70	10.46		2.80
31	6.12	6.93		4.03	5.85	8.92		2.54

Table 4.3: Daily AMSR-E SD mean (cm) within satellite coverage over 2007/2008 and 2008/2009 winter seasons.

Day	Dec 2007	Jan 2008	Feb 2008	Mar 2008	Dec 2008	Jan 2009	Feb 2009	Mar 2009
1	0.70	5.63	5.35	3.68	0.33	3.29	8.79	8.91
2	----	5.65	5.03	4.77	1.47	2.43	5.95	5.08
3	2.11	5.42	4.98	4.42	0.94	3.46	7.27	3.80
4	0.89	4.53	4.14	5.29	0.98	3.99	7.42	4.09
5	0.88	2.27	4.77	5.99	1.40	4.34	7.81	3.20
6	1.41	1.99	5.72	6.15	0.90	3.15	6.26	2.73
7	1.17	3.23	5.32	7.29	0.98	2.62	3.94	4.49
8	1.19	4.54	5.10	4.84	0.90	2.33	4.72	4.82
9	2.74	4.64	5.13	6.37	1.31	2.97	3.65	4.35
10	2.64	4.43	5.28	5.96	1.45	3.99	3.33	3.88
11	1.80	4.91	6.25	5.67	1.34	3.91	2.99	5.06
12	2.82	4.49	5.70	3.96	1.43	3.36	4.09	5.60
13	2.72	5.40	6.24	3.40	1.31	3.66	4.53	4.80
14	3.56	4.79	5.43	2.70	1.55	4.19	5.44	4.34
15	3.63	5.46	6.97	3.59	2.71	4.94	6.25	2.97
16	3.79	5.29	5.82	5.03	2.86	5.76	5.41	2.23
17	3.88	6.28	4.73	4.55	2.26	4.47	4.59	1.19
18	3.80	5.67	5.43	3.46	2.89	4.41	3.92	2.26
19	2.94	6.48	6.04	2.20	2.65	4.35	5.29	2.47
20	2.60	6.84	6.99	2.92	3.69	4.97	5.43	2.34
21	2.57	6.83	6.38	3.52	4.00	5.19	5.59	1.65
22	2.70	6.99	6.60	4.00	4.43	4.06	5.01	0.54
23	4.08	5.88	5.69	4.82	3.47	3.63	3.61	0.93
24	3.17	7.12	5.75	3.88	2.39	3.74	3.33	2.07
25	3.82	6.21	3.39	3.29	3.29	4.74	3.05	1.78
26	4.10	5.10	4.59	2.80	2.09	5.45	3.21	1.48
27	4.06	4.84	6.20	3.03	1.82	6.38	4.13	1.95
28	4.56	3.49	5.51	3.85	2.43	7.52	6.01	1.92
29	3.92	4.42	5.71	2.97	2.32	5.56		1.47
30	4.66	6.38		3.26	2.37	6.09		1.85
31	4.08	6.08		2.56	3.48	5.16		1.90

Table 4.4: Daily COOP number of reporting stations over 2007/2008 and 2008/2009 winter seasons.

Day	Dec 2007	Jan 2008	Feb 2008	Mar 2008	Dec 2008	Jan 2009	Feb 2009	Mar 2009
1	4301	4281	4041	4219	4319	4254	2004	1861
2	3245	4128	4194	4256	4612	4156	4119	3827
3	2706	4227	4089	4553	4368	4304	3893	3897
4	4257	4244	4169	4219	4477	4120	4023	3871
5	3229	4170	4241	4558	4456	4177	3820	3775
6	4197	4287	4211	4288	4429	4213	3894	3889
7	4541	4096	4277	4387	4417	4218	3931	3748
8	4062	4527	3988	4357	4195	4264	3866	3942
9	4286	4157	4305	4270	4558	4083	4043	3782
10	4235	4368	4031	4455	4167	4336	3809	3860
11	4340	4298	4310	4163	4401	4073	4081	3847
12	4335	4356	4208	4719	4307	4276	3761	3849
13	4223	4370	4279	4339	4337	4210	3898	3871
14	4386	4305	4281	4648	4279	4250	3799	3640
15	4067	4517	4088	4466	4175	4205	3783	3921
16	4238	4162	4269	4538	4242	4146	3913	3741
17	4076	4433	3992	4539	4024	4185	3821	3970
18	4173	3900	4370	4443	4177	4091	4002	3912
19	4302	4155	4184	4622	4026	4350	3823	3995
20	4320	4147	4314	4369	4045	4128	3949	4002
21	4411	4176	4313	4715	4102	4217	3737	3888
22	4057	4280	4270	4386	4178	4196	3752	4000
23	4376	3971	4227	4534	4156	4227	3897	3849
24	4031	4376	3946	4554	3902	4180	3835	4017
25	4162	4003	4373	4603	4144	4036	3958	3813
26	4257	4184	4058	4636	3927	4366	3744	3925
27	4371	4117	4303	4353	4052	4053	3998	3887
28	4291	4265	4230	4716	4006	4130	3666	3833
29	4143	4284	4369	4297	4175	4024		3797
30	4259	4152		4558	4201	4037		3637
31	4088	4341		4442	4161	4057		3842

Table 4.5: Date of the top 15 largest SD daily mean and number of reporting stations. Dates selected for spatial comparison shown in bold.

	Date	SD daily mean (cm/day)	Number of reporting stations
1	2/1/2009	14.30	2004
2	3/1/2009	10.88	1861
3	**1/29/2009**	**10.54**	**4024**
4	1/28/2009	10.54	4130
5	1/30/2009	10.46	4037
6	**2/13/2008**	**10.25**	**4279**
7	**2/6/2008**	**9.92**	**4211**
8	**2/22/2008**	**9.48**	**4270**
9	2/14/2008	9.40	4281
10	**12/22/2008**	**9.26**	**4178**
11	2/7/2008	9.25	4277
12	12/23/2008	9.23	4156
13	2/15/2008	9.11	4088
14	1/19/2009	9.09	4350
15	2/29/2008	9.08	4369

Table 4.6: Date of the top 15 smallest SD daily mean and daily station count. Dates selected for spatial comparison shown in bold.

	Date	SD daily mean (cm/day)	Station-in-use count
1	**12/2/2008**	**1.23**	**4612**
2	12/5/2008	1.28	4456
3	12/1/2008	1.33	4319
4	12/4/2008	1.38	4477
5	**12/1/2007**	**1.38**	**4301**
6	12/3/2008	1.39	4368
7	12/7/2008	1.50	4417
8	12/6/2008	1.54	4429
9	**3/21/2009**	**1.68**	**3888**
10	3/22/2009	1.76	4000
11	3/20/2009	1.79	4002
12	3/23/2009	2.09	3849
13	3/24/2009	2.12	4017
14	12/4/2007	2.17	4257
15	3/26/2009	2.19	3925

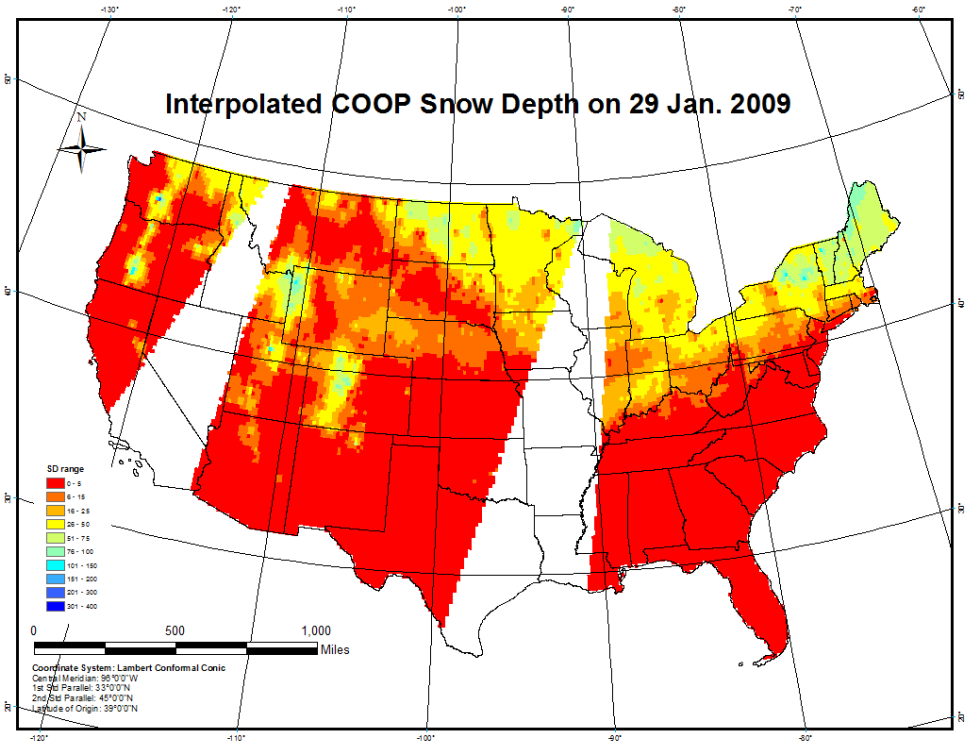

(a)

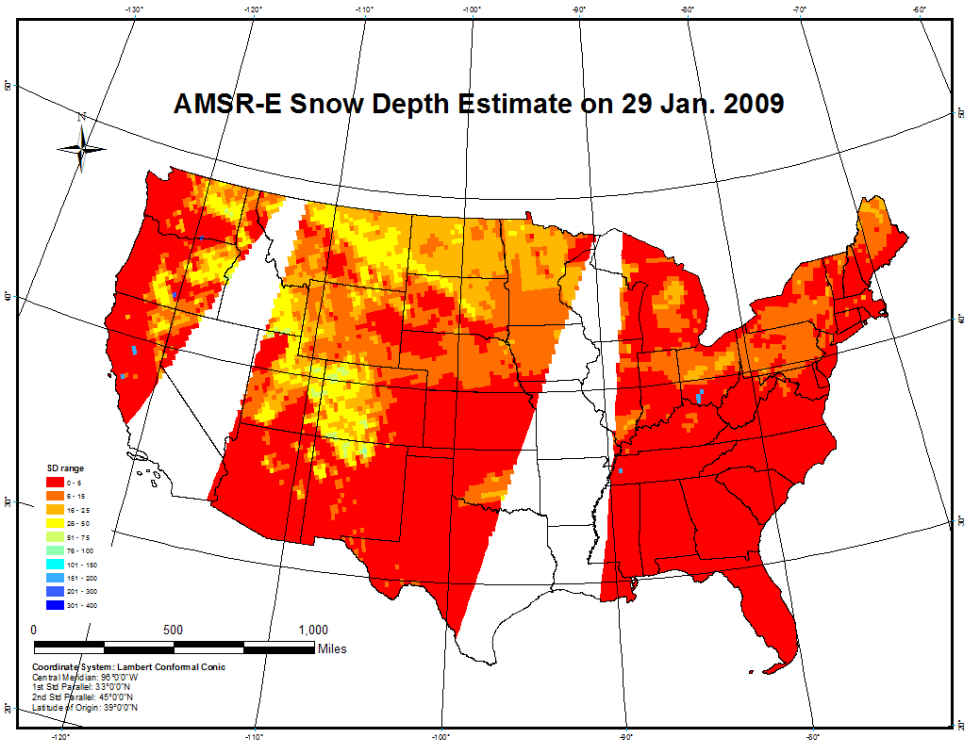

(b)

Figure 4.3: Interpolated COOP (a) and AMSR-E (b) SD (cm) on 29 Jan. 2009.

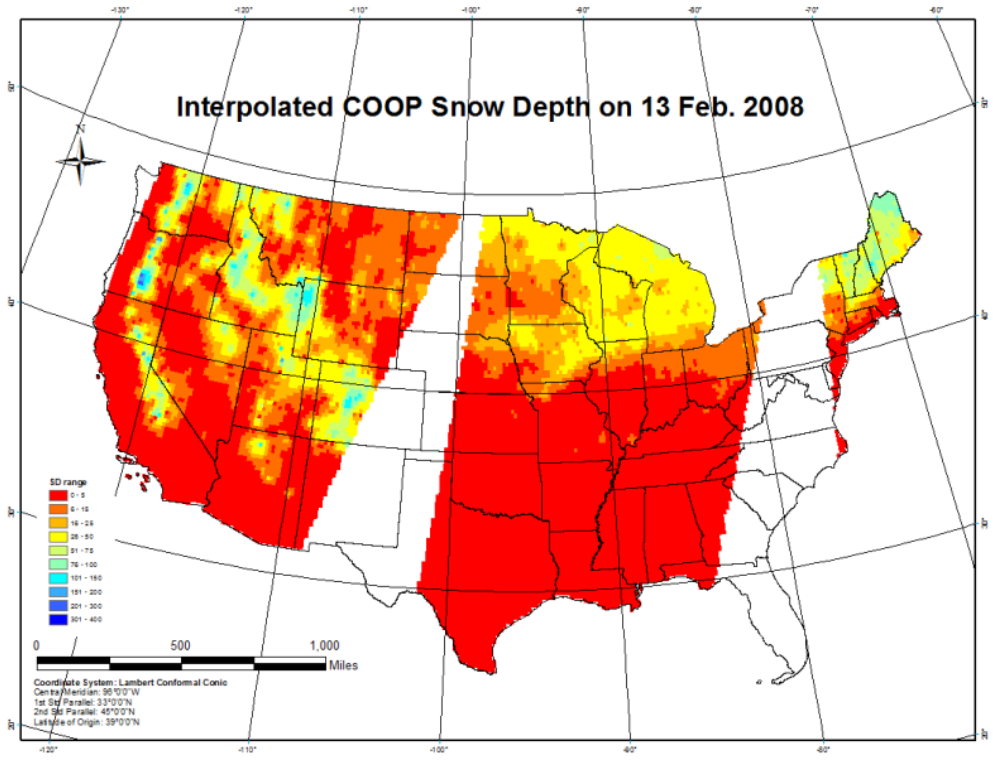

(a)

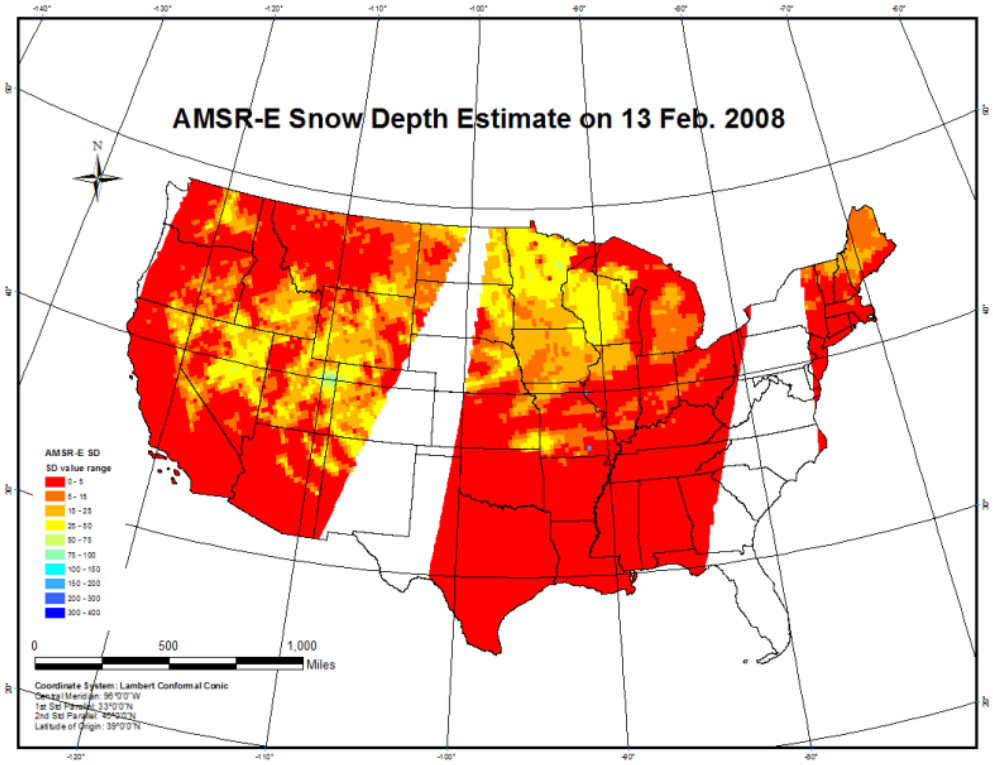

(b)

Figure 4.4: Interpolated COOP (a) and AMSR-E (b) SD (cm) on 13 Feb. 2008.

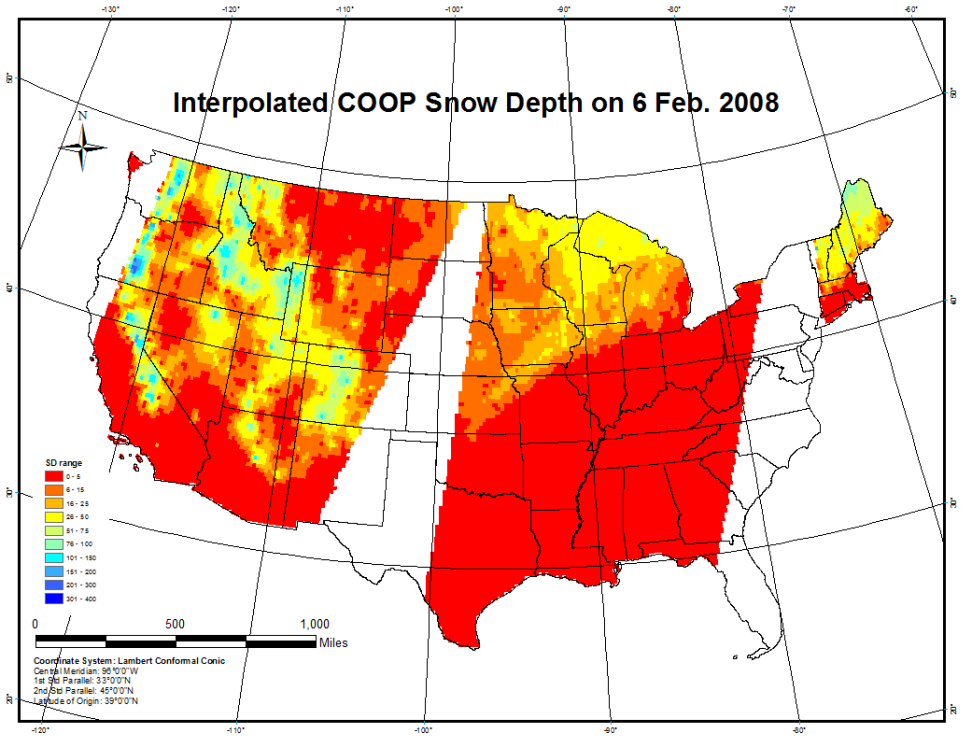

(a)

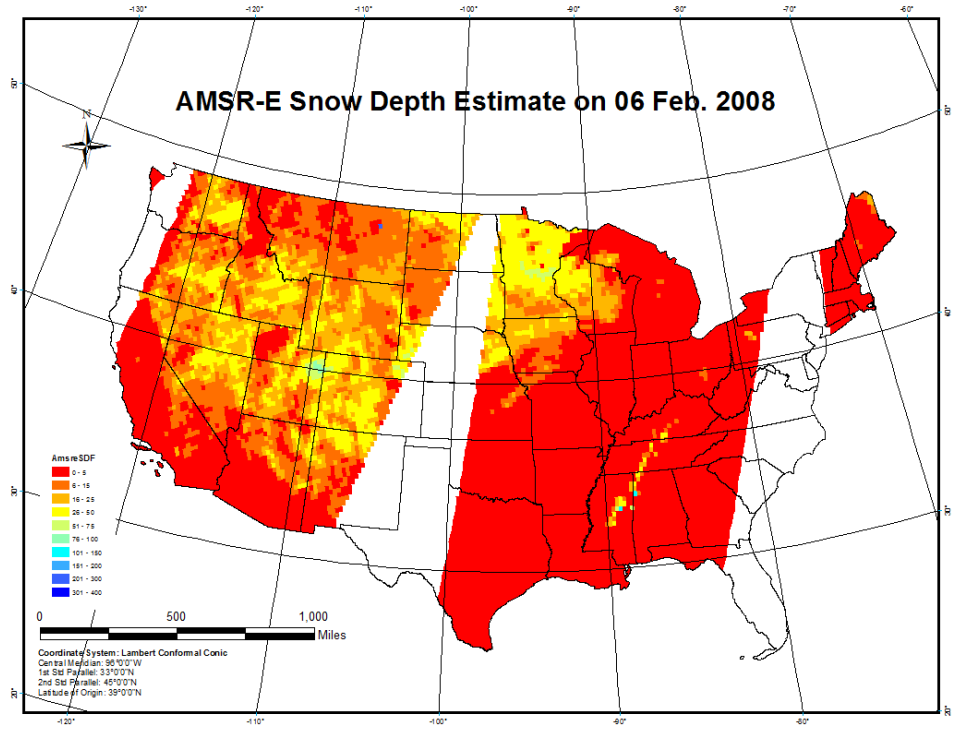

(b)

Figure 4.5: Interpolated COOP (a) and AMSR-E (b) SD (cm) on 6 Feb. 2008.

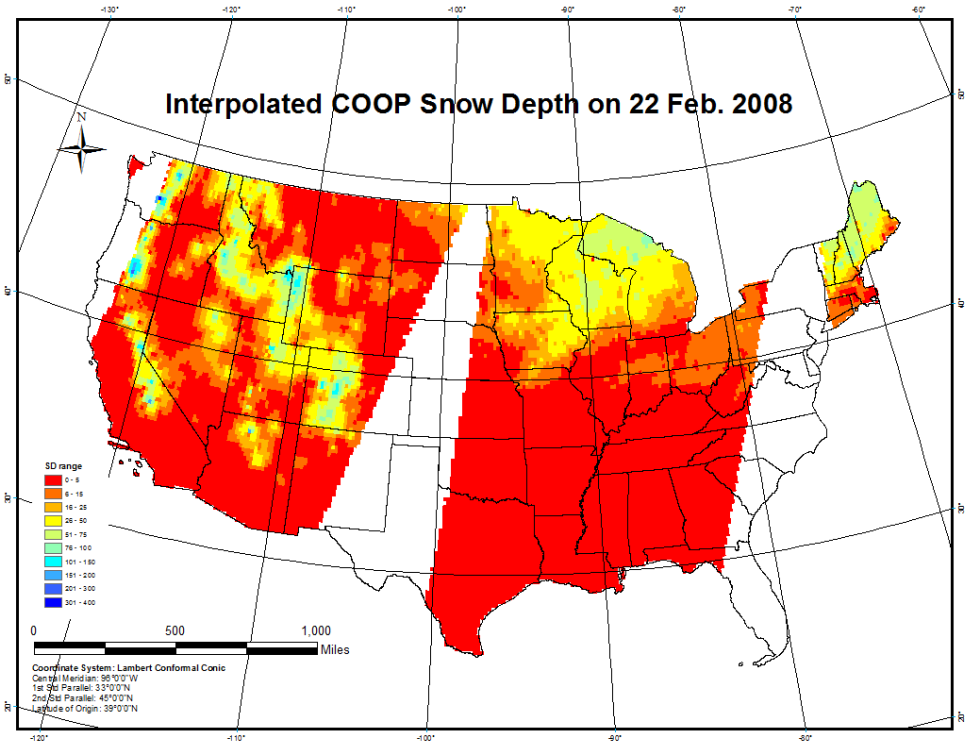

(a)

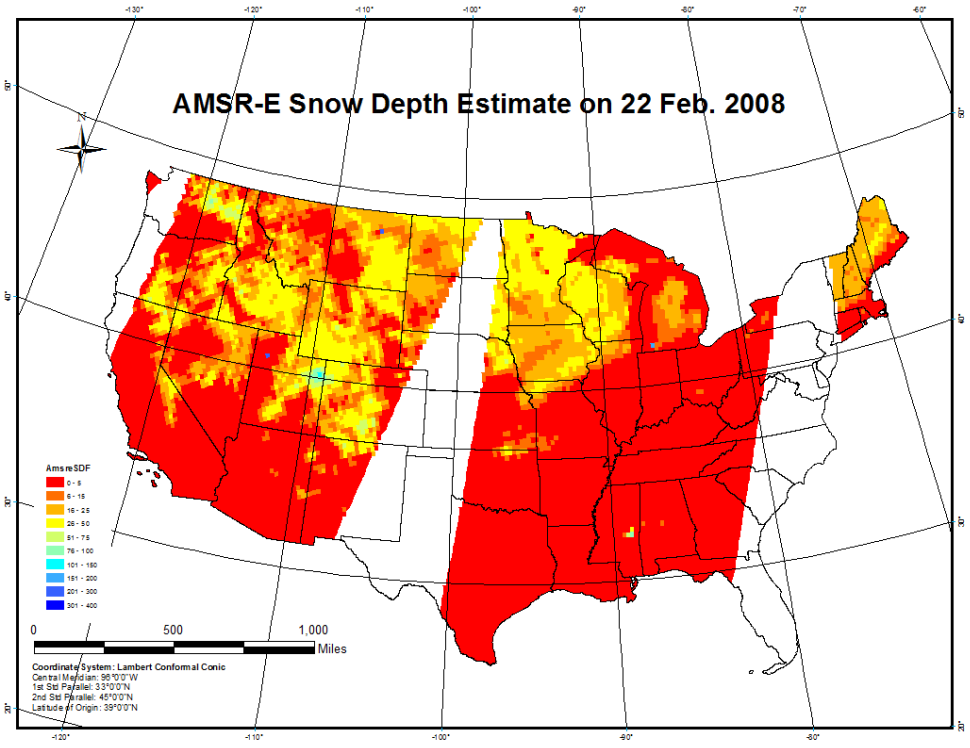

(b)

Figure 4.6: Interpolated COOP (a) and AMSR-E (b) SD (cm) on 22 Feb. 2008.

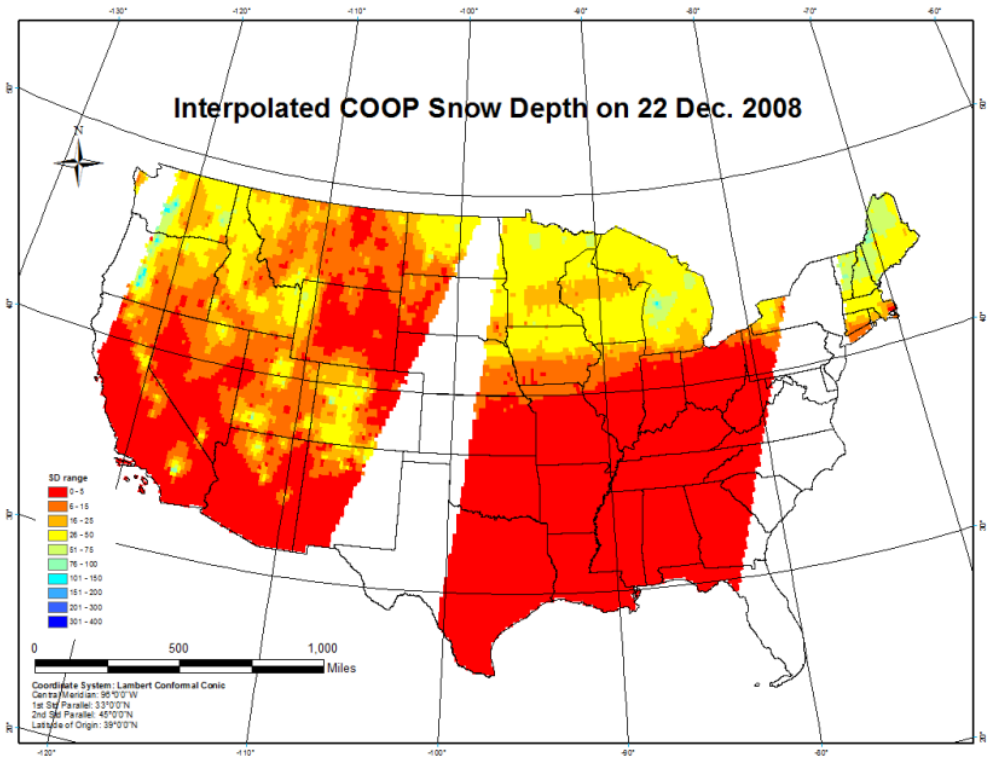

(a)

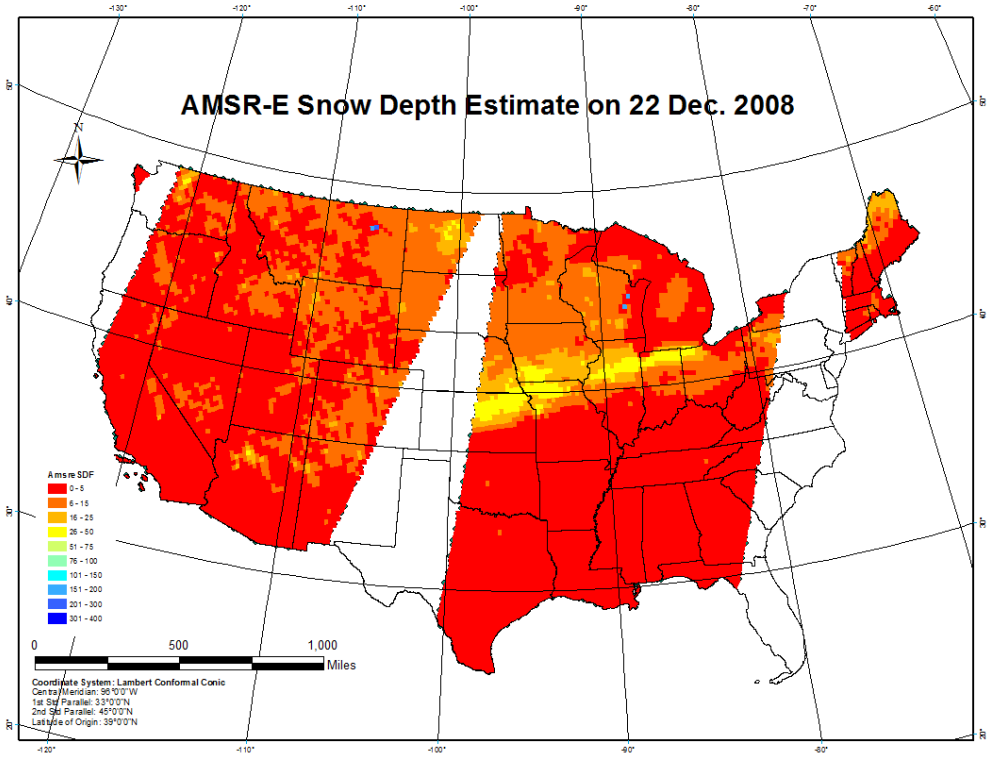

(b)

Figure 4.7: Interpolated COOP (a) and AMSR-E (b) SD (cm) on 22 Dec. 2008.

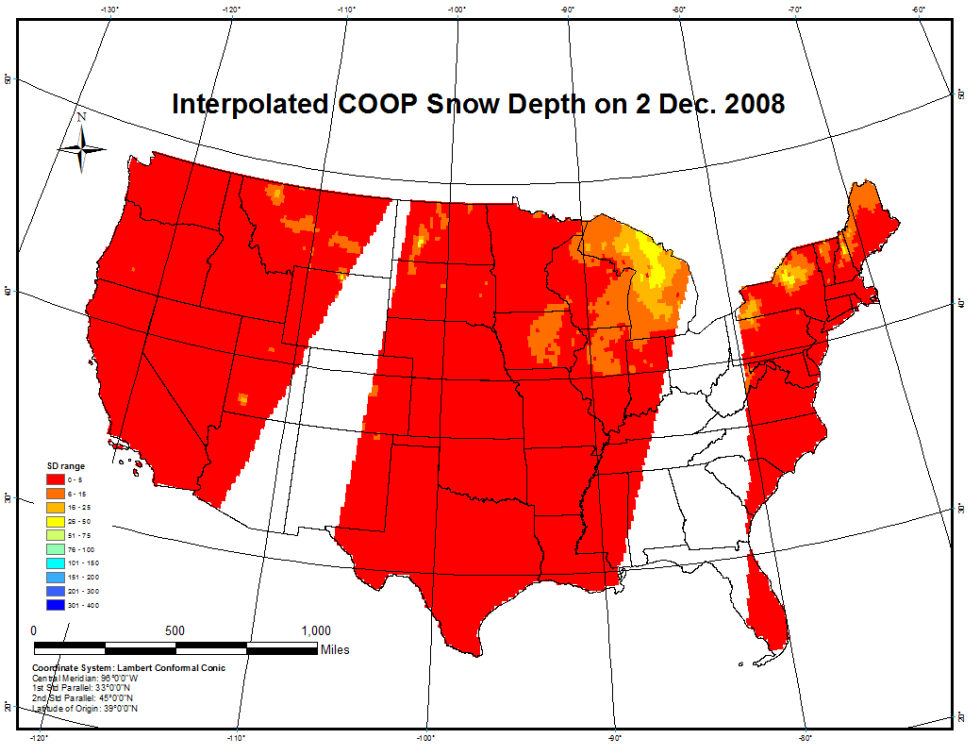

(a)

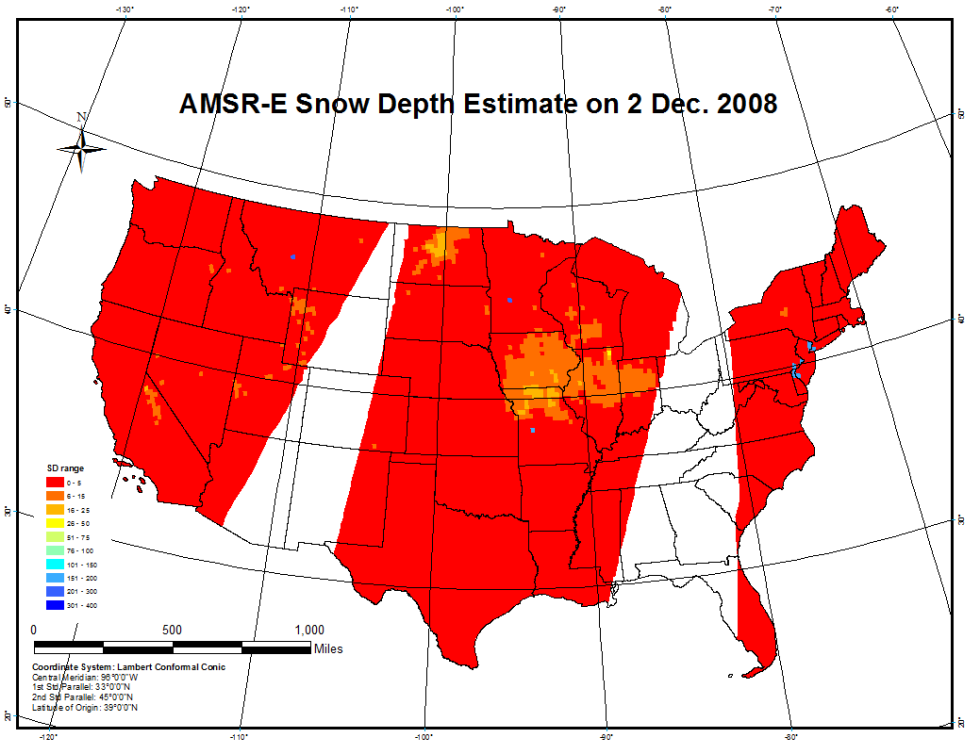

(b)

Figure 4.8: Interpolated COOP (a) and AMSR-E (b) SD (cm) on 2 Dec. 2008.

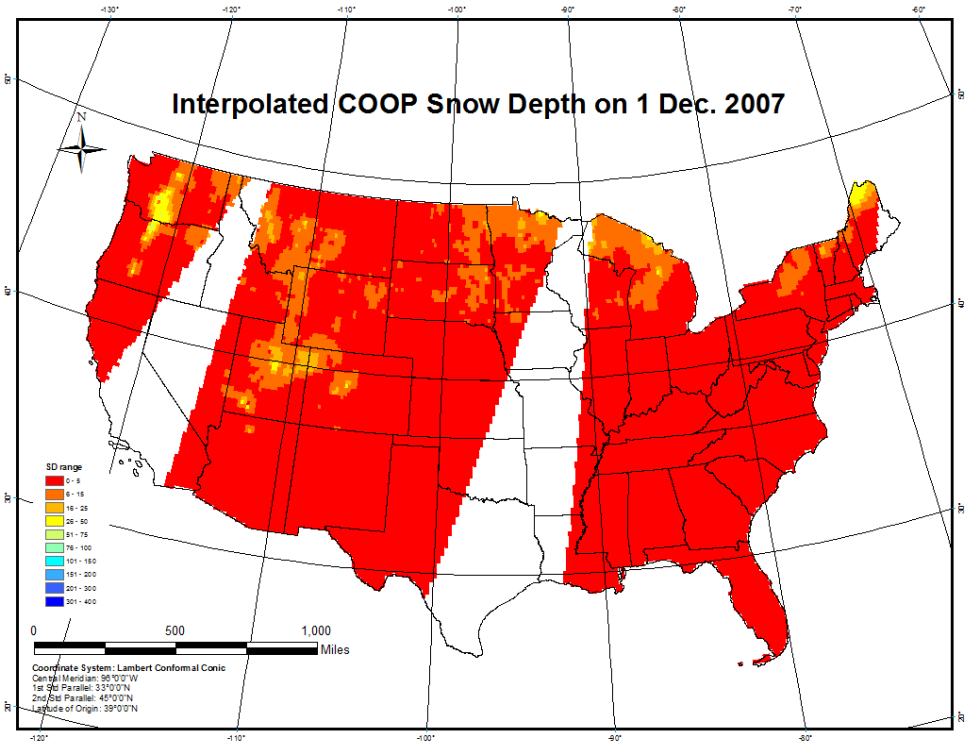

(a)

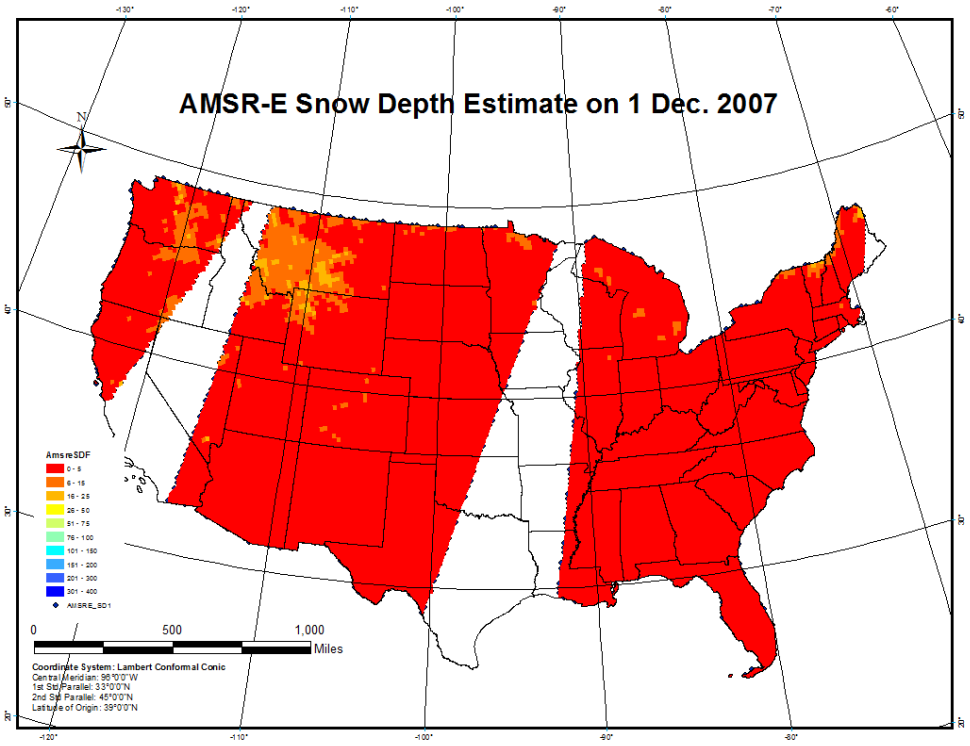

(b)

Figure 4.9: Interpolated COOP (a) and AMSR-E (b) SD (cm) on 1 Dec. 2007.

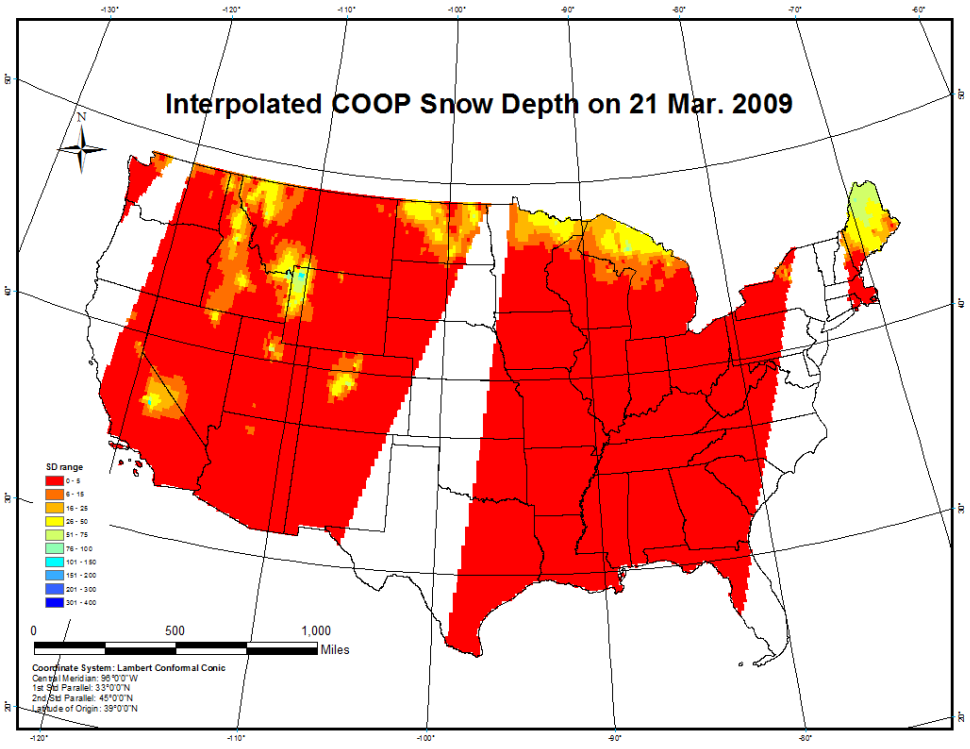

(a)

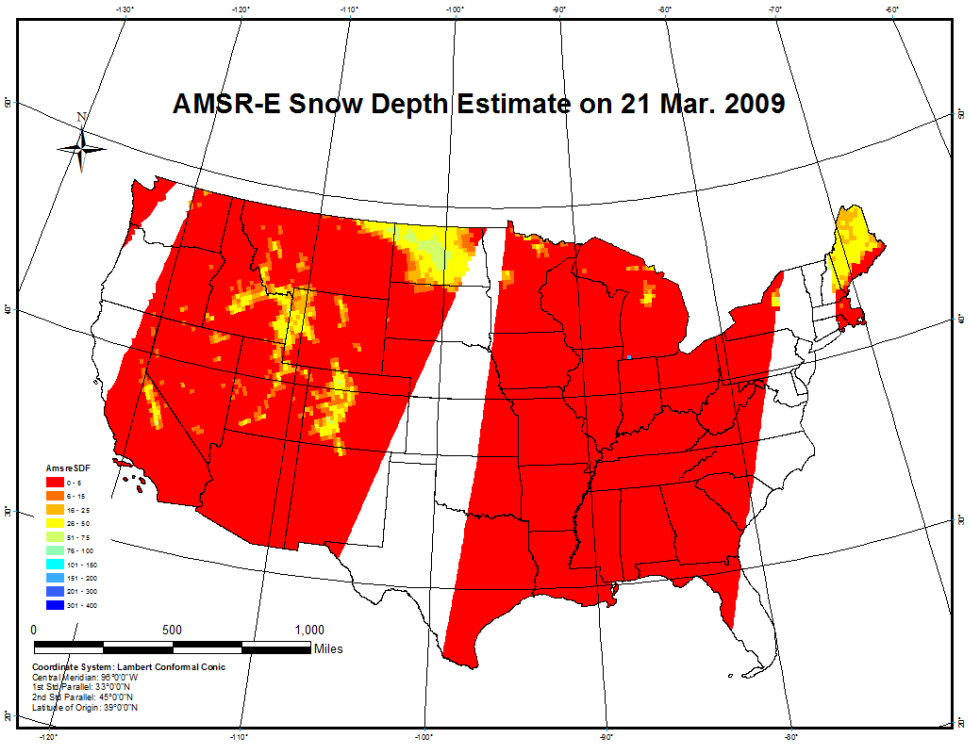

(b)

Figure 4.10: Interpolated COOP (a) and AMSR-E (b) SD (cm) on 21 Mar. 2009.

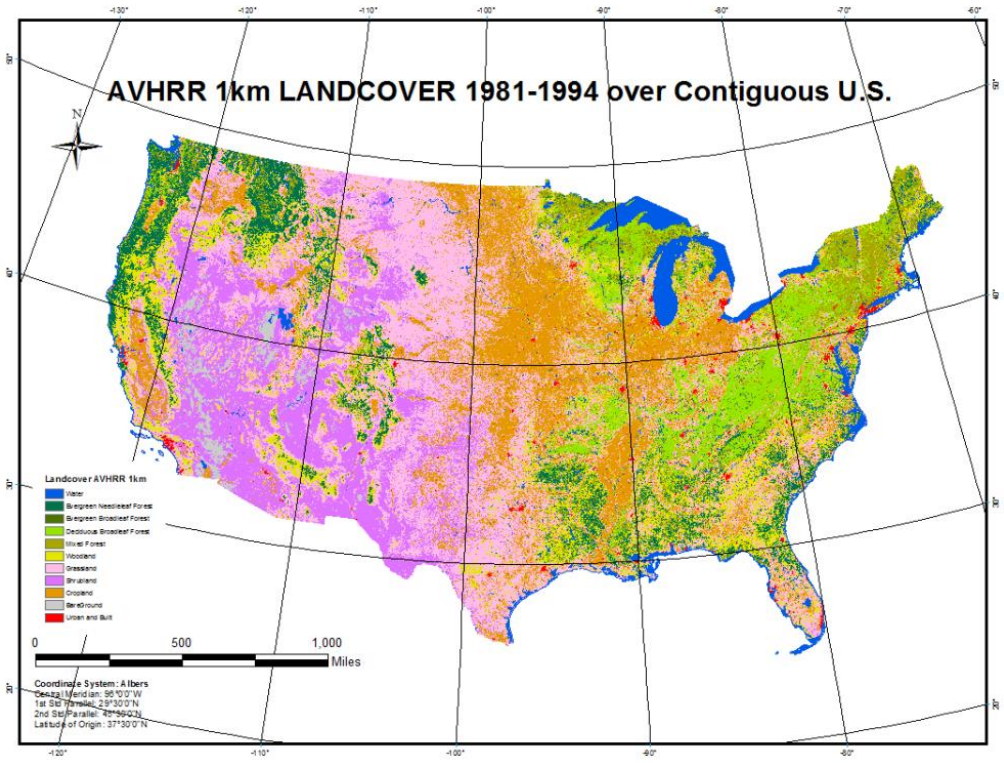

Figure 4.11: AVHRR 1km land cover over the contiguous U.S (1981-1994).

Figure 4.12: Forest density map. (United States aboveground woody biomass map with 66 ecoregions delineated. NASA Earth Observatory map by Robert Simmon. based on multiple data sets compiled and analyzed by the Woods Hole Research Center. Caption by Michael Carlowicz.).

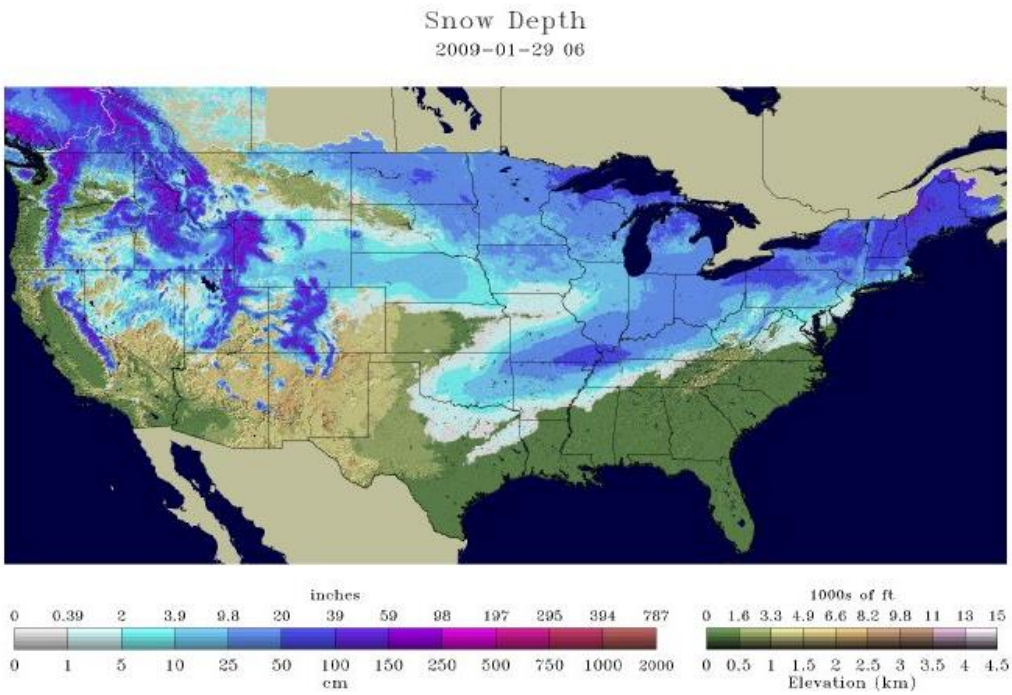

(a)

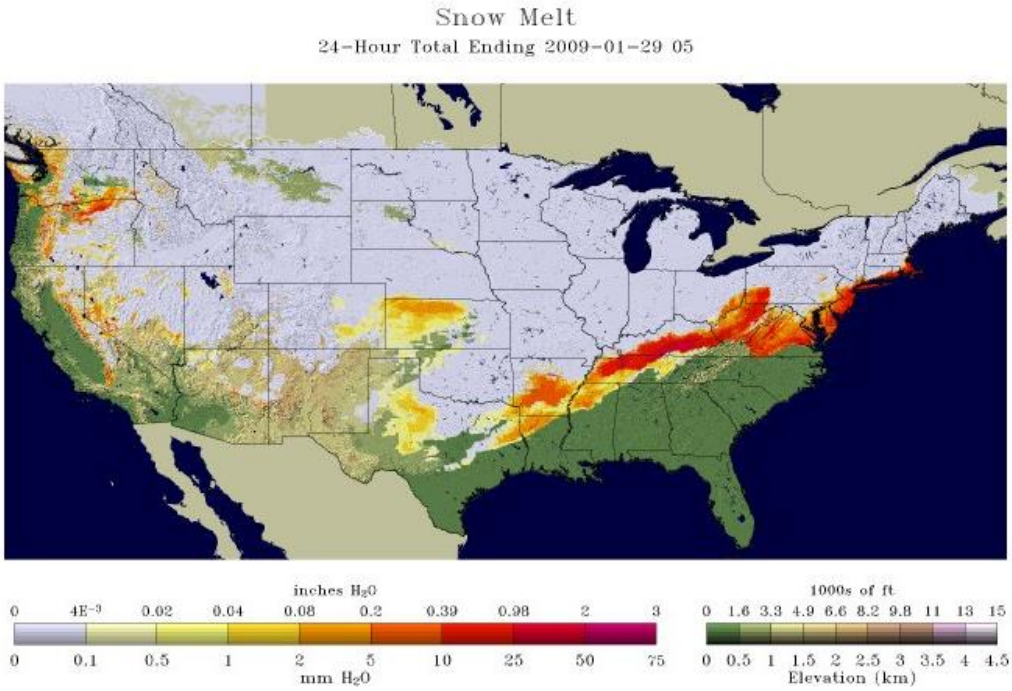

(b)

Figure 4.13: SNODAS snow depth (a) and snow melt (b) on 29 Jan. 2009.

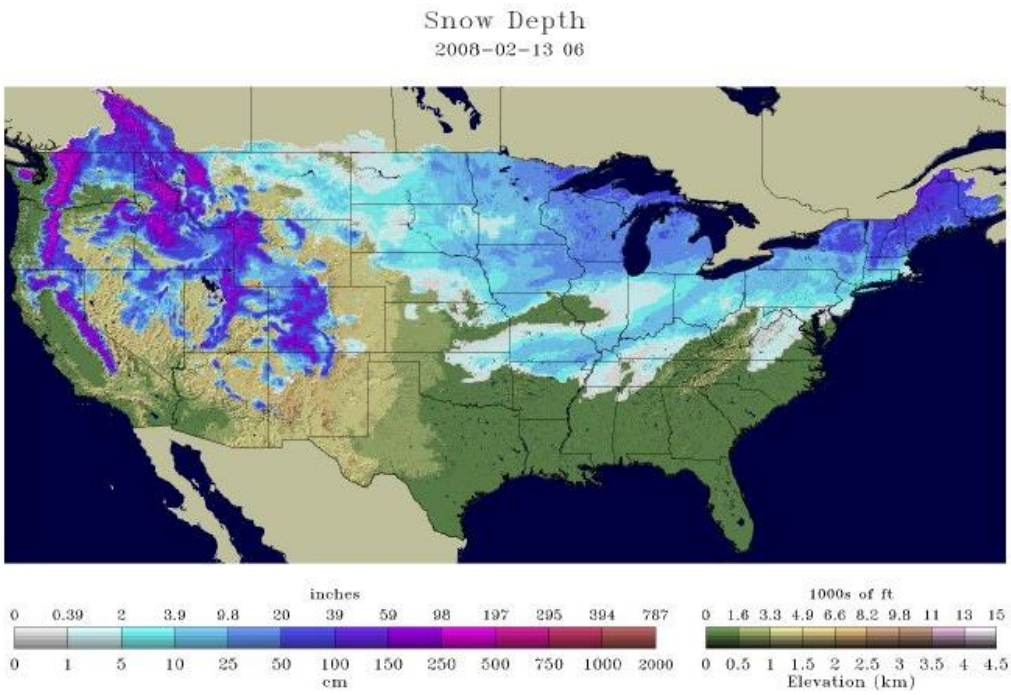

(a)

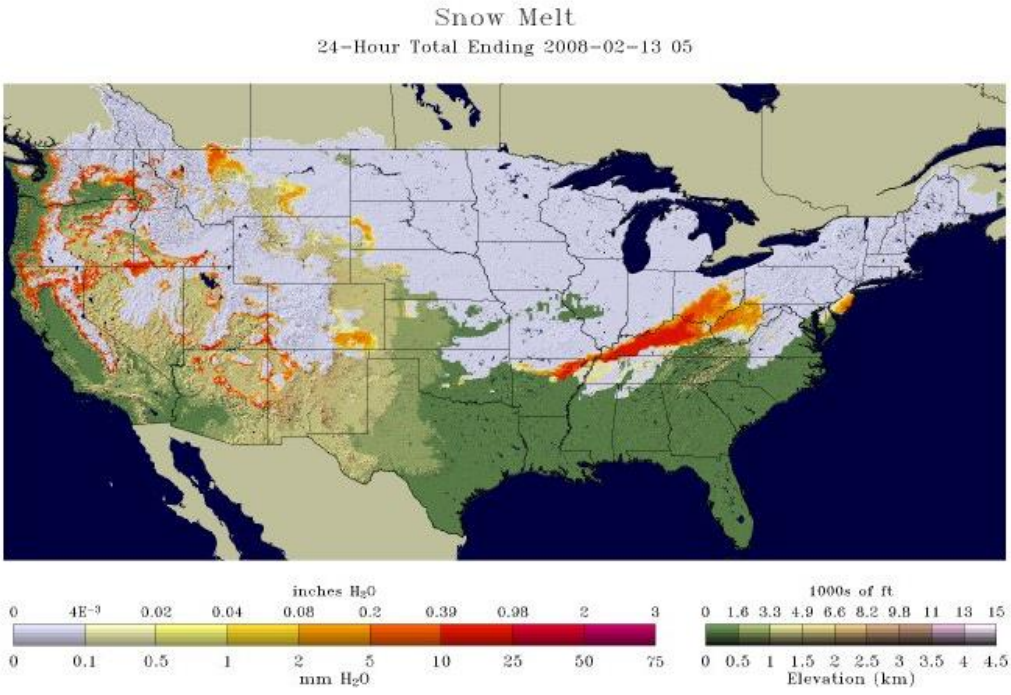

(b)

Figure 4.14: SNODAS snow depth (a) and snow melt (b) on 13 Feb. 2008.

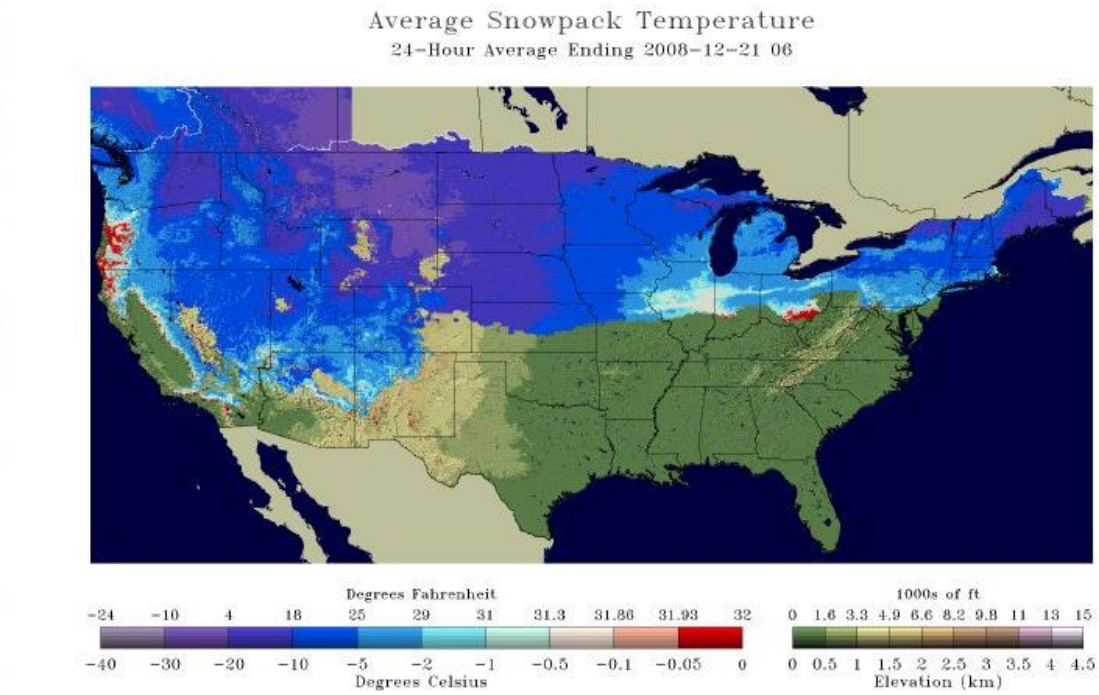

(a)

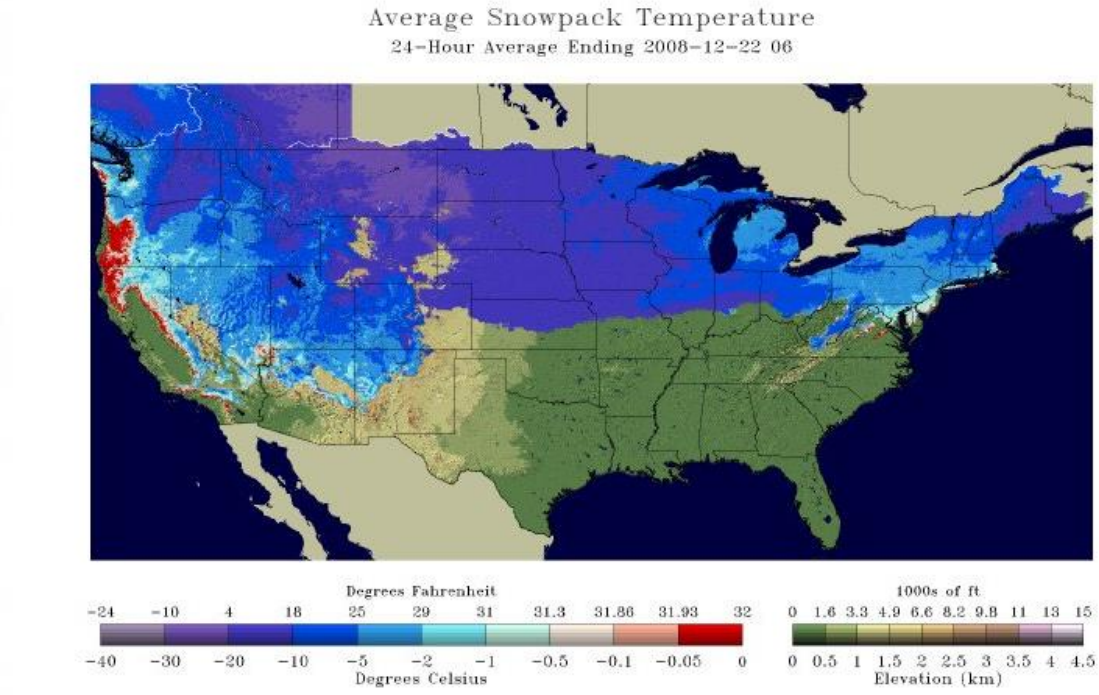

(b)

Figure 4.15: SNODAS snowpack temperature on 21 Dec. 2008 (a) and 22 Dec. 2008 (b).

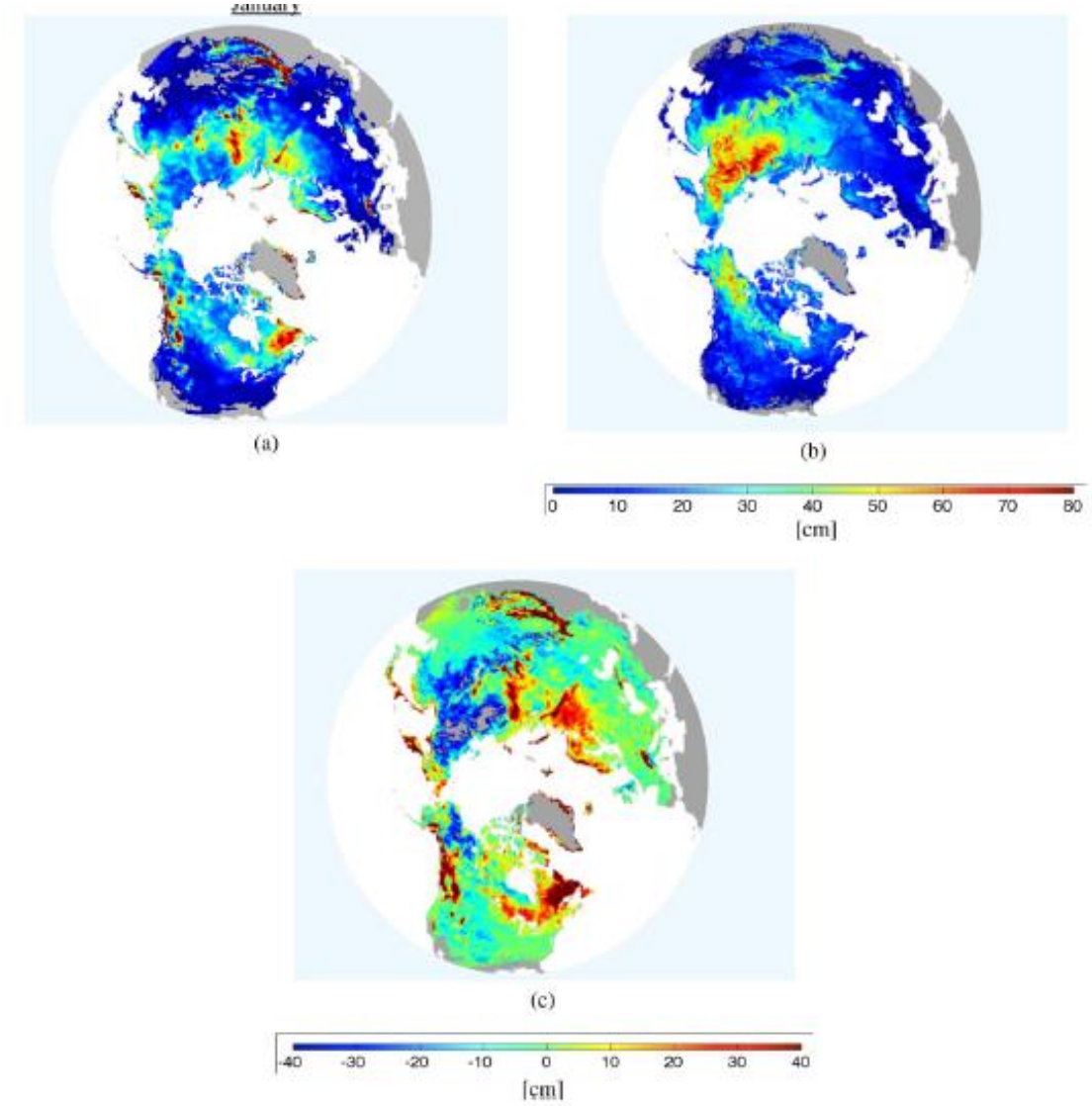

Figure 4.16: Comparison of AMSR-E and CMC SD for Jan. from Frei et al. (2012). (a) CMC estimated monthly mean snow depth. (b) AMSR-E estimated monthly mean snow depth. (c) Difference (CMC minus AMSR-E) in monthly mean snow depths.

4.2 Analysis of interpolation performance

The second objective was to evaluate the error of 10 classic interpolations on the COOP SD aimed at selecting the optimum interpolation technique. The methods used to address this objective were: (1) all of the COOP data were interpolated using different methods and evaluated using cross validation, (2) daily COOP data were split into two files with 20% of the data in one document for performance evaluation and 80% of the data in the second document for generating interpolation methods, and (3) different weights were assigned to cross validation (CV) and data splitting (DS) in order to see which interpolation technique suit dense/sparse network better.

4.2.1 Results of analysis of interpolation performance

Table 4.7 shows the CV results of the ten interpolation methods. A pattern was detected that the three months (January, February and March) with more SD had larger RMSE than month with less SD (December). By examining the seasonal average RMSE value of the ten interpolation approaches, cokriging (CO) was identified to have the best performance (17.27 cm), followed by completely regularized spline (CRS, 17.59 cm) and spline with tension (SWT, 17.61 cm).

Table 4.8 shows data splitting (DS) results of the ten interpolation methods. The same trend was seen in which large SD values are accompanied by greater error. CRS had the lowest RMSE (17.16 cm), followed by inverse distance weighted (IDW, 17.24 cm) and SWT (17.31 cm) of the 10 interpolation methods.

Figure 4.17 shows CV and DS evaluations for different interpolations. Global polynomial interpolation (GP) and thin plate spline (TPS) had comparatively higher CV and DS results. Other methods had similar RMSE around 10 cm, among which IDW and CRS had slightly lower RMSE than LP, kriging, CO, inverse multiquadric function (IMF), multiquadric function (MF)

and SWT. For most interpolation methods, CV and DS results were similar, however, CO (0.65 cm) and GP (0.3 cm) have comparatively larger differences between CV and DS.

Even though RMSE has been widely used to evaluate the performance of different models in the climate and environmental studies to assess accuracy, RMSE fails to take spatial consistency into consideration. For example, RMSE value can be largely enhanced (i.e. worse model performance) with extreme values over only couple of points (i.e., large error magnitude over very small amount of stations may cause large RMSE value for the interpolation method, which will further lead to inaccurate conclusion of bad model performance). To address the limitation of RMSE, a spatial analysis was generated in order to observe the patterns for all of the interpolation methods (i.e. to spatially examine extreme and unusual values). 29 January 2009 was selected for this analysis as it had the second largest daily SD over the time period with normal number of reporting stations. Figures 4.18–4.22 show SD interpolated using IDW and GP, LP and CO, OK and CRS, thin plate spline (TPS) and MF, and SWT and IMF.

The spatial patterns for the interpolation methods can be divided into five categories: (1) large SD values over the Great Lakes, Rocky Mountains, New England, and the mountainous areas of Washington, Oregon and California, and no snow over the South and west coast California (IDW, OK, CRS, SWT, LP and IMF), (2) the characteristics mentioned in the previous pattern and positive SD values over random locations over west coast California and the South (e.g., CO), (3) “bulls eye pattern” over the Great Lakes and Rocky Mountains (IDW, TPS and MF), (4) little SD values over mountainous areas of Washington, Oregon and California (OK and CO); (5) smooth pattern over the study area with less snow over the Rocky Mountains, and the mountainous areas of Washington, Oregon and California (GP). In addition to the spatial

patterns mentioned above, negative SD values were noted when interpolated using LP, GP, OK, TPS and MF.

Based on Sluiter (2009), CV is an evaluation for each individual station, and DS is an evaluation for multiple stations or an area. Therefore, if researchers focus on the individual location interpolation precision, CV is recommended. However, if multiple locations or a large area interpolation precision is more important, DS is recommended. Therefore, by assigning different weights to CV and DS results for interpolation methods, one can attempt to ascertain whether an interpolation method provides better results for a dense or sparse network.

Table 4.9 showed how weights were given to CV and DS based on previous CV and DS results. Different interpolation methods will be evaluated by different weighting systems and these are ranked in order of DS (DS_rank), CV (CV_rank), No Weight (Rank1), Weight1 (Rank2), Weight2 (Rank3), Weight3 (Rank4), Weight4 (Rank5).

Table 4.10 shows the results of using different weight combinations. From No Weight, Weight1 and Weight2 combinations, CRS had the best performance followed by IDW, CO and SWT. From Weight3 combination, CO had the lowest RMSE, followed by CRS and IDW. IDW was noted to have the best performance from Weight4 combination, followed by CRS and SWT.

Table 4.11 shows the rank results for different interpolation methods with different weighting systems. At first glance, the best interpolation methods for different weighting systems were IDW, CO, CRS, and SWT. However, by assigning different weights, the results change. For example, when looking at Rank1, CRS provided the best results followed by SWT and IDW. However, when looking at Rank 4, CO provided the best results, followed by CRS and SWT. A summary of the comparisons is shown in Figure 4.23.

Beginning with the simplest assumption, and lacking a reason to do otherwise, CV and DS were evenly important (i.e., No Weight combination is adopted), indicating that both individual location and areal interpolation precision are important. Therefore, the performance of interpolation can be ranked, from the best to the worst as follows: CRS, IDW, CO, SWT, LP, MF, IMF, kriging, TPS and GP. Based on visual analysis, LP, CO, and GP are found to have unreasonable SD values over some areas. For this reason, the use of the optimum interpolation method for further analysis was selected from the methods other than LP, CO and GP. Based on results from both statistical and spatial analyses, CRS was chosen as the optimal interpolation method for the COOP SD observations.

4.2.2 Discussion of analysis of interpolation performance

From the results of the interpolation optimization, it is shown that: (1) all of the interpolation methods except GP (CV = 21.68 cm, and DS = 20.87 cm) exhibited similar results ranging from 17.27 cm to 19.79 cm for CV, and 17.16 cm to 19.48 cm for DS, (2) CO provided the best CV results followed by CRS and SWT, although CRS had the best DS result followed by IDW and SWT and, (3) to interpolate values to large area with a limited number of COOP stations (CV and DS are added together as an index for interpolation optimization) CRS gave the best performance.

As mentioned by Harshburger et al. (2010), station numbers for generating interpolation can affect the performance of different interpolation techniques. This research also studied on which interpolation methods work bettered with more stations (dense network) or less stations (sparse network). As mentioned previously, CV used almost all the stations available for interpolation with only one station excluded for evaluation. Meanwhile, DS used three quarters of the stations and used another quarter of the data for evaluation. In other words, if the

interpolation technique has a lower CV rank (e.g. 1) than DS rank (e.g. 3) (i.e. a better CV evaluation performance than DS performance), it indicates that the interpolation works better with a dense network than a sparse network. On the other hand, if the interpolation method has a lower DS rank than CV rank, it indicates that the interpolation work better with a sparse network than a dense network. Therefore, by examining the CV and DS rank difference (CDRD) of each interpolation technique, it is possible to identify which interpolation method works better for a dense or sparse station network.

Table 4.12 lists the CDRD values for different interpolation methods. The CDRD values for IDW, LP, CRS and IMF were above zero, meaning they work better based on relatively sparse station networks, and likely better predict SD values over large areas. Meanwhile, the CDRD values for GP, kriging, SWT, MF and TPS were unchanged, meaning the interpolation results were not affected by either the change of station density, neither by single value prediction nor by values over large areas. CO was the only interpolation technique with negative CDRD value and was very likely sensitive to the station density. The CDRD value for CO further indicated a great potential of interpolation of SD by combining SD with DEM based on dense networks, consistent with previous studies of comparatively smaller regions (Fassnacht et al. 2003). However, the IMS SCE data was very important in the process of eliminating meaningless interpolated values over southern areas of the U.S. where no snow cover was present.

All interpolation techniques except kriging and CO are deterministic methods, which create surfaces from measured points, either based on degree of smoothing (e.g. CRS) or the extent of similarity (e.g. IDW). GP delivered the worst performance as a result of using the entire dataset to predict unknown values, thus, it was unable to detect regional variation. GP and LP are

both inexact interpolation methods. Each may provide better results when predicting a smooth surface without peak values. IDW and all RBF interpolations (CRS, SWT, MF, IMF and TPS) are exact interpolations; however, unlike IDW, RBF can predict values larger than the maximum or less than the minimum measured values. This may lead to better prediction when large snow variations exist.

As opposed to deterministic interpolation techniques, both kriging and cokriging are geostatistical methods that take spatial autocorrelation into account. Therefore, better kriging results can be obtained when the two stations are sufficiently close and the SD measurements from the two stations are spatially dependent. However, because the distance between COOP stations can be tens to hundreds of km, stand-alone kriging does not adequately model SD due to possible large variations of values over these distances. The RMSE for CO interpolation decreased greatly (i.e., better interpolation performance) based on both CV and DS values by incorporating a DEM as an additional source.

Table 4.7: Statistics of snow depth RMSE evaluated by cross validation.

Method	Dec 2007	Jan 2008	Feb 2008	Mar 2008	Dec 2008	Jan 2009	Feb 2009	Mar 2009	AVE	Rank
IDW	9.35	17.15	22.18	27.85	9.79	15.19	17.74	22.27	17.69	4
LP	9.23	17.10	22.39	28.30	9.92	15.31	18.18	23.02	17.93	6
GP	12.05	21.20	27.79	33.21	12.32	18.71	21.82	26.37	21.68	10
Kriging	9.74	18.00	23.47	29.37	10.30	16.05	18.92	23.70	18.69	8
CO	8.97	16.73	22.12	27.19	9.45	14.85	17.35	21.50	17.27	1
CRS	9.26	16.86	22.05	27.74	9.70	15.11	17.81	22.19	17.59	2
SWT	9.26	16.93	22.13	27.75	9.72	15.17	17.67	22.21	17.61	3
MF	9.56	17.26	22.24	27.90	10.08	15.52	18.00	22.42	17.87	5
IMF	9.72	17.91	23.51	28.51	10.10	15.99	18.39	22.43	18.32	7
TPS	10.78	19.39	24.50	30.33	11.35	17.46	19.91	24.62	19.79	9

Table 4.8: Statistics of snow depth RMSE evaluated by data splitting.

Method	Dec 2007	Jan 2008	Feb 2008	Mar 2008	Dec 2008	Jan 2009	Feb 2009	Mar 2009	AVE	Rank
IDW	9.76	16.90	21.27	26.83	9.86	15.13	17.24	20.90	17.24	2
LP	9.70	16.77	21.11	26.64	9.86	15.03	17.75	21.77	17.33	4
GP	12.05	20.59	26.40	31.65	12.24	18.37	20.73	24.94	20.87	10
Kriging	10.06	17.83	22.59	27.91	10.31	15.79	18.39	22.27	18.14	8
CO	10.11	17.94	22.73	28.04	10.36	15.88	16.83	22.39	18.04	7
CRS	9.79	16.86	21.25	26.71	9.84	15.17	17.22	20.42	17.16	1
SWT	9.90	17.06	21.34	26.91	9.94	15.31	17.38	20.68	17.31	3
MF	9.97	17.24	21.46	26.93	10.08	15.40	17.66	21.23	17.50	5
IMF	10.27	17.67	21.97	27.79	10.26	15.93	17.74	20.88	17.82	6
TPS	11.09	19.48	23.84	29.74	11.31	17.21	19.57	23.64	19.48	9

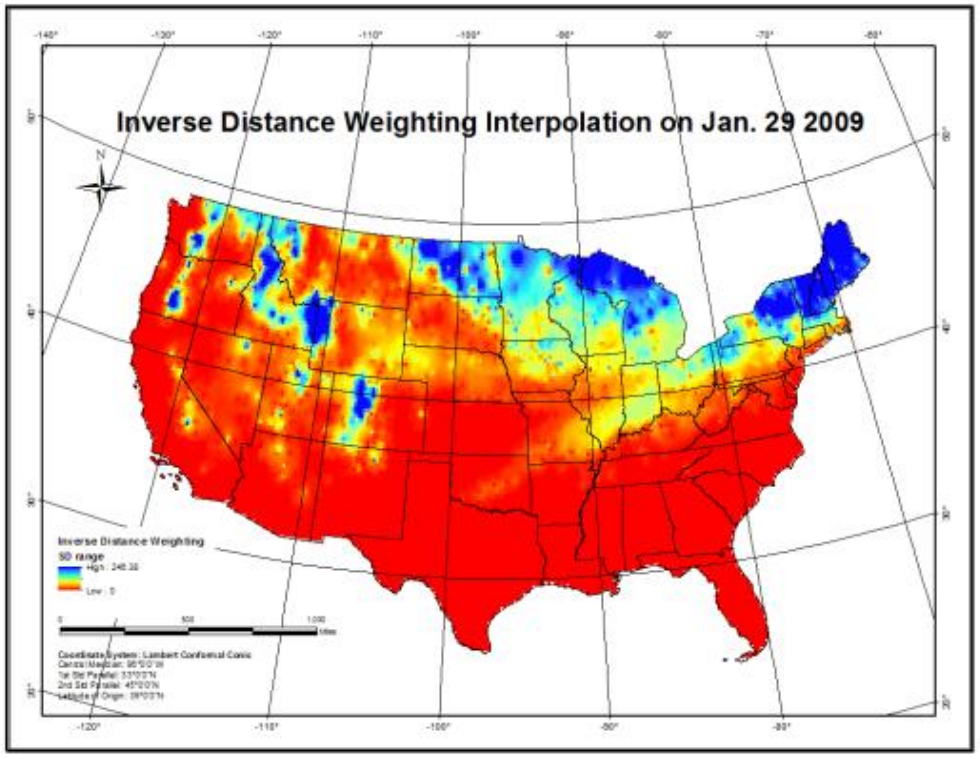

(a)

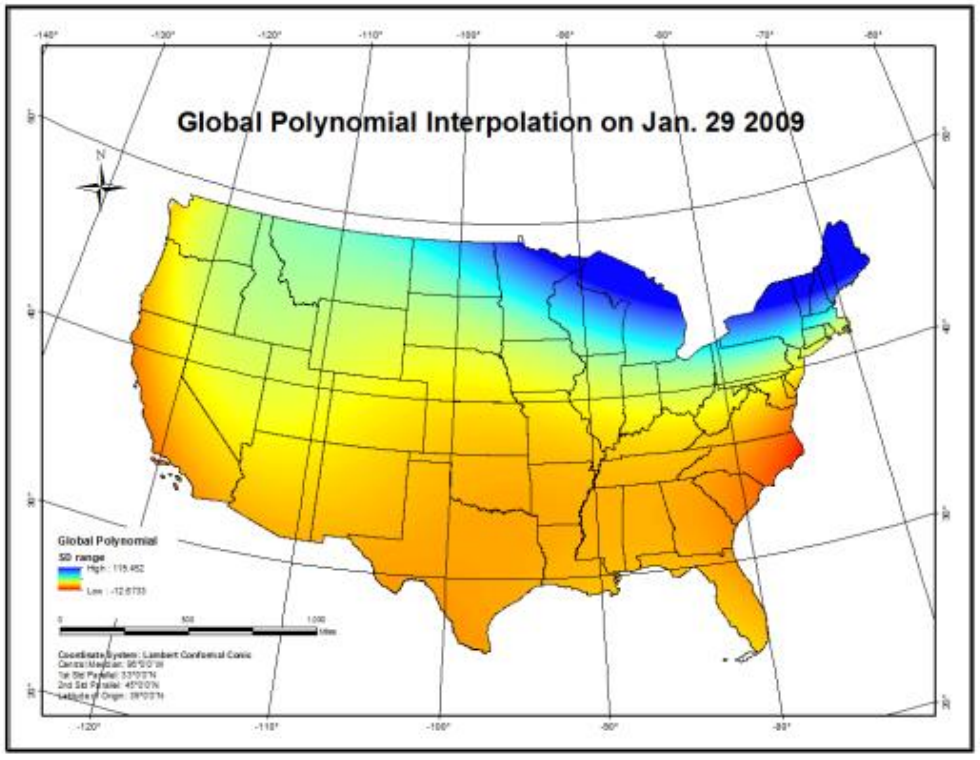

(b)

Figure 4.17: IDW (a) and GP (b) interpolation for 29 Jan. 2009.

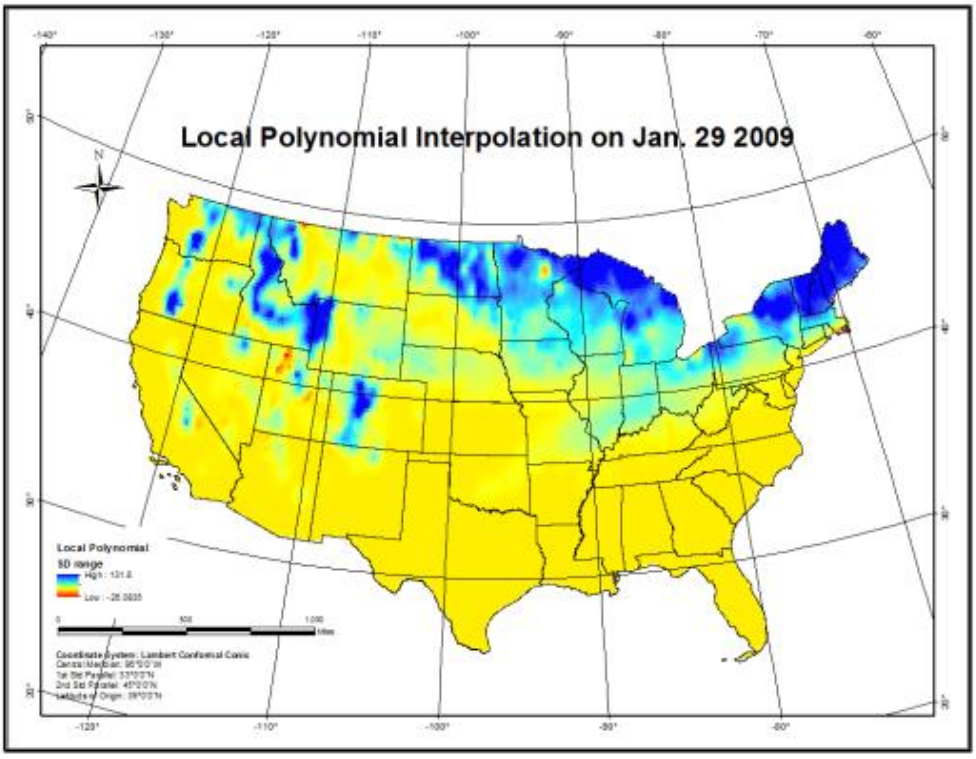

(a)

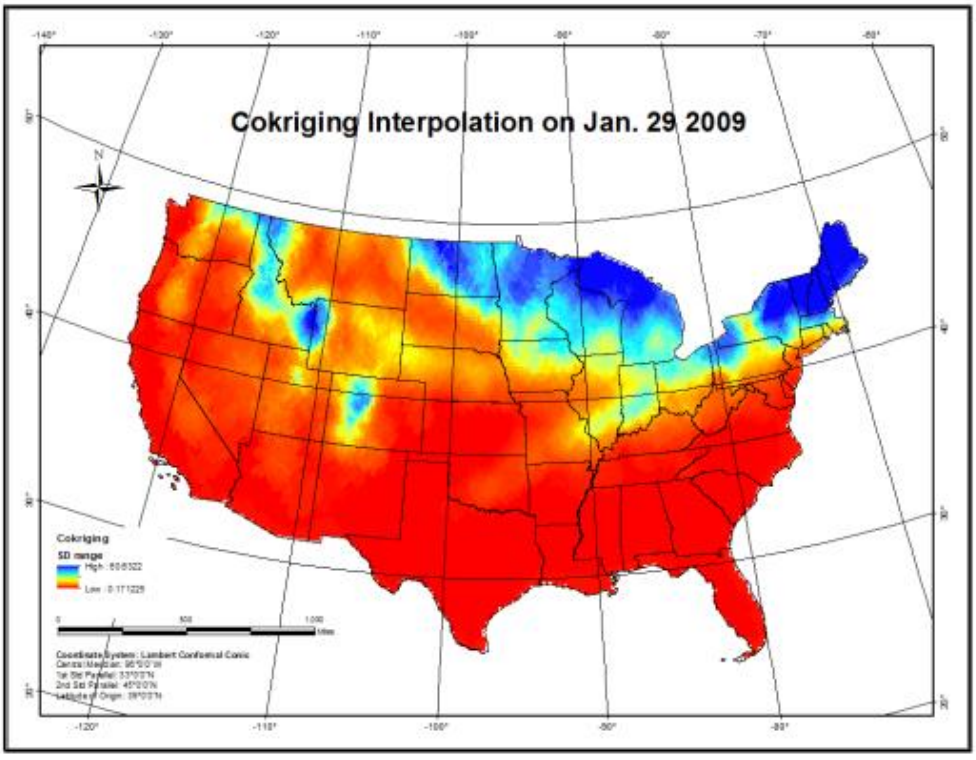

(b)

Figure 4.18: LP (a) and CO (b) interpolation for 29 Jan. 2009.

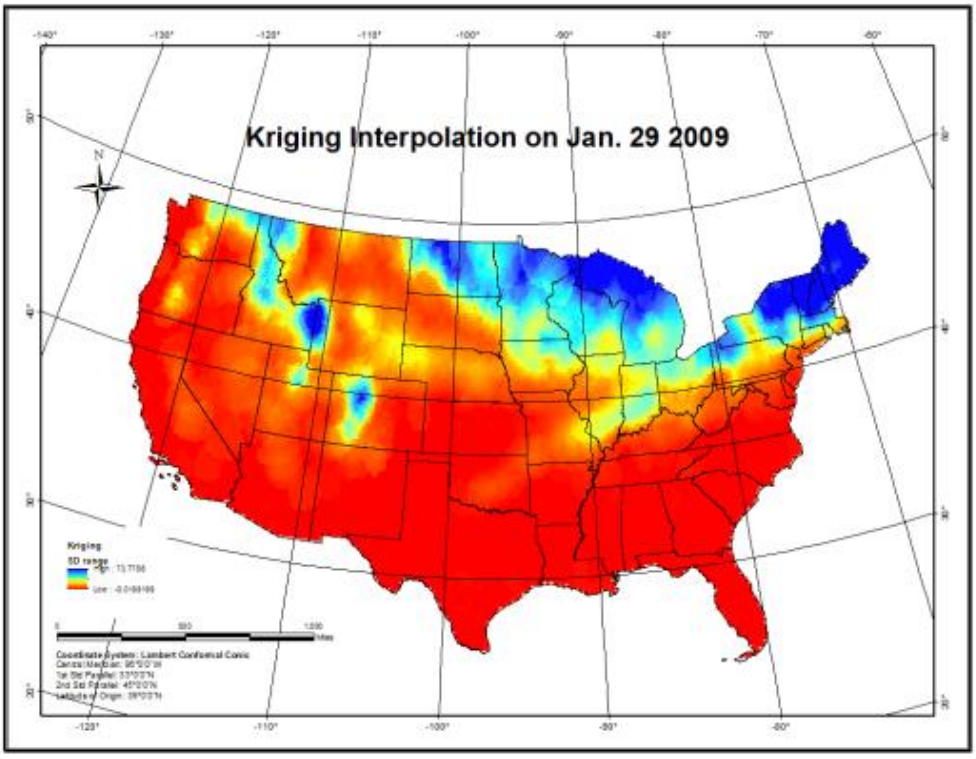

(a)

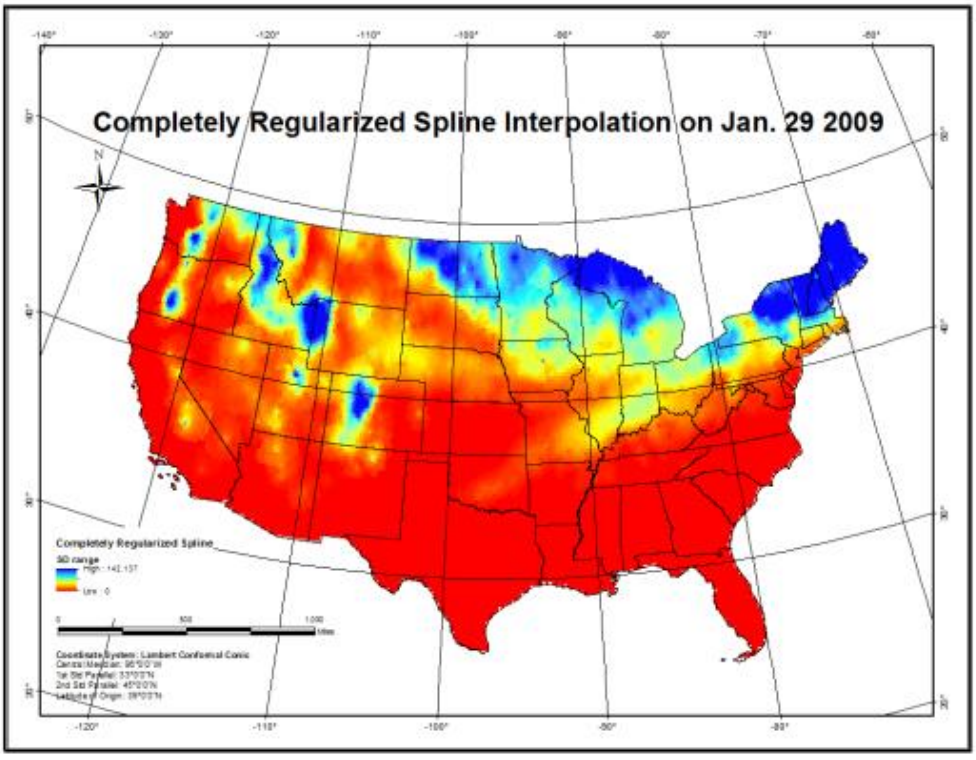

(b)

Figure 4.19: OK (a) and CRS (b) interpolation for 29 Jan. 2009.

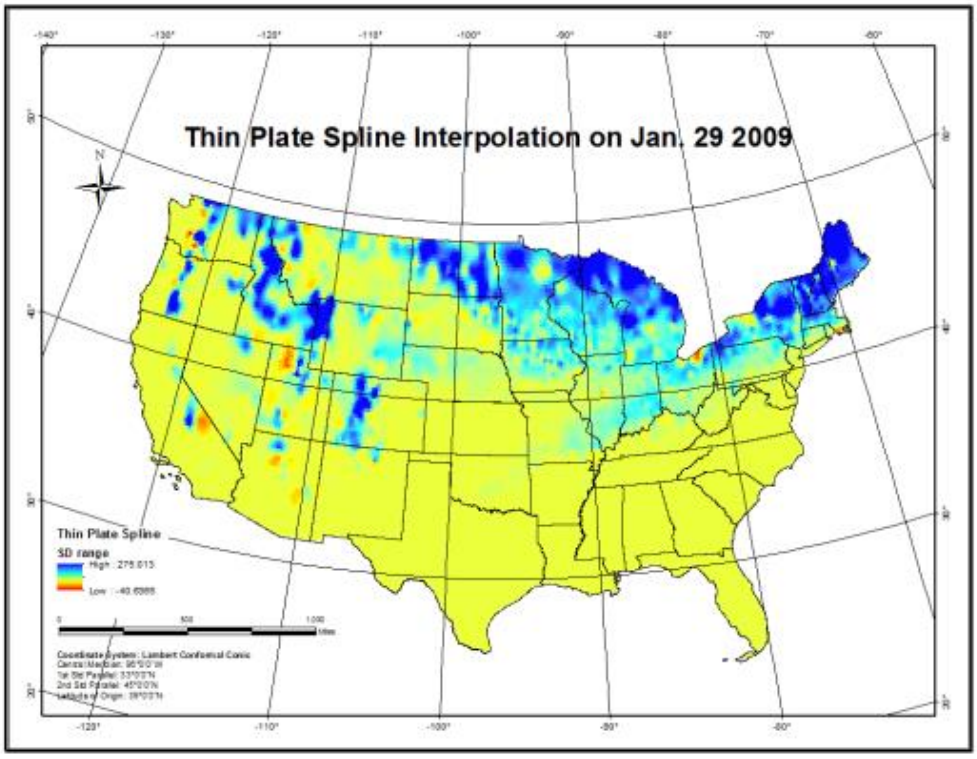

(a)

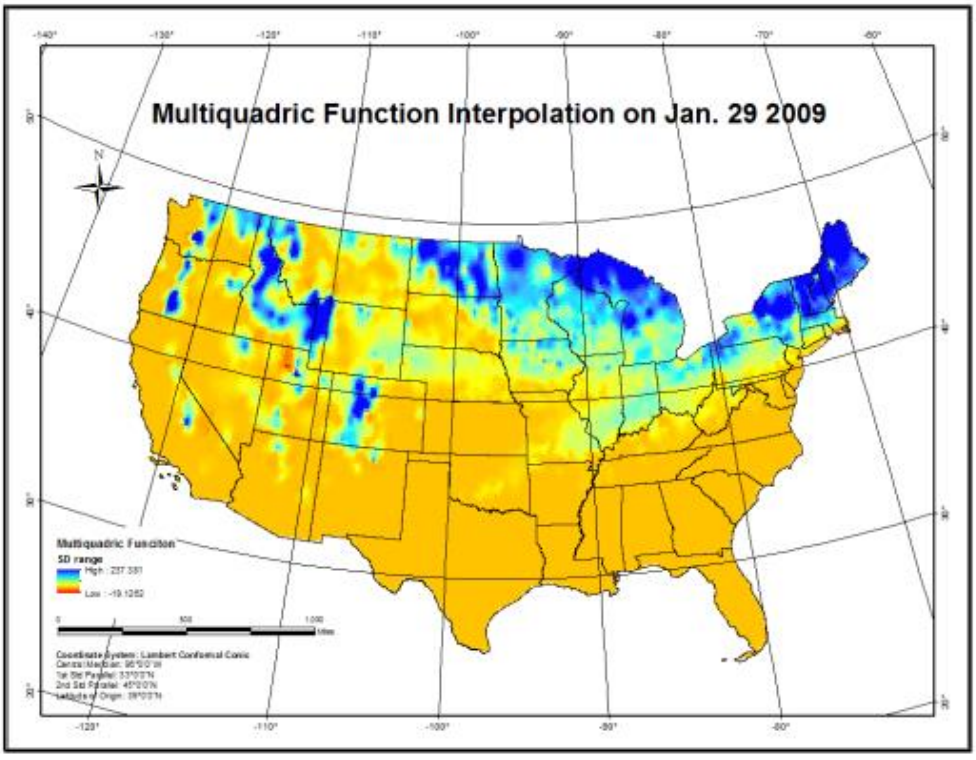

(b)

Figure 4.20: TPS and MF interpolation for 29 Jan. 2009.

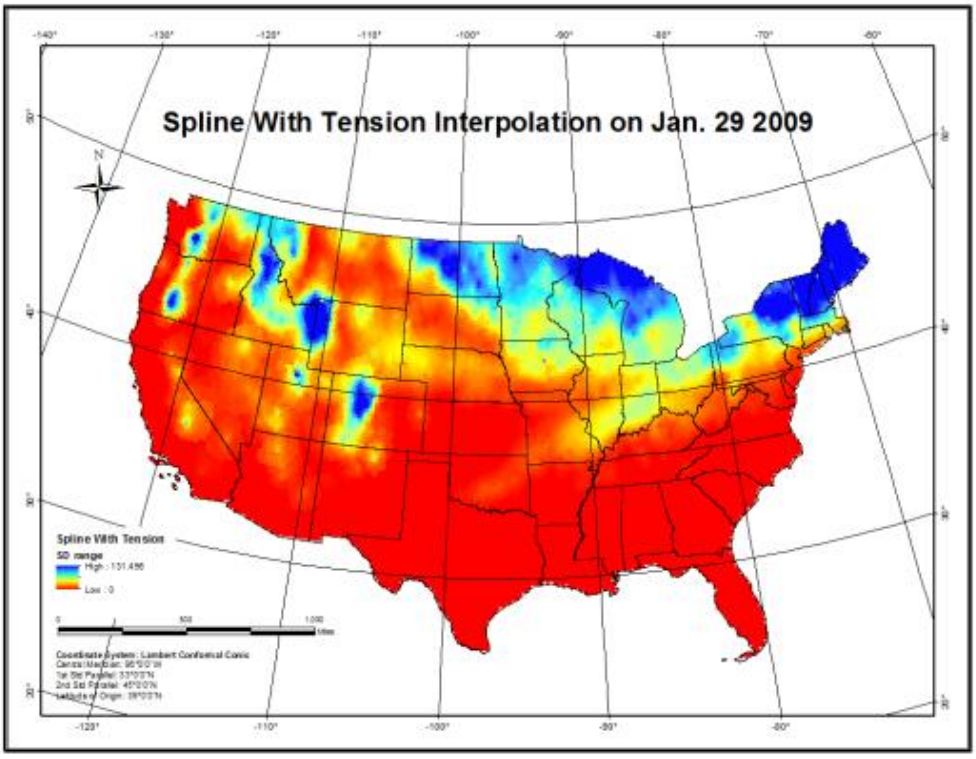

(a)

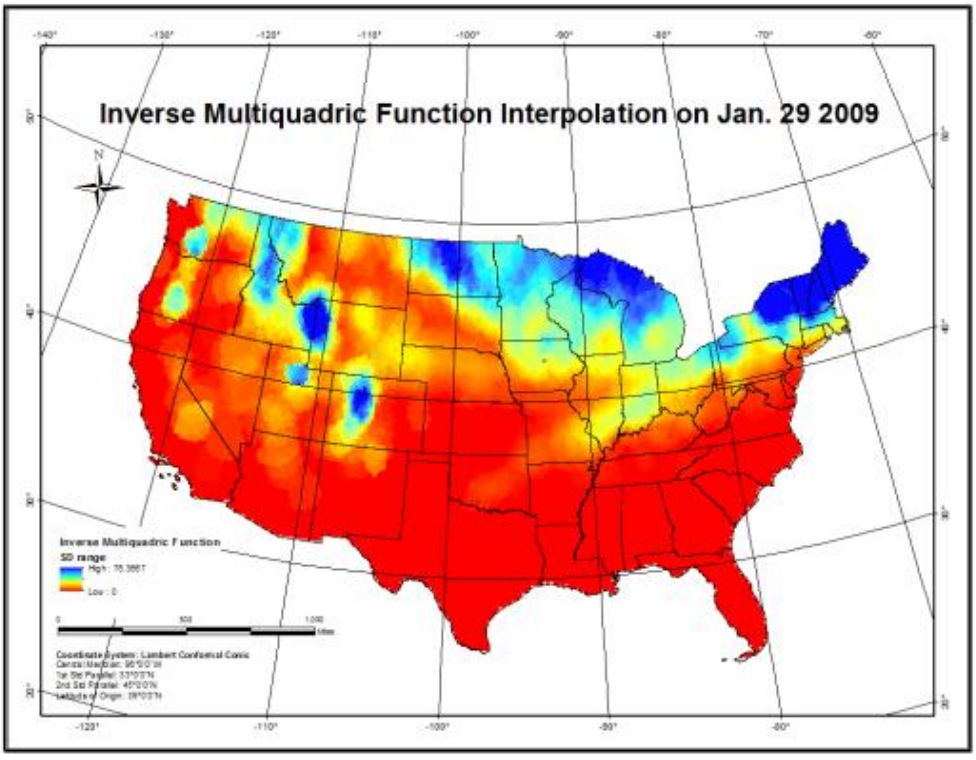

(b)

Figure 4.21: SWT (a) and IMF (b) interpolation for 29 Jan. 2009.

Table 4.9: Variable calculation methods.

Variable	Equation	Rank
No Weight	CV+DS	Rank1
Weight1	2*CV+DS	Rank2
Weight2	CV+2*DS	Rank3
Weight3	4*CV+DS	Rank4
Weight4	CV+4*DS	Rank5

Table 4.10: Result of using different weighting systems.

Method	DS_Ave	CV_Ave	No Weight	Weight1	Weight2	Weight3	Weight4
IDW	17.33	17.69	35.02	52.71	52.35	88.09	87.00
LP	17.82	17.93	35.75	53.68	53.56	89.54	89.19
GP	20.87	21.68	42.55	64.24	63.42	107.60	105.16
Kriging	18.14	18.69	36.84	55.53	54.98	92.92	91.26
CO	17.16	17.27	34.43	51.70	51.59	86.25	85.91
CRS	17.24	17.59	34.83	52.42	52.06	87.60	86.53
SWT	17.31	17.61	34.92	52.52	52.23	87.74	86.86
MF	17.50	17.87	35.37	53.24	52.86	88.98	87.86
IMF	18.04	18.32	36.36	54.68	54.39	91.32	90.46
TPS	19.48	19.79	39.28	59.07	58.76	98.65	97.73

Table 4.11: Rank of different interpolation methods with different weighting system.

Method	DS_Rank	CV_Rank	Rank1	Rank2	Rank3	Rank4	Rank5
IDW	3	4	3	4	2	4	2
LP	4	6	4	5	4	6	4
GP	10	10	10	10	10	10	10
Kriging	8	8	8	8	8	8	8
CO	5	1	5	3	6	1	6
CRS	1	2	1	1	1	2	1
SWT	2	3	2	2	3	3	3
MF	6	5	6	6	5	5	5
IMF	7	7	7	7	7	7	7
TPS	9	9	9	9	9	9	9

Table 4.12: CV and DS rank difference (CV - DS).

Method	CV Rank	DS Rank	Rank difference (CV-DS)
IDW	4	2	2
LP	6	4	2
GP	10	10	0
Kriging	8	8	0
CO	1	7	-6
CRS	2	1	1
SWT	3	3	0
MF	5	5	0
IMF	7	6	1
TPS	9	9	0

4.3 Synthesis modeling and evaluation

The third objective was to use five interpolation methods from Cao (2012) and produce a best synthesis combining satellite SD, SCE and COOP SD observations and then compare to stand-alone SD products. The methods used to address this objective were: (1) mean absolute error (MAE), r, and root mean square error (RMSE) were calculated based on CoCoRaHS SD observations, (2) a spatial analysis of all synthesis results on 29 January 2009 was conducted. For both evaluation procedures, the optimum synthesis results were compared to stand-alone satellite estimates and stand-alone interpolated COOP SD.

4.3.1 Results of synthesis modeling and evaluation

The MAE, RMSE and r for the five methods, SD retrievals from AMSR-E SWE, interpolation techniques incorporating ground stations and SCE (ISCE) over the study period are listed in Table 4.13, Table 4.14 and Table 4.15, respectively. In this research, the best detection performance is assured when the method has (1) the lowest MAE value, (2) the lowest RMSE value, and (3) an r value closest to 1.

From Table 4.13, all of the bias correction methods (DC, DMC, RMC, and SC) improved the AMSR-E estimates, except RC. Of those, DC (6.80 cm) had the best performance followed by DMC (9.23 cm) and RMC (9.23 cm). However, none of the bias correction methods performed as well as ISCE. Similar to previous MAE results, ISCE revealed the best results with a RMSE equal to 11.27 cm and r equal to 0.61, followed by DC (RMSE = 14.37 cm, r = 0.56). All of the DMC (17.70 cm), RMC (17.78 cm), and SC (17.80 cm) methods had better RMSE results compared to the stand-alone AMSR-E SWE value. Compared to MAE results, all of the stand-alone AMSR-E SD retrievals (r = 0.16), RC (r = 0.25) and SC (r = 0.22) had higher r values than DMC (r = 0.05) and RMC (r = 0.02) (see Tables 4.14 and 4.15). Table 4.16 lists the MAE, RMSE, and r values generated from the seven methods, the five methods from Cao et al

(2012) and stand-alone AMSR-E and interpolated COOP. The corresponding graph is shown in Figure 4.24 (r values shown multiplied by 10). The results showed that both DC and SC had better results than stand-alone AMSR-E SD retrievals; however, all of them showed less promising results than ISCE.

Figures 4.25–4.28 represented the spatial analysis for the five methods, stand-alone AMSR-E SD retrievals, and ISCE on 29 January 2009. Figures 4.24–4.27 show the stand-alone AMSR-E SD and ISCE, post DC SD and post RC SD, post DMC SD and post RMC SD, and post SC SD, respectively. Darker blue depicts larger SD, while darker red depictes smaller SD.

Post DMC SD, post RMC SD and post SC SD shared a similar pattern with stand-alone AMSR-E SD. Deep snow was detected over western Colorado, southeastern Idaho, Washington, Oregon, Montana, North Dakota and Minnesota. Post DC SD shared a similar pattern with the interpolated COOP SD (i.e., large SD values mainly over New England, Great Lakes, Rocky mountains, especially over mid-western Colorado and boundary between Idaho and Wyoming). Post RC had an unusual pattern with shallow snow over a large area. Some snow was detected over New England, parts of New York and Pennsylvania, the Great Lakes, western Colorado, over the boundary between Idaho and Wyoming, and northwestern Montana. Large SD was detected in limited New England and Great Lakes areas. However, the SD detected after RC was in either dot shape or a band shape. From the stand-alone AMSR-E SD map, we can identify some snow over southwestern New Mexico and western Texas.

The SD ranges for stand-alone AMSR-E SD, ISCE, post DC, post RC, post DMC, post RMC and post SC were 0.00 - 200.64 cm, 0.00 - 158.8 cm, 0.00 - 204.83 cm, 0.00 - 1630.31 cm, 0 - 12.40 cm, 0 - 10.58 cm, 0.00 - 232.43 cm, respectively.

4.3.2 Discussion of synthesis modeling and evaluation

All of the potential methods for synthesis optimization proposed in this paper gave lower MAE and RMSE values (with the exception of RC) compared to stand-alone AMSR-E SD retrievals. Among all the methods, DC provided the best results (MAE = 6.80 cm, RMSE = 13.31 cm, r = 0.56). However, none of the DMC, RMC and SC methods worked well with pattern correction. Each increased the SD values over central and New England, which might be the main reason of low MAE and RMSE when evaluated by CoCoRaHS dataset. Both DMC and RMC had a very low r because (1) they were able to correct the spatial SD distribution and (2) due to the low correlation between the ground truth SD and the SD retrieved after analysis. Post SD ranges were found to be 0–12.41 cm and 0–10.58 cm, respectively.

RC gave a comparably high r value, which suggested that the post RC SD data had a better spatial agreement with the ground truth data when compared to DMC and RMC. RC had a very high MAE (16.34 cm) and RMSE (60.99 cm) owing to the original COOP SD values equaled to 0 being set to a small non-zero value (0.0001) cm for interpolation. Therefore, the post RC SD would be exaggerated even if the stand-alone AMSR-E were set to a higher non-zero value (e.g., 0.01 cm).

A spatial evaluation of DC performance was conducted following Eqn. 4.1 below:

$$\mathrm{CACD} = (\mathrm{Xcocorahs} - \mathrm{Xamsre}) - (\mathrm{Xcocorahs} - \mathrm{Xdc}) \tag{4.1}$$

where:

Xcocorahs = CoCoRaHS SD measurement;

Xamsre = extracted AMSR-E SD estimates for CoCoRaHS locations;

Xdc = extracted post DC SD estimates for CoCoRaHS locations.

Figure 4.29 shows the CoCoRaHS stations utilized to evaluate correction methods on 29 January 2009. Higher (lower) value represented better (worse) performance. The dots in Figure 4.29 represent CoCoRaHS station distribution on 29 Jan. 2009. The darker red represent worse DC performance and darker blue represent better performance. Most stations within the snow boundary have been successfully corrected, especially those stations over Indiana, eastern Illinois, Michigan, New York State, western Iowa, northern Idaho, North Dakota and Indiana. However, stations along the snow boundary over Tennessee, Maryland, New Jersey, western Ohio, and Oregon are noted with negative values, indicating worse performance. Some negative values can also be identified over eastern Colorado and Kansas. Both positive and negative values were found evenly distributed over Wyoming, Nebraska, Utah, Montana and Colorado. Reduced accuracy of AMSR-E SD was noted over part of central region and the areas outside of SCE, although this may be due to the inaccuracy of IMS SCE.

A natural break has been used to symbolize the spatial evaluation results in Figure 4.29. Therefore, the success of the correction results can be more clearly identified. The best DC performance (blue) was found over western Colorado, North Dakota, northeastern South Dakota, west central Iowa, Michigan, central region of Indiana and central New York State. The least successful DC performance (red) was noted over central Colorado and northern Washington.

Different observation time may be an important factor influencing SD comparison between different data sources. For most of COOP stations, SD measurements are taken around 7 am local time. As CoCoRaHS is a relatively new station network, CoCoRaHS observation time has not been well documented. Table 4.17 showed CoCoRaHS observation counts over 24 hours. A corresponding figure is shown in Figure 4.30. From Table 4.17, over 90% of SD observations were taken between 6am to 9am (7am - 8am = 67%, 8am – 9am = 16% and 6am – 7am = 9%),

which indicated that most of the CoCoRaHS measurements had similar observation time with COOP, which has a preponderance of morning observers.

Stand-alone interpolation indicated a better performance than all the post correction methods with MAE equal to 5.74 cm, RMSE equal to 11.27 cm and r equal to 0.61. DC performance was not as good as stand-alone interpolated COOP SD result. This may due to the CoCoRaHS data used for evaluation is clustered (i.e., most CoCoRaHS data are clustered over Colorado, Wyoming, Nebraska, Michigan, Indiana, eastern Illinois, Tennessee, Maryland, Delaware, Pennsylvania and New York), DC performance may better than stand-alone interpolated COOP if there is a more regularly distributed dataset available. This may also due to the adequacy of the station density for correct interpolation over contiguous U.S. Nevertheless, even though interpolation provides better SD estimates, many of the snow measurement networks in other countries are not as dense (e.g., Russia). Therefore, an easy to retrieve SD product based on accurate global datasets is still needed for research outside the U.S.

Table 4.13: MAE obtained with interpolated value, AMSR-E, and all the correction methods over time period.

	AMSR-E	DC	RC	DMC	RMC	SC	Interpolation
Dec 07	7.78	8.49	49.71	7.06	7.11	7.60	3.67
Jan. 08	10.18	5.87	8.48	7.78	7.80	11.23	5.09
Feb 08	11.00	6.76	11.08	10.28	10.36	11.93	5.92
Mar 08	10.88	7.87	15.44	10.32	10.40	11.16	7.64
Dec 08	9.52	5.08	11.75	8.31	8.26	8.76	4.15
Jan. 09	11.95	5.99	12.74	11.08	10.97	10.66	5.22
Feb 09	9.37	6.44	10.28	8.89	8.80	9.36	6.35
Mar 09	10.29	7.91	11.19	10.10	10.16	9.49	7.91
Average	10.12	6.80	16.34	9.23	9.23	10.02	5.74

Table 4.14: RMSE obtained with interpolated values, AMSR-E, and all the correction methods over time period.

	AMSR-E	DC	RC	DMC	RMC	SC	Interpolation
Dec 07	11.34	12.15	183.28	10.83	10.89	11.01	6.16
Jan. 08	15.92	10.34	15.83	14.39	14.52	16.80	8.85
Feb 08	19.80	13.39	27.90	19.70	19.81	20.09	11.46
Mar 08	21.13	15.99	95.10	22.82	23.03	21.18	14.91
Dec 08	15.55	9.37	86.39	13.48	13.38	14.06	7.12
Jan. 09	20.19	12.31	27.63	18.36	18.19	18.83	9.84
Feb 09	19.36	14.15	23.58	18.80	19.07	19.11	13.58
Mar 09	22.43	18.78	28.18	23.24	23.32	21.33	18.20
Average	18.22	13.31	60.99	17.70	17.78	17.80	11.27

Table 4.15: r obtained with interpolated values, AMSR-E, and all the correction methods over time period.

	AMSR-E	DC	RC	DMC	RMC	SC	Interpolation
Dec 07	0.13	0.41	0.57	0.06	0.06	0.20	0.65
Jan. 08	0.16	0.68	0.29	0.05	0.04	0.23	0.70
Feb 08	0.19	0.64	0.22	0.05	0.05	0.27	0.66
Mar 08	0.27	0.61	0.08	0.04	0.04	0.35	0.63
Dec 08	0.06	0.67	0.44	0.03	0.03	0.08	0.68
Jan. 09	0.14	0.65	0.24	0.07	0.07	0.21	0.65
Feb 09	0.19	0.52	0.08	0.05	0.05	0.25	0.53
Mar 09	0.17	0.32	0.07	0.03	0.03	0.19	0.34
Average	0.16	0.56	0.25	0.05	0.05	0.22	0.61

Table 4.16: Average MAE, RMSE, r through time series obtained with interpolated values, AMSR-E and all the correction methods.

	AMSR-E	DC	RC	DMC	RMC	SC	Interpolation
MAE	10.12	6.8	16.34	9.23	9.23	10.02	5.74
r	0.16	0.56	0.25	0.05	0.05	0.22	0.61
RMSE	18.22	13.31	60.99	17.7	17.78	17.8	11.27

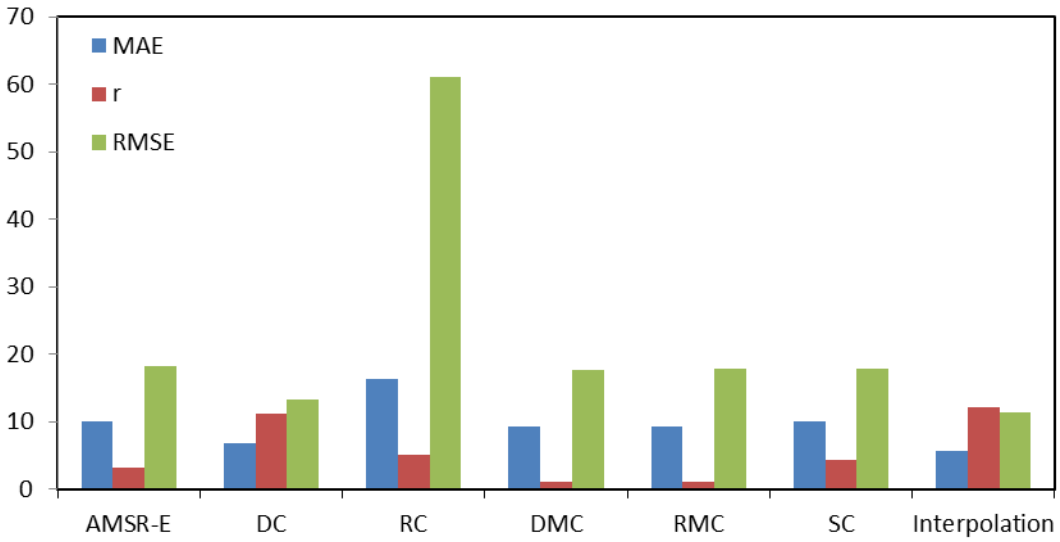

Figure 4.22: Average MAE, RMSE, r through time series obtained with interpolated values, AMSR-E and all the correction methods.

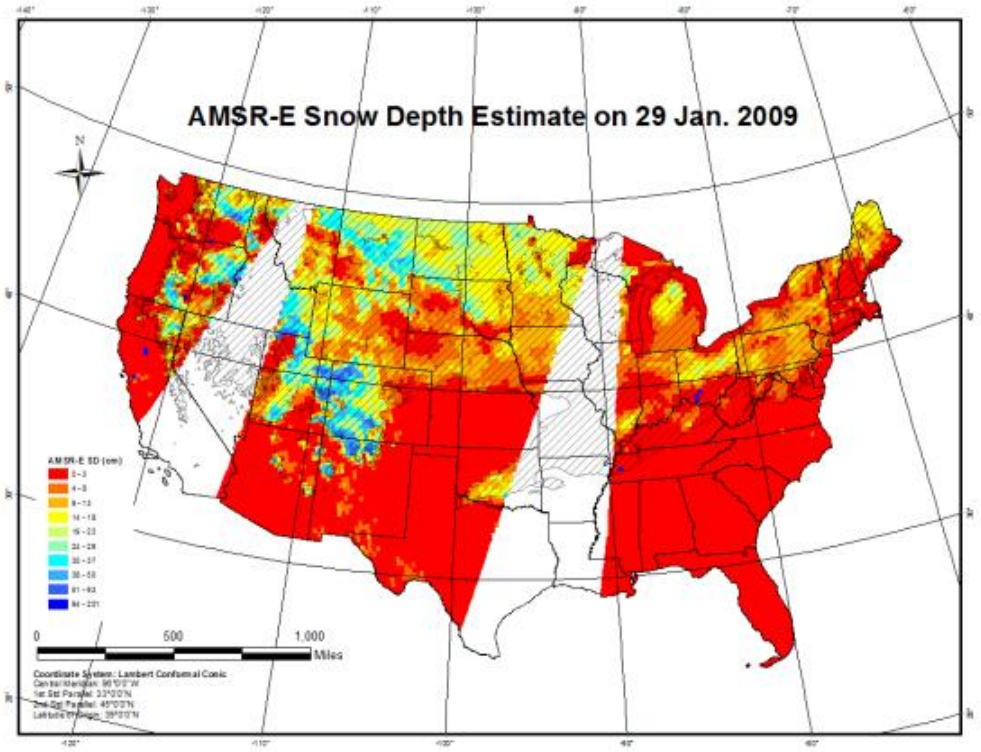

(a)

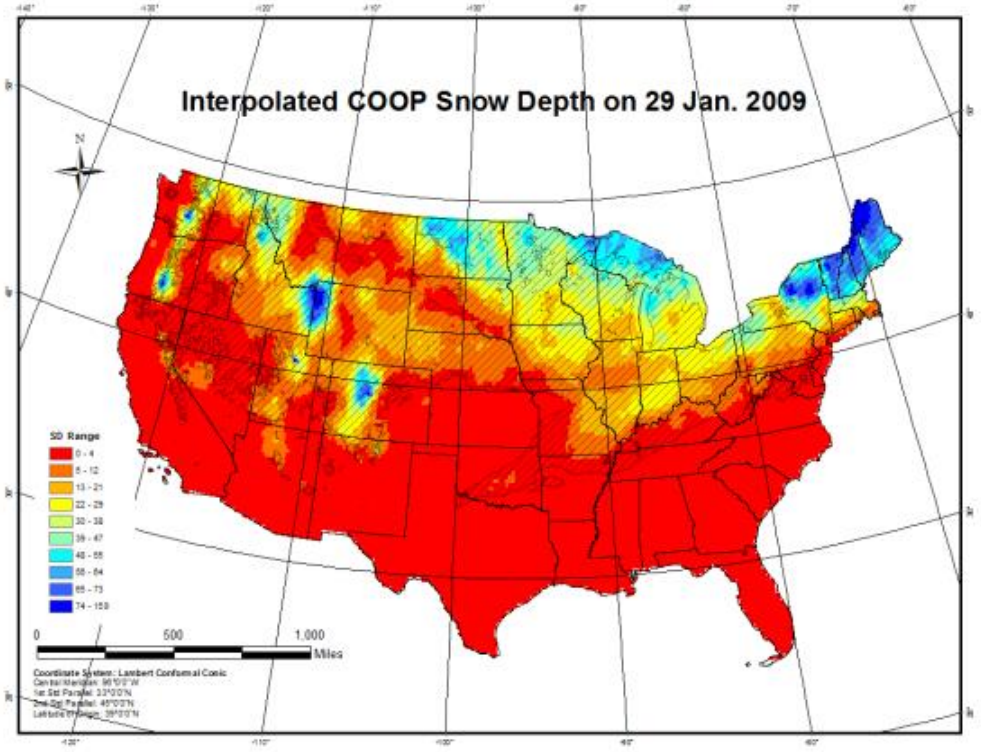

(b)

Figure 4.23: AMSR-E SD estimate (a) and ISCE (b) on 29 Jan. 2009.

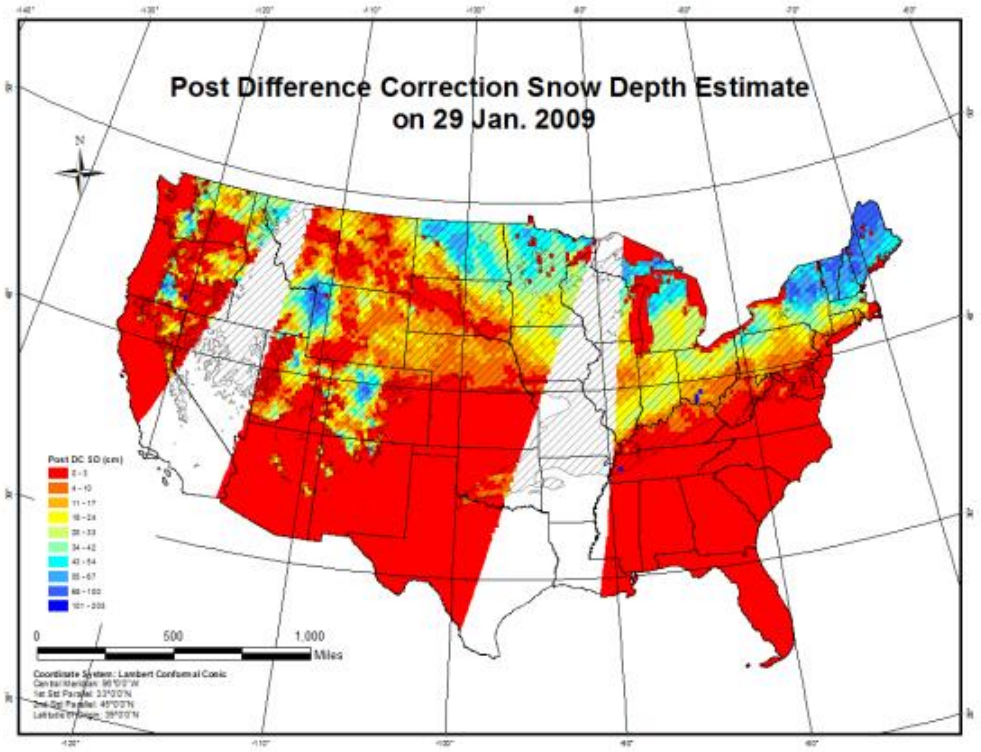

(a)

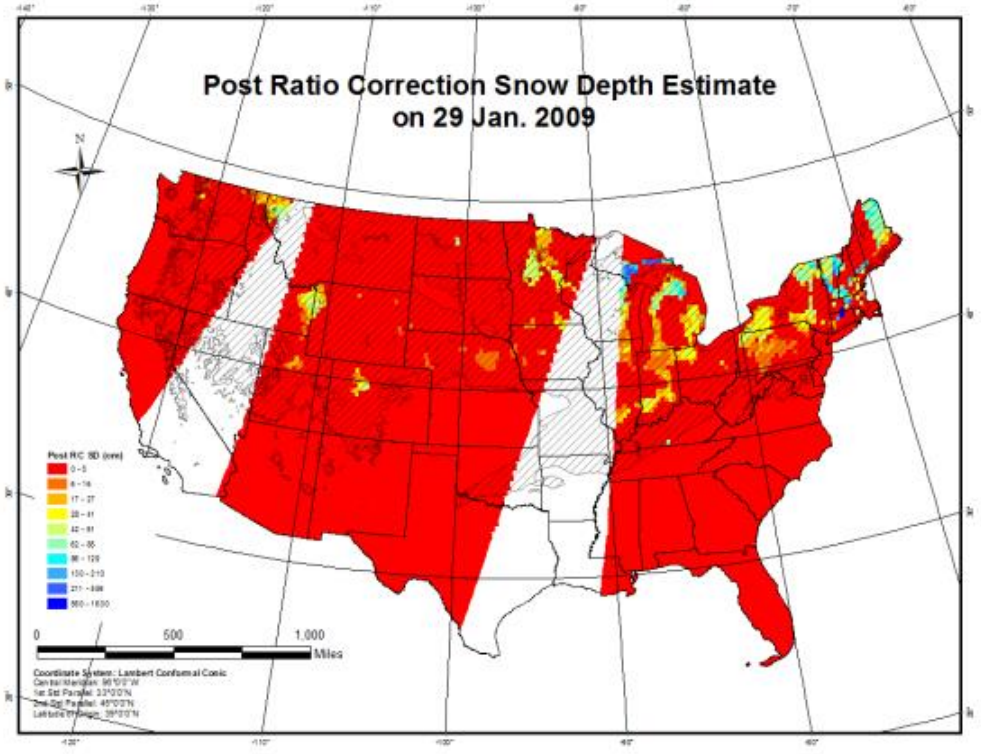

(b)

Figure 4.24: Post DC (a) and post RC (b) SD estimate on 29 Jan. 2009.

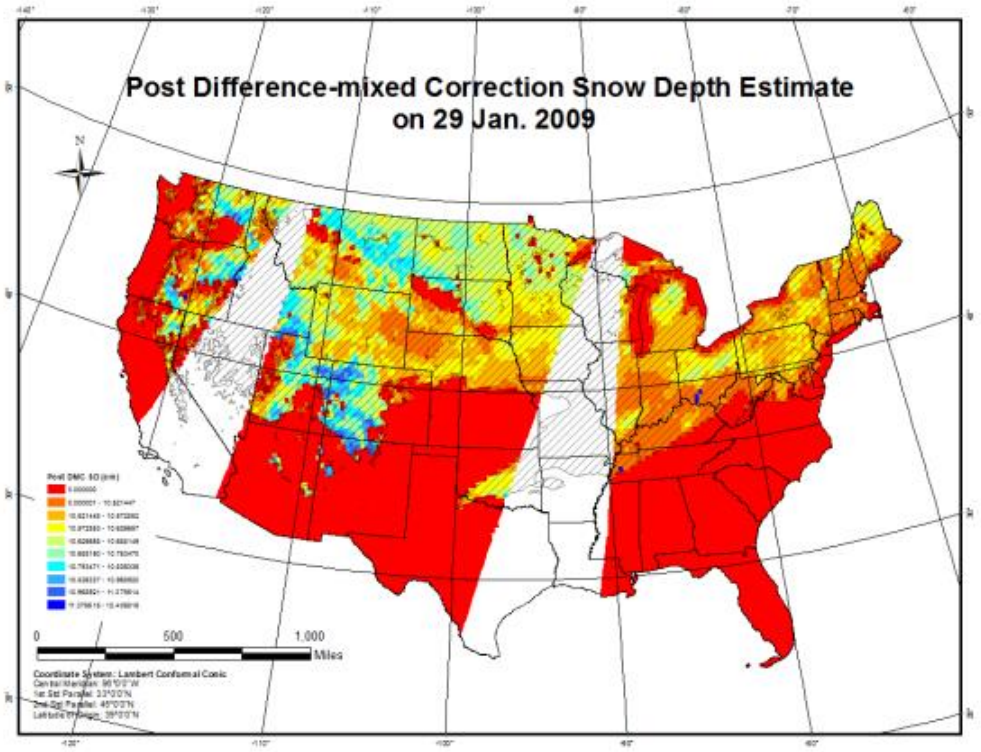

(a)

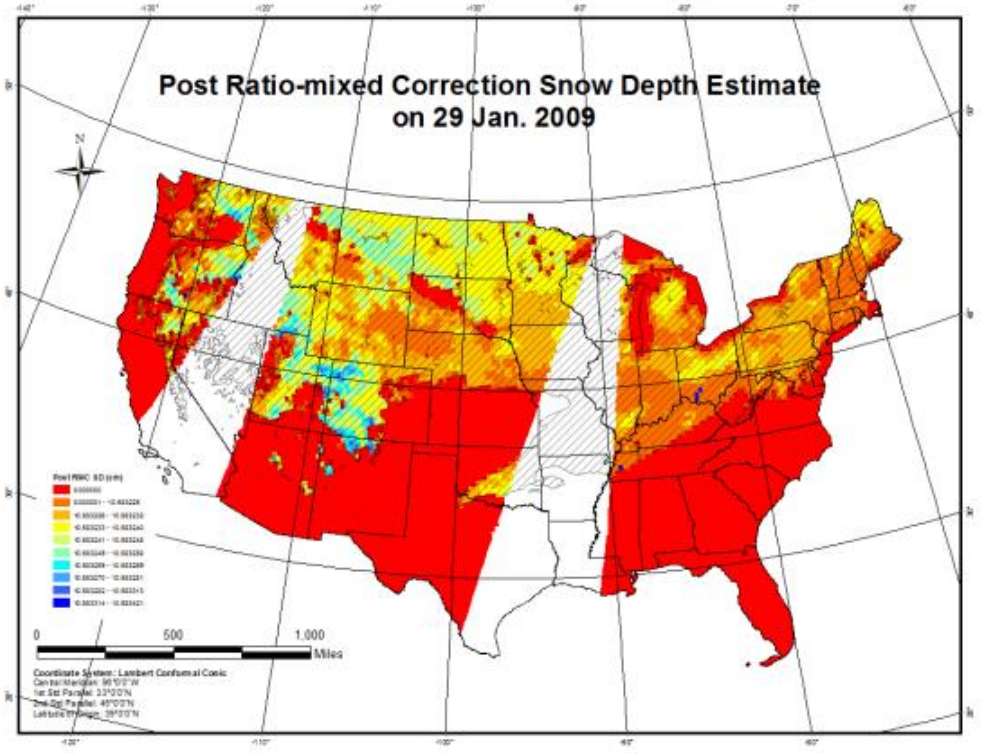

(b)

Figure 4.25: Post DMC (a) and post RMC (b) SD estimate on 29 Jan. 2009.

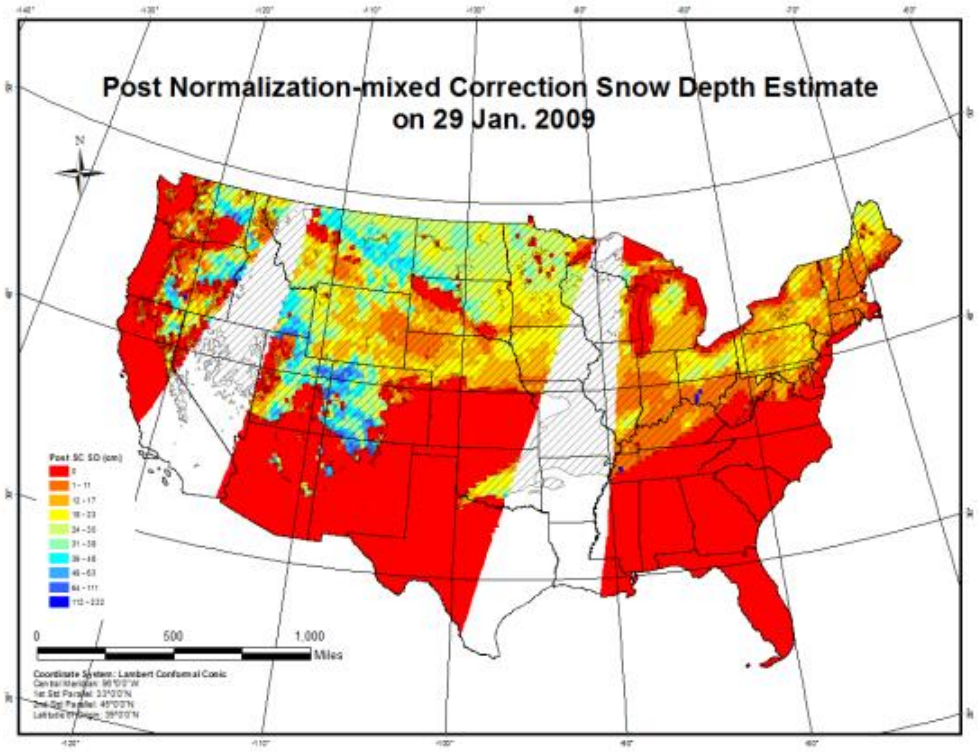

Figure 4.26: Post SC SD estimate on 29 Jan. 2009.

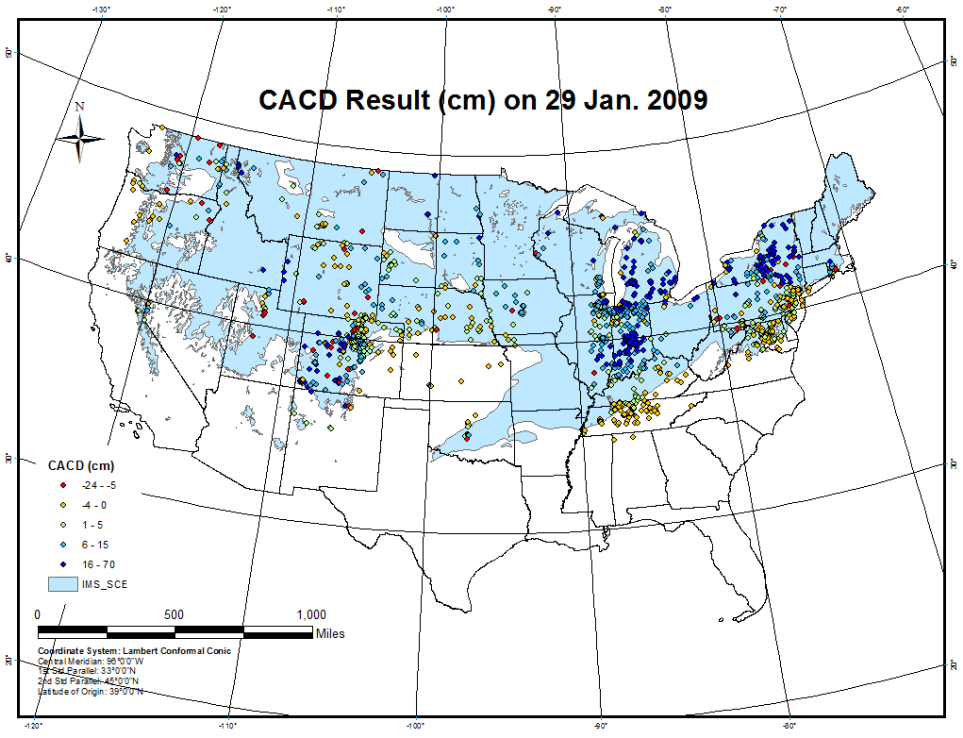

Figure 4.27: CACD result of DC performance on 29 Jan. 2009.

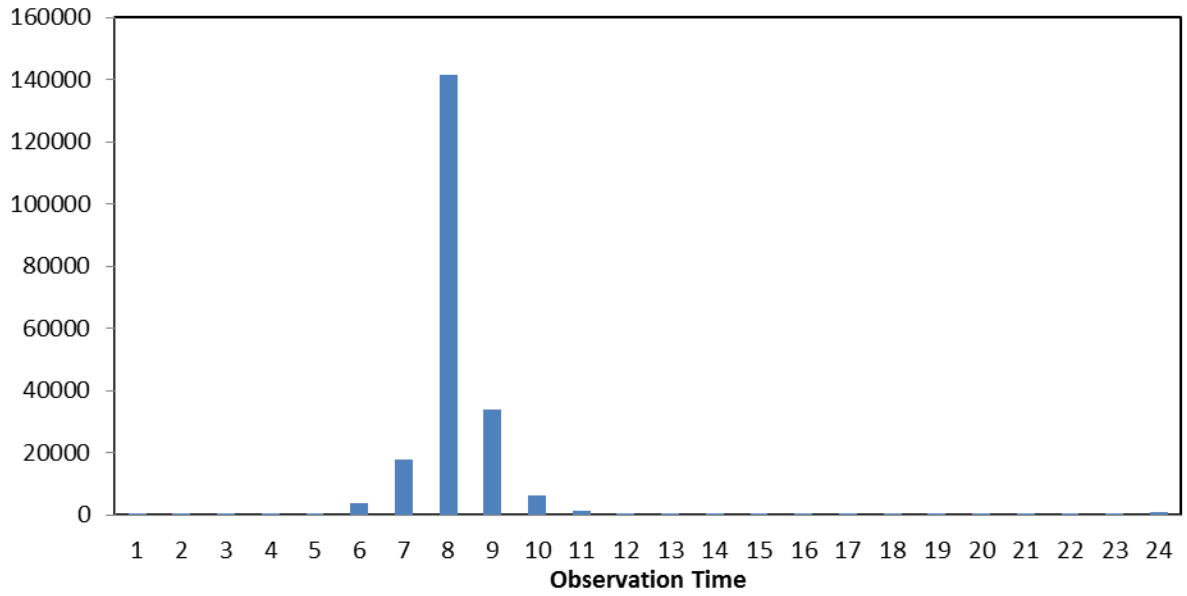

Figure 4.28: CoCoRaHS time of observation (LST) frequency.

Table 4.17: CoCoRaHS observation frequency by time (LST).

Observation Time	Observation Count
0–1	420
1–2	11
2–3	116
3–4	51
4–5	609
5–6	3954
6–7	17911
7–8	141348
8–9	34112
9–10	6287
10–11	1203
11–12	485
12–13	409
13–14	294
14–15	150
15–16	156
16–17	222
17–18	411
18–19	367
19–20	441
20–21	189
21–22	101
22–23	143
23–24	933

CHAPTER 5

CONCLUSIONS

Snow plays an important role in the hydrological cycle. SCE can greatly influence the radiation and surface energy budgets. SWE and SD are crucial components for water management, notably flood prevention. Snow detection techniques have consistently improved over time. Among all the snow detection methods, satellite snow detection is one of the most important techniques, especially for large-scale studies, which dates back to 1978. Passive microwave technique, among all the satellite snow detection methods, is comparatively new. This technique provides better snow detection performance because it is able to penetrate clouds and it is insensitive to solar illumination. For this reason, many passive microwave snow products have been developed and used in snow research. Passive microwave snow estimates can be affected by forest, snow grain size, and snow density, among other factors. In this research, I proposed a simple interpolation-based synthesis combining satellite SWE, SCE and ground observation datasets aimed at providing a large-scale SD product with comparatively higher accuracy compared to stand-alone satellite retrievals.

5.1 Major findings

In this research, AMSR-E SD values were first compared with COOP ground SD observations (i.e. objective one). In general, daily SD means were found to be significantly different between the two datasets. This statistical result was probably due to the overall underestimation of SD by AMSR-E. The correlations between AMSR-E and COOP daily means were relatively high for two winter-seasons (2007/2008 and 2008/2009), indicating that AMSR-

E adequately detects snow variations over time. However, the SD spatial distributions of the two datasets were significantly different. Based on eight individual day comparisons, AMSR-E greatly underestimated the SD values over the northern Rocky Mountains and the mountainous areas over Washington, Oregon, California. Meanwhile, it occasionally overestimated SD values over the north central U.S.. Based on previous studies and the findings from this research, the possible explanations include effects of forest cover, elevation, snow melt and algorithm-related error of not accounting for dynamic snow density and snow grain size.

The completely regularized spline (CRS) interpolation was found to have the best data splitting (DS) results and cokriging (CO) was found to have the best performance when using cross-validation (CV) (i.e. result of objective two). In this research, CV plus DS was used to optimize interpolation techniques. Results suggested that CRS surpasses other interpolation techniques in terms of accuracy. The number and distribution of the ground stations may affect the performance of different interpolation techniques. The difference between CV and DS results can be used as an measure to determine which interpolation works better for dense or sparse ground observation networks. Based on previous studies, spatial dependence also appeared to play a crucial role in applying geostatistical methods (e.g. kriging).

Five syntheses of SD observations, satellite SWE product and satellite SCE products based on Cao et al. (2012) were modeled using ArcGIS and evaluated by comparison with CoCoRaHS data (i.e. objective three). The difference correction (DC) method was found to provide the best synthesis of COOP and AMSR-E data. The synthesis had a better performance compared to stand-alone AMSR-E SD values. However, the results were not as good as stand-alone interpolation methods when taking IMS SCE into account. This observation is probably due to the adequate number of ground stations in use over the study area for interpolation. This

may also due to the CoCoRaHS data used for evaluation was clustered; DC performance might be better than stand-alone interpolated COOP if there was a more regularly distributed dataset available. However, regions outside the U.S. may not have dense station network. Therefore, more analysis should be conducted over other regions. A worldwide or hemispheric-scale station network including either governmental or volunteer networks would be ideal for large-scale snow studies.

Since the methodology was rather simple with limited modeling, the stand-alone satellite SD estimates have been largely improved. The methodology may also prove to be relatively easy for water managers and other operational forecasters to generate accurate gridded estimates of SWE in a timely manner, especially with the benefit of global availability of ArcGIS software.

5.2 Limitations

Although this research has been carefully conducted, limitations still exist such as missing data, data spatial-temporal resolution, time series and study area.

Almost all of the data sources used have missing data except the DEM. AMSR-E lacks an entire day data on 2 December 2007. IMS SCE product lacks four days (i.e., 17 January 2008, 28 February 2009, 26 March 2009 and 31 March 2009). Both COOP and CoCoRaHS have stations with no measurements on some days, and the missing data stations vary on a daily basis. However, COOP is noted to be much more consistent (i.e., less clustered spatial distribution distribution variation and more consistent observation time) than CoCoRaHS.

Data spatio-temporal resolution is another limitation that should be taken into consideration. The spatial resolution of IMS SCE is 1 km, which is coarse compared to visible and infrared and combined products (e.g., ANSA). Both COOP and CoCoRaHS are volunteer station networks. Not all the stations from the two datasets are noted to have consistent

measurement over time. Inconsistent datasets may lead to less dense networks and a "clustering" effect, especially for the CoCoRaHS dataset. With finer spatial resolution and more consistent ground station networks, a more accurate product is expected.

Utilizing RMSE as a metric for selecting an optimum interpolation method is another limitation. RMSE fails to take data spatial consistency into account (i.e. small amount of extreme values can increase the RMSE value for the whole model). Although a comparison study of different interpolation techniques has been conducted to evaluate the spatial pattern of various methods (i.e. spatially evaluate the extreme value) to address this limitation, additional error metrics need to be included in order to get a more accurate evaluation result. Finally, in this study, only two winter seasons over the contiguous U.S. have been studied. However, with a longer time series and different study region, the results could vary greatly. The density of station networks varies substantially for different regions, and even areas with dense networks may not make the data publically available.

5.3 Future directions

Future studies may consider suggestions including: use of more recently developed satellite SCE products with high resolution and careful validation, exploration of refined regression relationships between satellite estimates and ground observations, defining a threshold of stations density to decide whether to use stand-alone interpolation methods, stand-alone satellite estimates or the synthesis proposed in this study, and implementation of a worldwide or hemispheric scale station network for large-scale meteorological studies. However, establishing a worldwide or a hemispheric scale station network is not an easy task (e.g., many stations have been erroneously recorded as "zero" when they should have been recorded as "missing" (Christy, 2012)).

Developing interpolation models such as Artificial Neural Networks (ANN) and regression tree (RT) by using ArcGIS for better synthesis results can also be a future study. According to Sluiter (2009), a feature of ANNs is their adaptive nature of "learning" during the classification/prediction process. For this reason, ANNs are powerful and popular for solving complex, non-linear processes. RT is another interpolation technique, which has been more recently adopted, especially for modeling snow. According to Breiman et al. (1984), RT models are non-parametric methods that rely on the recursive splitting of the values from the predictor variables aimed at minimizing the squared residuals of each group. In general, the tree size is selected based on a threshold in the change of the unexplained variance while a new group is obtained.

Funded by the European Space Agency (ESA), GlobSnow currently provides snow extent (SE) and SWE data at the hemispherical scale. The SWE product combines satellite retrievals with ground observations following algorithm proposed by Pullianinen (2006). SWE output was noted to have better performance compared to stand-alone interpolated ground observations. (Pullianinen 2006). However, some limitations exist when applying this approach at a hemisphere or global scale including: (1) the SWE algorithm is developed for boreal and sub-arctic zones, whether the algorithm fits other regions still needs to be explored; (2) and the interpolation used for ground observation is ordinary kriging, while, as concluded in Section 4.2, ordinary kriging is not recommended as the interpolation method. Therefore, one of the most important contributions from this thesis research may come from applications of the findings to the GlobSnow productr.

REFERENCES

Barrett, A. 2003: *National Operational Hydrologic Remote Sensing Center SNOw Data Assimilation System (SNODAS) Products at NSIDC*. NSIDC Special Report 11. Boulder, CO, USA: National Snow and Ice Data Center. Digital media.

Burakowski, E. A., C. P. Wake, B. Braswell, and D. P. Brown, 2008: Trends in wintertime climate in the northeastern United States: 1965–2005. *J. Geophys. Res.*, 113, *D20114.*

Brodzik, M. J. and K. W. Knowles, 2002: EASE-Grid: A Versatile Set of Equal-Area Projections and Grids in M. Goodchild (Ed.) Discrete Global Grids. Santa Barbara, California USA: National Center for Geographic Information & Analysis.

Cao, Y., Y. He, X. Qiu, Y. Zeng, Q. Luo, and T. Gao, 2012: Correction methods of MODIS cloud product based on ground observation data. *J. Remote Sens.*, **16**, 326-342

Chang, A. T. C., P. Gloersen, T. Schmugge, T. T. Wilheit, and H. J. Zwally, 1976: Microwave emission from snow and glacier ice. *J. Glaciol.*, **16**, 23–39.

Chang, A. T. C., J. L. Foster, and D. K. Hall, 1987: Nimbus-7 SMMR derived global snow cover parameters. *Ann. Glaciol.*, **9**, 39–44.

Chang, A.T.C., J. L. Foster, and A. Rango, 1991: Utilization of surface cover composition to improve the microwave determination of SWE in a mountain basin. *Intl. J. Remote Sensing*, **12**, 2311–2319.

Chang, A. T. C., R. E. J. Kelly, 2005: Analysis of ground-measured and passive-microwave-derived snow depth variations in midwinter across the northern Great Plains. *J. Hydrometeor.*, **6**, 20–33.

Chi, J., 2011: *Proficient in ArcGIS: Geographic Information System*. Tsinghua University Press, 457 pp.

Christy, J. R., 2012: Searching for information in 133 years of California snowfall observations. *Bull. Amer. Meteor. Soc.,* **13**, 895–912.

Climate Change 2007: Synthesis Report. *Contribution of Working Groups I, II and III to the Fourth Assessment Report of the Intergovernmental Panel on Climate Change,* Core

Writing Team, R. K. Pachauri, and A. Reisinger, Ed., Geneva, Switzerland: IPCC, 104 pp.

Community Collaborative Rain, Hail and Snow Network, cited 2013: General information about CoCoRaHS.
[Available online at http://www.cocorahs.org/Content.aspx? page=aboutus#what.]

De Lannoy, G. J. M., R. H. Reichle, K. R. Arsenault, P. R. Houser, S. Kumar, N. E. C. Verhoest, and V. R. N. Pauwels, 2012: Multiscale assimilation of Advanced Microwave Scanning Radiometer–EOS snow water equivalent and Moderate Resolution Imaging Spectroradiometer snow cover fraction observations in northern Colorado. *Water Resour. Res.*, **48**, W01522.

Dyer, J. L., and T. L. Mote, 2006: Spatial variability and trends in observed snow depth over North America. *Geophys. Res. Lett.*, **33**, L16503, doi:10.1029/2006GL027258.

Easterling, D. R., T. R. Karl, E.H. Mason, P. Y. Hughes, and D. P. Bowman 1996. United States Historical Climatology Network (U.S. HCN) Monthly Temperature and Precipitation Data. ORNL/CDIAC-87, NDP-019/R3. Carbon Dioxide Information Analysis Center, Oak Ridge National Laboratory, U.S. Department of Energy, Oak Ridge, Tennessee.

Engen, G., T. Gunerjussen, and O. Overrein, 2004: Delta-K interferometric SAR technique for SWE (SWE) retrieval. *IEEE Geosci. Remote Sens. Lett.*, **1**, 57–61.

England, A. W. 1975: Thermal microwave emission from a scattering layer. *J. Geophys. Res.* **80**, 4484-4496.

Erxleben, J., K. Elder and R. Davis, 2002: Comparison of spatial interpolation methods for estimating snow distribution in the Colorado Rocky Mountains. *Hydrol. Process*. **16**. 3627–3649.

Fassnacht, S. R., K. A. Dressler, and R. C. Bales, 2003: SWE interpolation for the Colorado River Basin from snow telemetry (SNOTEL) data. *Water Resour. Res*., **39**, 1208.

Fiebrich, C. A. 2009: History of surface weather observations in the United States. *Earth Sci. Rev.*, **93**, 77-84.

Foster, J. L., A. T. Chang, and D. K. Hall, 1997: Comparison of snow mass estimation from a prototype passive microwave snow algorithm, a revised algorithm and snow depth climatology. *Remote Sensing Envirion.*, **62**, 132–142.

Foster, J. L., D. K. Hall, J. B. Eylander, G. A. Riggs, S. V. Nghiem, M. Tedesco, E. Kim, P. M. Montesano, R. E. J. Kelly, K. A. Casey, and B. Choudhury, 2011: A blended global snow product using visible, passive microwave and scatterometer satellite data. *Int. J. Remote Sens.*, **32**, 1371–1395.

Foppa, N., A. Stoffel, and R. Meister, 2007: Synergy of in situ and space borne observation for snow depth mapping in the Swiss Alps. *Int. J. Appl. Earth Obs.*, **9**, 294–310.

Frei, A., M. Tedesco, S. Lee, J. Foster, D. K. Hall, R. Kelly, and D. A. Robinson, 2012: A review of global satellite-derived snow products. *Adv. Space Res.*, **50**, 1007–1029.

Fuhrmann, C. M., D. K. Hall, L. B. Perry, and G. A. Riggs, 2010: Spatial patterns of snow cover in North Carolina: surface and satellite perspectives. *Proceedings of the Annual Eastern Snow Conference*, **67**, R.A. Hellstrom and S. Frankenstein, Ed., Eastern Snow Conference, 183-195 pp.

Gan, T. Y., O. Kalinga, and P. R. Singh, 2009: Comparison of SWE retrieved from SSM/I passive microwave data using artificial neural network, projection pursuit and nonlinear regressions. *Remote Sens. Environ.*, **113**, 919–927.

GCOS, 2009: Snow Cover Standards Report on the Assessment of the Status of the Development of the Standards for the Terrestrial Essential Climate Variables. Version 8 21 May 2009. [Available online: http://www.fao.org/gtos/doc/ECVs/T05/T05.pdf]

Ge, Y., and G. Gong, 2009: North American Snow Depth and Climate Teleconnection Patterns. *J. Climate*, **22**, 217–233.

Goodison, B. E., I. Rubinstein, F. W. Thirkettle, and E. J. Langham, 1986: Determination of SWE on the Canadian prairies using microwave rediometry. *Modelling Snowmelt-Induced Processes, Proceedings of the Budapest Symposium, IAHS Publ.*, **155**, 163–173.

Green, J., C. Kongoli, A. Prakash, M. Sturm, C. Duguay, and S. Li, 2012: Quangtifying the relationships between lake fraction, SWE and snow depth, and microwave brightness temperatures in an arctic tundra landscape. *Remote Sens. Environ.*, **127**, 329–340.

Grundstein, A., and T. L. Mote, 2010: Trends in average snow depth across the western united states. Phys. Geog., **31**, 172–185.

Hall, D. K., J. L. Foster, V. V. Salomonson, A. G. Klein, and J. Y. L. Chien, 2001: Development of a technique to assess snow-cover mapping errors from space. *IEEE Trans. Geosci. Remote Sensing*, **39**, 432–438.

Hallikainen, M. T., 1984 : Retrieval of SWE from Nimbus-7 SMMR data: Effect of land-cover categories and weather conditions. *IEEE J. Oceanic Engr.*, **9**, 372–376.

Hallikainen, M. T., F. T. Ulaby, and T.E. Van Deventer, 1987: Extinction behavior of dry snow in the 18-Ghz to 90-Ghz range. *IEEE Trans. Geosci. Remote Sens.*, **25**, 737–745.

Hallikainen, M. T., 1989: Microwave radiometry on snow. *Adv. Space Res*., **9**, 267–275.

Harshburger, B. J., K. S. Humes, V. P. Walden, T. R. Blandford, B. C. Moore, and R. J. Dezzani, 2010: Spatial interpolation of snow water equivalency using surface observations and remotely sensed images of snow-covered area. *Hydrol. Process*., **24**, 1285–1295.

Hyvarinen, O., K. Eerola, N. Siljamo, and J. Koskinen, 2009: Comparison of snow cover from satellite and numerical weather prediction models in the Northern Hemisphere and Northern Europe. *J. Appl. Meteor. Climatology*, **48**, 1199–1216.

Konstantinos, M. A., P. Storck, and D. P. Lettenmaier, 2009: Modeling snow accumulation and ablation processes in forested environments. *Water Resour. Res*., **45**, W05429.

Kunkel, K., E., M. Palecki, L. Ensor, K. G. Hubbard, D. Robinson, K. Redmond, D. Easterling, 2009: Trends in Twentieth-Century U.S. snowfall using a quality-controlled dataset. *J. Atmos. Oceanic Tech..,* **26**, 33–44.

Larson, K. M., E. D. Gutmann, V. U. Zavorotny, J. J. Braun, M. W. Williams, and F. G. Nievinski, 2009: Can we measure snow depth with GPS receivers? *Geophys. Res. Lett.,* **36**, L17502.

Liang, T., X. Zhang, H. Xie, C. Wu, Q. Feng, X. Huang, and Q. Chen, 2008: Toward improved daily snow cover mapping with advanced combination of MODIS and AMSR-E measurements. *Remote Sens. Enviorn.,* **112**, 3750–3761.

Liu, Y., Q., C. D. Peters-Lidard, S. Kumar, J. L. Foster, M. Shaw, Y. Tian, and G. M. Fall, 2013: Assimilating satellite-based snow depth and snow cover products for improving snow predictions in Alaska. *Adv. Water Resour.*, **54**, 208–227.

López-Moreno, J. I., and D. Nogués-Bravo, 2006: Interpolating local snow depth data: an evaluation of methods. *Hydrol. Process.,* **20**, 2217–2232.

Lucas, R. M., and A. R. Harrison., 1990: Snow observation by satellite: A review. *Remote Sens. Rev*., **4**, 285–348.

Luzi, G., L. Noferini, D. Mecatti, G. Macaluso, M. Pieraccini, C. Atzeni, A. Schaffhauser, R. Fromm, T. Nagler, 2009: Using a ground-based SAR interferometer and a terrestrial laser scanner to monitor a snow-covered slope: Results from an experimental data collection in Tyrol (Austria). *IEEE Trans. Geosci. Remote Sens.*, **47**, 382–393.

Matzler C., 1994: Passive microwave signatures of landscapes in winter. *Meteor. Atmos. Physics*, **54**, 241–260.

McGrew, J. C., and Jr. C. B. Monroe, 2009: *An Introduction to Statistical Problem Solving in Geography*. Waveland Press, Inc., 254 pp.

Molotch, N. P., M. T. Colee, R. C. Bales, and J. Dozier, 2005: Estimating the spatial distribution of SWE in an alpine basin using binary regression tree models: the impact of digital elevation data and independent variable selection. *Hydrol. Process.*, **19**, 1459–1479.

Moser, C. L., G. A. Tootle, A. A. Oubeidillah, and V. Lakshmi, 2011: A comparison of SNOTEL and AMSR-E snow water equivalent data sets in western U.S.watersheds. *Int. J. Remote Sens.*, **32**, 6611-6629.

Mote, P. W., A. F. Hamlet, M. P. Clark, and D. P. Letternmaier, 2005: Declining mountain snowpack in western North Amricca. *Bull. Amer. Meteor. Soc.*, **86**, 39–49.

Mote, T., 2008: On the association between air temperatures and snow depth. J. Appl. Meteor. Climatol., **47**, 2008–2022.

NOAA/NESDIS/OSDPD/SSD, 2004: IMS Daily Northern Hemisphere Snow and Ice Analysis at 4 km and 24 km Resolution. Boulder, Colorado USA: National Snow and Ice Data Center.
[Available online at http://dx.doi.org/10.7265/N52R3PMC]

NOAA's National Weather Service Cooperative Observer Program, cited 2013: What is the COOP Program?
[Available online at http://www.nws.noaa.gov/om/coop/what-is-coop.html].

Peng, S., S. Piao, P. Ciais, J. Fang, and X. Wang, 2010: Change in winter snow depth and its impacts on vegetation in China. *Glob. Change Biol.*, **16**, 3004–3013.

Pulliainen, J., 2006: Mapping of SWE and snow depth in boreal and sub-arctic zones by assimilating space-borne microwave radiometer data and ground-based observations. *Remote Sens. Environ.*, **101**, 257–269.

Robinson, D. A., 1989: Construction of a United States historical snow data base. *Proc. Eastern Snow Conf*., **45**, 50–59.

Romanov, P., G. Gutman, and I. Csiszar, 2000: Automated monitoring of snow cover over North America with multispectral satellite data. *J. Appl. Meteor.*, **39**, 1866–1880.

Rozante, J. R., S. M. Demerval, G. G. G. Luis, and A. V. Daniel, 2010: Combining TRMM and Surface Observations of Precipitation: Technique and Validation over South America. *Wea. Forecasting*, **25**, 885–894.

Singh, P.R., and T.Y. Gan, 2000: Retrieval of SWE using passive microwave brightness temperature data. *Remote Sens. Environ.*, **74**, 275–286.

Sluiter, R., 2009: Interpolation methods for climate data. KNMI, R&D Information and Observation Technology.

Takala, M., K. Luojus, J. Pulliainen, C. Derksen, J. Lemmetyinen, J-P. Kärnä, J. Koskinen, and B. Bojkov, 2011: Estimating northern hemisphere SWE for climate research through assimilation of space-borne radiometer data and ground-based measurements. *Remote Sens. Environ.*, **115**, 3517–3529.

Tedesco, M., R. Kelly, J. L. Foster, and A. T.C. Chang, 2004: *AMSR-E/Aqua Daily L3 Global Snow Water Equivalent EASE-Grids*. Version 2. Boulder, Colorado USA: NASA DAAC at the National Snow and Ice Data Center.

Tedesco, M., R. Reichle, A. Low, T. Markus, and J.L. Foster, 2010: Dynamic approaches for snow depth retrieval from spaceborne microwave brightness temperature. *IEEE Trans. Geosci. Remote Sens.*, **48**, 1955–1967.

Tedesco, M., and Narvekar, P., S., 2010: Assessment of the NASA AMSR-E SWE Product. *IEEE J. Sel. Top. Appl. Earth Obs. Remote Sens.*, **3**,141–159.

Tedesco, M., C. Derksen and J. Pulliainen, 2012: Hemispheric SWE: The need for a synergistic approach, *Eos Trans.*, **93**, 305.

Tedesco, M., 2012: Algorithm Theoretical Basis Document (ATBD) for the AMSR-E Snow Water Equivalent Algorithm, NASA GSFC.

Tekeli, A. E., 2008: Early findings in comparison of AMSR-E/Aqua L3 global SWE EASE-grids data with in situ observations for Eastern Turkey. *Hydrol. Process*., **22**, 2737–2747.

Tveito, O.E., M. Wegehenkel, F. Van der Wel and H. Dobesch, 2006: The Use of Geographic Information Systems in Climatology and Meteorology, Final Report COST Action 719.

U.S. Geological Survey, cited in 2013: The National Map Seamless Server. [Available online at http://seamless.usgs.gov]

Wu, X. Q., H. Y. Zhang, R. G. Li, Z. X. Zhang, and G. H. Dong, 2009: *ArcGIS 9: Geographic Information System Application and Practice.* 4th ed. Tsinghua University, 330–336.

Zhu, M., 2009: Validation of passive microwave remotely sensed snow depth data. M.S. thesis, School of Remote Sensing and Information Engineering, Wuhan University, Hubei, China, 69.

Zhu, M., J.Y. Li, and M.D. Zhou, 2009: The research on snow depth validation data densification at regional scale. *Application Remote Sensing*, 44–47.